NASA TM X-209

TECHNICAL MEMORANDUM

X-209

STATIC LONGITUDINAL, DIRECTIONAL, AND LATERAL STABILITY AND CONTROL DATA FROM AN INVESTIGATION AT A MACH NUMBER OF 6.83 OF TWO DEVELOPMENTAL X-15 AIRPLANE CONFIGURATIONS

By David E. Fetterman, Jr., and Jim A. Penland

Langley Research Center
Langley Field, Va.

NATIONAL AERONAUTICS AND SPACE ADMINISTRATION
WASHINGTON
March 1960

NATIONAL AERONAUTICS AND SPACE ADMINISTRATION

TECHNICAL MEMORANDUM X-209

STATIC LONGITUDINAL, DIRECTIONAL, AND LATERAL STABILITY AND CONTROL DATA FROM AN INVESTIGATION AT A MACH NUMBER OF 6.83 OF TWO DEVELOPMENTAL X-15 AIRPLANE CONFIGURATIONS*

By David E. Fetterman, Jr., and Jim A. Penland

SUMMARY

An investigation has been conducted in the Langley 11-inch hypersonic tunnel to determine the static longitudinal, lateral, and directional stability and control on two preliminary developmental X-15 configurations with various component modifications. The tests were made at a Mach number of 6.83 and a Reynolds number of 640,000 based on wing mean aerodynamic chord. The majority of the data were obtained over an angle-of-attack range from -4° to 24° at sideslip angles of 0° and -5°. The longitudinal stability data are referred to the stability axes system, and the directional and lateral stability data are referred to the body axes system. Analysis of the data has been omitted in order to expedite release of this information.

INTRODUCTION

An investigation at the Langley Research Center has been under way over the past few years to supply hypersonic static stability and control data on airplane-type configurations for use in establishing the X-15 configuration. The results of this early investigation are reported in references 1 to 7. These results were utilized to establish the developmental X-15 configurations which were tested at various speeds. This paper presents the static stability and control data obtained in the Langley 11-inch hypersonic tunnel at a Mach number of 6.83 for the two preliminary X-15 configurations with their various component modifications. The results of tests on these two preliminary X-15 configurations at other Mach numbers can be obtained from references 8 to 16.

Analysis of the data presented herein has been omitted in order to expedite release of this information.

SYMBOLS

The longitudinal stability data are referred to the stability axes system, and the directional and lateral stability data are referred to the body-axes system. The body-axes and stability-axes systems are illustrated in figure 1. The moment reference is at 25 percent of the wing mean aerodynamic chord.

The coefficients and symbols are defined as follows:

C_D drag coefficient, $\frac{F_D}{qS}$

C_L lift coefficient, $\frac{F_L}{qS}$

C_m pitching-moment coefficient, $\frac{M_Y}{qS\bar{c}}$

C_l rolling-moment coefficient, $\frac{M_X}{qSb}$

C_n yawing-moment coefficient, $\frac{M_Z}{qSb}$

C_Y side-force coefficient, $\frac{F_Y}{qS}$

F_D force along $-X_s$-axis

F_L force along $-Z_s$-axis

F_Y force along Y-axis

M_X moment about X-axis

M_Y moment about Y-axis

M_Z moment about Z-axis

b wing span

c	chord
$\bar{c}$	wing mean aerodynamic chord
d	body maximum diameter
M	Mach number
q	free-stream dynamic pressure
S	total wing area including body intercept
X,Y,Z	longitudinal, lateral, and normal axes, respectively
x	distance along chord from leading edge
y	distance perpendicular to chord
α	angle of attack
β	angle of sideslip
Γ	dihedral angle
δ_e	equivalent pitch deflection of differentially deflected horizontal tails, positive to produce positive C_L, $\frac{1}{2}(\delta_{HL} + \delta_{HR})$
δ_H	horizontal-tail deflection, positive to produce positive C_L
δ_h'	differential horizontal-tail deflection, positive to produce positive M_X, $(\delta_{HL} - \delta_{HR})$
δ_J	speed-brake deflection
δ_V	vertical-tail deflection, positive to produce positive C_Y
C_{Y_β}	rate of change of side-force coefficient with sideslip angle
C_{n_β}	rate of change of yawing-moment coefficient with sideslip angle
C_{l_β}	rate of change of rolling-moment coefficient with sideslip angle

$C_{Y_{\delta V}}$ rate of change of side-force coefficient with vertical-tail deflection

$C_{n_{\delta V}}$ rate of change of yawing-moment coefficient with vertical-tail deflection

$C_{l_{\delta V}}$ rate of change of rolling-moment coefficient with vertical-tail deflection

$C_{Y_{\delta h'}}$ rate of change of side-force coefficient with differential horizontal-tail deflection

$C_{n_{\delta h'}}$ rate of change of yawing-moment coefficient with differential horizontal-tail deflection

$C_{l_{\delta h'}}$ rate of change of rolling-moment coefficient with differential horizontal-tail deflection

L 7 4 0

Subscripts:

B body

F fairing

L lower when used with vertical tail; left when used with horizontal tail

R right

r root

s stability

t tip

U upper

Model component designations:

B body

H horizontal tail

J speed brake

V vertical tail

W wing

X side fairing

APPARATUS

Wind Tunnel

The tests were conducted in the Mach number 6.86 test section of the Langley 11-inch hypersonic tunnel which is equipped with a single-step, two-dimensional nozzle constructed of Invar. Tunnel operation is of the intermittent type, and a test run duration of about 80 seconds is possible. The nozzle was designed by the method of characteristics with a correction made for boundary layer. The tunnel-wall boundary-layer thickness and likewise free-stream Mach number are dependent upon the tunnel stagnation pressure. For these tests (at a stagnation pressure of 26 atmospheres absolute) the average free-stream Mach number was 6.83. The variation in Mach number after the first 10 seconds of operating time is about 1 percent.

During these tests the stagnation temperature was maintained at about 675° F by means of a variable-frequency electrical heater equipped with Nichrome tube resistance elements. This high temperature is necessary to avoid air liquefaction in the test section. In order to eliminate the effects of water condensation, the absolute humidity of the air was kept less than 1.87×10^{-5} pounds of water vapor per pound of air for all tests.

Further details of the Langley 11-inch hypersonic tunnel facility may be found in reference 17.

Balance and Model Support

Force and moment measurements were made through the use of a six-component, strain-gage force balance, the design of which allows four components to be located internally in the model. The other two components - axial force and rolling moment - are mounted externally at the rear of the balance and are shielded from the air flow during the tests. The model and balance were mounted in the test section on a movable support strut which could be rotated through an angle-of-attack range. During each test the period of essentially constant Mach number flow was long enough to permit testing through the angle-of-attack range of the investigation. Angles of sideslip were obtained by offsetting the model and balance support to the desired sideslip angle prior to each test. Thus, the data were obtained at an essentially constant sideslip angle over an angle-of-attack range.

MODELS

The two preliminary versions of the X-15 are designated as configurations 1 and 2, and three-view drawings of these configurations are presented in figures 2 and 3, respectively. An additional designation is employed herein to define these configurations in terms of their various components. The designation $BWXHV_UV_L$, then, unless otherwise specified, refers to configuration 1 as shown in figure 2; the designation $B_2W_2X_3H_3V_{U2}V_L$ refers to configuration 2 as shown in figure 3.

On configuration 2 two different horizontal-tail airfoil sections were tested, one having a modified NACA 66-005 section designated as H_3, and one having a 5° semiangle wedge section designated as H_2. These horizontal-tail modifications are shown in figure 3.

A comparison of configurations 1 and 2 is shown in figure 4. The primary differences between the configurations are that, for configuration 2, the nose of the fuselage was more blunt and the diameter of the cylindrical portion was increased; the leading-edge radii of the horizontal tail were increased and the wing was moved rearward and the horizontal tail was moved forward; the rear portions of the side fairings were enlarged and the landing skids were moved from under the wing to a position beneath the horizontal tail.

Two modifications to the side fairings of configuration 1 forward of the 6.105 body station were tested. These side-fairing modifications are designated X_{1A} and X_{1B} and are shown together with the original side fairing in figure 5.

Details and designations of the vertical-tail modifications and the various vertical-tail combinations tested on configuration 1 are shown in figure 6; the vertical-tail combinations tested on configuration 2 are shown in figure 7.

The various speed-brake configurations investigated are divided into vertical-tail speed brakes, fuselage speed brakes, and fairing speed brakes; details and designations of each are shown in figure 8. For the vertical-tail speed brakes (fig. 8(a)) and fairing speed brakes (fig. 8(c)) the surfaces shown are the true views of the brake surfaces. In addition to the location shown in figure 8(c) the fairing speed brakes were also tested with boundary-layer gaps of 0.0558d and 0.112d to offset the effects of flow separation ahead of the brakes.

The horizontal tail of configuration 1 was tested at different locations and with 0° and -15° dihedral. Details and designations of these horizontal-tail modifications are shown in figure 9.

Details for configuration 1 and its component modifications not covered in the aforementioned figures are included in table I, and those for configuration 2 are included in table II. The root-chord and tip-chord ordinates and leading-edge radii for the wing and horizontal-tail configurations are given in tables III and IV, respectively.

TESTS

The tests were conducted at a stagnation pressure of 26 atmospheres absolute. At this stagnation pressure the average test-section Mach number for test durations of 60 seconds is 6.83. These conditions in combination with the stagnation temperature mentioned previously resulted in a Reynolds number of 640,000 based on wing mean aerodynamic chord.

Six-component force and moment data were obtained at sideslip angles of 0° and -5° over an angle-of-attack range from -4° to 24° for the majority of the configurations. For configuration 1 with various horizontal-tail locations and dihedral angles and for configuration 2 with a 20° speed-brake deflection, the angle-of-attack range was from -20° to 24°. Directional control data were obtained by testing vertical-tail deflections δ_v of 0° and -5°, and lateral control data were obtained by testing differential horizontal-tail deflections δ_h' of 0°, -10°, and -20°.

The angles of attack were set by use of a lens prism imbedded in the model surface to reflect and focus a spot from a light source onto a previously calibrated screen. By using this method the true angles of attack were obtained directly irrespective of deflection under load.

During all tests the base pressure was measured, and the axial force was adjusted to correspond to the condition of base pressure equal to free-stream pressure.

PRECISION OF DATA

The probable uncertainties in the force and moment coefficients due to balance repeatability and variations in dynamic pressure have been estimated and are presented as follows:

C_L	±0.02
C_D	±0.006
C_m	±0.006
C_Y	±0.005
C_n	±0.001
C_l	±0.0005

The inaccuracies in α and β were ±0.10°.

PRESENTATION OF RESULTS

The data are presented in the form of comparison plots to show the effects of component breakdown and component modifications. For convenience in locating these various effects and configurations an index to the data figures is presented in table V.

The basic longitudinal stability data C_L, C_D, and C_m are presented in figures 10 to 27. No variations of the basic lateral and directional stability data C_Y, C_n, and C_l with sideslip angle are presented since the majority of the tests were made over the angle-of-attack range only at sideslip angles of 0° and -5°. Straight-line slopes between the basic data at these sideslip angles were then used to obtain the lateral and directional stability parameters presented in figures 28 to 39. This method is believed to yield sufficiently accurate results since the slopes so obtained agreed very well with those obtained from a limited number of tests wherein the model was tested over a sideslip-angle range at $\alpha = 0°$. These data are not included inasmuch as zero values of C_Y, C_n, and C_l were obtained at $\beta = 0°$ and essentially linear variations of the coefficients C_Y, C_n, and C_l with sideslip angle were obtained so that the data between $\beta = \pm 5°$ are adequately represented by the stability parameters. For similar reasons the straight-line-slope method was used to obtain the directional and lateral control parameters presented in figures 40 to 45.

Although an analysis of the data has been omitted from this report, a few cautionary comments concerning portions of the data are in order. For instance, the anomalous behavior of the pitching-moment curves for horizontal-tail deflections less than -10° in the angle-of-attack range between ±5° (for example, figs. 14, 18, and 22) is the result of submersion of the horizontal tail in the wing wake. (Compare figs. 17 and 18.) This phenomenon was previously reported in references 5 and 18. A few

tests at Reynolds numbers other than that reported herein indicated that this behavior of the pitching-moment curves is aggravated at lower Reynolds numbers and diminishes at higher Reynolds numbers.

The results for the configurations with speed brakes deflected are also affected to some extent by the Reynolds number level of the tests inasmuch as flow separation occurred over and ahead of the brake surfaces in the vicinity of the hinge line. In view of the length of fuselage or fairing surface ahead of the fuselage and fairing speed brakes, these configurations are affected to the greatest extent. Various boundary-layer gaps were tested with the fairing speed brakes J_F in an effort to offset the effects of flow separation.

For the remaining configurations with undeflected horizontal tails and speed brake closed, no significant effects of Reynolds number on the longitudinal, lateral, and directional stability and control characteristics were observed.

Langley Research Center,
National Aeronautics and Space Administration,
Langley Field, Va., September 22, 1959.

[redacted]

REFERENCES

1. Penland, Jim A., Ridyard, Herbert W., and Fetterman, David E., Jr.: Lift, Drag, and Static Longitudinal Stability Data From an Exploratory Investigation at a Mach Number of 6.86 of an Airplane Configuration Having a Wing of Trapezoidal Plan Form. NACA RM L54L03b, 1955.

2. Ridyard, Herbert W., Fetterman, David E., Jr., and Penland, Jim A.: Static Lateral Stability Data From an Exploratory Investigation at a Mach Number of 6.86 of an Airplane Configuration Having a Wing of Trapezoidal Plan Form. NACA RM L55A21a, 1955.

3. Dunning, Robert W., and Ulmann, Edward F.: Static Longitudinal and Lateral Stability Data From an Exploratory Investigation at Mach Number 4.06 of an Airplane Configuration Having a Wing of Trapezoidal Plan Form. NACA RM L55A21, 1955.

4. Dunning, Robert W., and Ulmann, Edward F.: Exploratory Investigation at Mach Number 4.06 of an Airplane Configuration Having a Wing of Trapezoidal Plan Form - Longitudinal and Lateral Control Characteristics. NACA RM L55B28, 1955.

5. Fetterman, David E., Jr., Penland, Jim A., and Ridyard, Herbert W.: Static Longitudinal and Lateral Stability and Control Data From an Exploratory Investigation at a Mach Number of 6.86 of an Airplane Configuration Having a Wing of Trapezoidal Plan Form. NACA RM L55C04, 1955.

6. Dunning, Robert W., and Ulmann, Edward F.: Exploratory Investigation at Mach Number 4.06 of an Airplane Configuration Having a Wing of Trapezoidal Plan Form - Effects of Various Tail Arrangements on Wing-On and Wing-Off Static Longitudinal and Lateral Stability Characteristics. NACA RM L55D08, 1955.

7. Penland, Jim A., Fetterman, David E., Jr., and Ridyard, Herbert W.: Static Longitudinal and Lateral Stability and Control Characteristics of an Airplane Configuration Having a Wing of Trapezoidal Plan Form With Various Tail Airfoil Sections and Tail Arrangements at a Mach Number of 6.86. NACA RM L55F17, 1955.

8. Osborne, Robert S.: Aerodynamic Characteristics of a 0.0667-Scale Model of the North American X-15 Research Airplane at Transonic Speeds. NASA TM X-24, 1959.

9. Leupold, Mathias J., and Freeman, Elizabeth M.: Supersonic Force Tests for Stabilizer-Control Effectiveness on the Full-Span Model X-15 for North American Aviation, Inc. Wind Tunnel Rep. 164, Naval Supersonic Lab., M.I.T., Oct. 1957.

10. Leupold, Mathias J., and Freeman, Elizabeth M.: A Second Series of Supersonic Force Tests on the Full-Span Model X-15 for North American Aviation, Incorporated. Wind Tunnel Rep. 200, Naval Supersonic Lab., M.I.T., Sept. 1958.

11. Leupold, Mathias J., and Freeman, Elizabeth M.: A Third Series of Supersonic Force Tests on the Full-Span Model X-15 for North American Aviation, Incorporated. Wind Tunnel Rep. 228, Naval Supersonic Lab., M.I.T., Nov. 1958.

12. Leupold, Mathias J., and Freeman, Elizabeth M.: A Fourth Series of Supersonic Force Tests on the Full-Span Model X-15 for North American Aviation, Incorporated. Wind Tunnel Rep. 239, Naval Supersonic Lab., M.I.T., Dec. 1958.

13. Franklin, Arthur E., and Silvers, H. Norman: Investigation of the Aerodynamic Characteristics of a 0.067-Scale Model of the X-15 Airplane (Configuration 2) at Mach Numbers of 2.29, 2.98, 3.96, and 4.65. NASA MEMO 4-27-59L, 1959.

14. Boisseau, Peter C.: Investigation of the Low-Speed Stability and Control Characteristics of a 1/7-Scale Model of the North American X-15 Airplane. NACA RM L57D09, 1957.

15. Lopez, Armando E., and Tinling, Bruce E.: The Static and Dynamic-Rotary Stability Derivatives at Subsonic Speeds of a Model of the X-15 Research Airplane. NACA RM A58F09, 1958.

16. Tunnell, Phillips J., and Latham, Eldon A.: The Static and Dynamic-Rotary Stability Derivatives of a Model of the X-15 Research Airplane at Mach Numbers From 1.55 to 3.50. NASA MEMO 12-23-58A, 1959.

17. McLellan, Charles H., Williams, Thomas W., and Beckwith, Ivan E.: Investigation of the Flow Through a Single-Stage Two-Dimensional Nozzle in the Langley 11-Inch Hypersonic Tunnel. NACA TN 2223, 1950.

18. Ulmann, Edward F., and Ridyard, Herbert W.: Flow-Field Effects on Static Stability and Control at High Supersonic Mach Numbers. NACA RM L55L19a, 1956.

TABLE I.- GEOMETRIC CHARACTERISTICS OF CONFIGURATION 1

(0.02-SCALE MODEL OF X-15 AIRPLANE)

Wing:	
Area, total, sq in.	11.520
Area, exposed, sq in.	6.080
Span, in.	5.366
Aspect ratio	2.5
Root chord, in.	3.578
Root chord, exposed, in.	2.645
Tip chord, in.	0.716
Mean aerodynamic chord, exposed, in.	2.465
Sweepback angles, deg:	
Leading edge	36.75
25-percent element	25.64
Trailing edge	-17.74
Taper ratio	0.2
Dihedral angle, deg	0
Incidence angle, deg	0
Airfoil section, parallel to fuselage center line	NACA 66-005 (modified)
Horizontal tail:	
Area, exposed, sq in.	2.878
Semispan (panel span), in.	1.330
Aspect ratio, per exposed panel	1.229
Taper ratio	0.328
Root chord, exposed, in.	1.658
Tip chord, in.	0.506
Mean aerodynamic chord, exposed, in.	1.184
Sweepback angles, deg:	
Leading edge	50.58
25-percent element	45
Trailing edge	19.28
Dihedral, deg	-15
Airfoil section, parallel to fuselage center line	NACA 66-005 (modified)
Fuselage:	
Length, in.	11.76
Maximum diameter	1.060
Maximum width, including side fairings	1.750
Fineness ratio	11.100
Base diameter	0.960
Upper vertical tail:	
Area, exposed, sq in.	2.294
Span, exposed, in.	1.700
Aspect ratio	1.260
Taper ratio	0.277
Root chord, in.	2.112
Tip chord, in.	0.586
Mean aerodynamic chord, exposed, in.	1.493
Sweepback angles, deg:	
Leading edge	32.17
Trailing edge	-15.08

Lower vertical tails:

	V_L	V_{L2}	V_{L3}
Area, exposed, sq in.	0.775	1.740	1.506
Span, exposed, in.	0.480	0.975	0.860
Aspect ratio	0.297	0.546	0.491
Taper ratio	0.612	0.455	0.705
Root chord, in.	2.147	2.635	2.128
Tip chord, in.	1.315	1.200	1.500
Mean aerodynamic chord, in.	1.765	2.007	1.833
Sweepback angles, deg:			
Leading edge	60	59.66	38.13
Trailing edge	0	0	0

TABLE II.- GEOMETRIC CHARACTERISTICS OF CONFIGURATION 2

(0.02-SCALE MODEL OF X-15 AIRPLANE)

Wing:	
Area, total, sq in.	11.520
Area, exposed, sq in.	6.050
Span, in.	5.366
Aspect ratio	2.5
Root chord, in.	3.578
Root chord, exposed, in.	2.640
Tip chord, exposed, in.	0.716
Mean aerodynamic chord, exposed, in.	2.465
Sweepback angles, deg:	
Leading edge	36.75
25-percent element	25.64
Trailing edge	-17.74
Taper ratio	0.2
Dihedral angle, deg	0
Incidence angle, deg	0
Airfoil section, parallel to fuselage center line	NACA 66-005 (modified)
Horizontal tail:	
Area, exposed, sq in.	2.878
Semispan (panel span), in.	1.330
Aspect ratio, per exposed panel	1.229
Taper ratio	0.328
Root chord, exposed, in.	1.658
Tip chord, in.	0.506
Mean aerodynamic chord, exposed, in.	1.184
Sweepback angles, deg:	
Leading edge	50.58
25-percent element	45.00
Trailing edge	19.28
Dihedral, deg	-15
Airfoil section, parallel to fuselage center line	NACA 66-005 (modified)
Fuselage:	
Length, in.	11.76
Maximum diameter, in.	1.12
Maximum width, including side fairings	1.76
Fineness ratio	10.50
Base diameter	0.960

Upper vertical tails:

	V_{U2}	V_{U3}	V_{U4}
Area, exposed, sq in.	2.272	1.135	2.280
Span, exposed, in.	1.700	1.202	1.000
Aspect ratio	1.272	1.273	0.438
Taper ratio	0.266	0.266	0.774
Root chord, in.	2.112	1.493	2.570
Tip chord, in.	0.561	0.397	1.990
Mean aerodynamic chord, exposed, in.	1.487	1.051	2.292
Sweepback angles, deg:			
Leading edge	32.7	32.67	30
Trailing edge	-15.08	-15.04	0

Lower vertical tails:

	V_{L2}	V_{L3}	V_{L4}
Area, exposed, sq in.	0.775	0.7632	2.237
Span, exposed, in.	0.480	0.720	1.00
Aspect ratio	0.297	0.679	0.4470
Taper ratio	0.612	0.536	0.774
Root chord, in.	2.147	1.380	2.570
Tip chord, in.	1.315	0.740	1.990
Mean aerodynamic chord, in.	1.765	1.091	2.292
Sweepback angles, deg:			
Leading edge	60	32.66	30.1
Trailing edge	0	-13.89	0

TABLE III.- ORDINATES OF MODIFIED NACA 66-005 AIRFOIL SECTION FOR WING CONFIGURATIONS W AND W_2[a]

x, percent c	y_r, percent c (b)	y_t, percent c
0	0	0
1.25	.358	1.048
2.5	.533	1.123
5.0	.854	1.263
7.5	1.137	1.395
10	1.382	1.523
15	1.759	1.769
20	2.001	2.001
25	2.182	2.182
30	2.318	2.318
35	2.416	2.416
40	2.476	2.476
45	2.500	2.500
50	2.485	2.485
55	2.432	2.432
60	2.332	2.332
65	2.151	2.151
67	2.085	2.085
100	.500	.500

[a]Basic airfoil modified for linear taper between root and tip forward of 17-percent-chord station. Basic airfoil modified to straight side rearward of 67-percent-chord station to 1-percent-chord blunt trailing edge.

Leading-edge radius, in., for -			
Configuration W		Configuration W_2	
Root	Tip	Root	Tip
0.004	0.001	0.015	0.008

[b]Exposed root chord.

TABLE IV.- ORDINATES OF MODIFIED NACA 66-005 AIRFOIL SECTION FOR HORIZONTAL-TAIL CONFIGURATIONS H AND H_3[a]

x, percent c	y_r, percent c (b)	y_t, percent c
0	0	0
.1	.269	.348
.25	.408	.538
.5	.531	.728
.75	.590	.846
1.25	.650	.969
2.50	.791	1.052
5.00	1.048	1.206
7.5	1.268	1.353
10	1.458	1.495
15	1.765	1.768
20	2.001	2.001
25	2.182	2.182
30	2.318	2.318
35	2.416	2.416
40	2.476	2.476
45	2.500	2.500
50	2.485	2.485
55	2.432	2.432
60	2.332	2.332
75	1.653	1.653
90	.961	.961
100	.500	.500

[a]Basic airfoil section modified to straight side rearward of 67-percent-chord station to 1-percent-chord blunt trailing edge. Basic airfoil modified for linear taper between root and tip forward of 5-percent-chord station at root and 15-percent-chord station at tip.

Leading-edge radius, in., for -			
Configuration H		Configuration H_3	
Root	Tip	Root	Tip
0.003	0.001	0.010	0.005

[b]Exposed root chord.

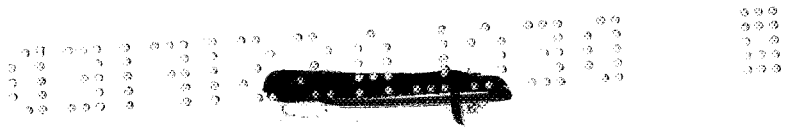

TABLE V.- INDEX OF DATA FIGURES

(a) Configuration 1

Effect of -	Configuration	Speed-brake deflection, deg		Figure for -	
		δ_{J_U}	δ_{J_L}	C_L, C_D, C_m	C_{Y_β}, C_{n_β}, C_{l_β}
Component parts of configuration 1	B	---	---	10	28
	BX	---	---		
	BW	---	---		
	BWX	---	---		
	BWXH	---	---		
	$BWXHV_U$	0	---		
	$BWXHV_L$	---	0		
	$BWXHV_UV_L$	0	0		
Speed-brake components	$BWXHV_UV_L$	0	0	11	29
	$BWXHV_UV_LJ_U$	45	0		
	$BWXHV_UV_LJ_L$	0	45		
	$BWXHV_UV_LJ_UJ_L$	45	45		
Wing dihedral	$BWXHV_UV_L$	0	0	12	30
Lower vertical-tail modifications	$BWXHV_UV_L$	0	0	13	31
	$BWXHV_UV_{L2}$	0	0		
	$BWXHV_UV_{L3}$	0	0		
Horizontal-tail deflection, location, and dihedral	$BWXHV_UV_L$	0	0	14	32
	$BWXH_6V_UV_L$	0	0		
	$BWXH_7V_UV_L$	0	0		
	$BWXH_8V_UV_L$	0	0		
Fuselage fairing modifications	BX	---	---	15	
	BX_{1A}	---	---		
	BX_{1B}	---	---		
	B_2X_2	---	---		

TABLE V.- INDEX OF DATA FIGURES - Continued

(b) Configuration 2

Effect of -	Configuration	Speed-brake deflection, deg		Figure for -	
		δ_{J_U}	δ_{J_L}	C_L, C_D, C_m	C_{Y_β}, C_{n_β}, C_{l_β}
Component parts of configuration 2	B_2X_3	---	---	16	33
	$B_2X_3H_3$	---	---		
	$B_2W_2X_3H_3$	---	---		
	$B_2W_2X_3H_3V_{U2}V_L$	0	0		
	$B_2W_2X_3H_3V_{U2}V_LJ_UJ_L$	5	7.5	---	
Horizontal-tail deflection (wing off)	$B_2X_3H_3V_{U2}V_LJ_UJ_L$	20	20	17	
Horizontal-tail deflection (wing on)	$B_2W_2X_3H_3V_{U2}V_LJ_UJ_L$	5	7.5	18	
	$B_2W_2X_3H_3V_{U2}V_LJ_UJ_L$	20	20		
	$B_2W_2X_3H_3V_{U2}V_LJ_UJ_L$	45	45		
Speed-brake components	$B_2W_2X_3H_3V_{U2}V_L$	0	0	19	34
	$B_2W_2X_3H_3V_{U2}V_LJ_L$	0	45		
	$B_2W_2X_3H_3V_{U2}V_LJ_UJ_L$	45	45		
Sideslip	$B_2W_2X_3H_3V_{U2}V_L$	0	0	20	
	$B_2W_2X_3H_3V_{U2}V_LJ_UJ_L$	20	20		
	$B_2W_2X_3H_3V_{U2}V_LJ_UJ_L$	45	45		
Differential horizontal-tail deflection	$B_2W_2X_3H_3V_{U2}V_LJ_UJ_L$	20	20	21	
Horizontal-tail deflection	$B_2W_2X_3H_2V_{U2}V_LJ_UJ_L$	20	20	22	
Fuselage conical speed brakes, J_{B2}	$B_2W_2X_3H_3V_{U2}V_L$	0	0	23	35
	$B_2W_2X_3H_3V_{U2}V_LJ_{B2}$; $\delta_{J_{B2}} = 20°$	0	0		
Vertical-tail components, V_{U3}, V_{L4}	$B_2W_2X_3H_3$	---	---	24	36
	$B_2W_2X_3H_3V_{L4}$	0	0		
	$B_2W_2X_3H_3V_{U3}V_{L4}$	0	0		
Fuselage conical speed brakes, J_{B1}	$B_2W_2X_3H_3V_{U3}V_{L4}$	0	0	25	37
	$B_2W_2X_3H_3V_{U3}V_{L4}J_{B1}$; $\delta_{J_{B1}} = 20°$	0	0		
	$B_2W_2X_3H_3V_{U3}V_{L4}J_{B1}$; $\delta_{J_{B1}} = 45°$	0	0		
Vertical-tail components, V_{U4}, V_{L5}	$B_2W_2X_3H_3V_{U4}J_{U1}$	0, 20, 45	0	26	38
	$B_2W_2X_3H_3V_{L5}J_{L1}$	0	0, 20, 45		
	$B_2W_2X_3H_3V_{U4}V_{L5}J_{U1}J_{L1}$	0, 20, 45	0, 20, 45		
	$B_2W_2X_3H_3$	---	---		
	$B_2W_2X_3V_{U4}V_{L5}J_{U1}J_{L1}$	45	45		
Boundary-layer gap and speed-brake deflections J_F	$B_2W_2X_3H_3V_{U4}V_{L5}J_F$; $\delta_{J_F} = 40°$	0	0	27	39
	$B_2W_2X_3H_3V_{U4}V_{L5}J_F$; $\delta_{J_F} = 75°$	0	0		

TABLE V.- INDEX OF DATA FIGURES - Concluded

(b) Configuration 2 - Concluded

Effects of -	Configuration	Speed-brake deflection, deg		Figure for -					
		δ_{J_U}	δ_{J_L}	$C_{Y_{\delta_V}}$, $C_{n_{\delta_V}}$, $C_{l_{\delta_V}}$			$C_{Y_{\delta_h}}$', $C_{n_{\delta_h}}$', $C_{l_{\delta_h}}$'		
Speed-brake deflection	$B_2W_2X_3H_3V_{U2}V_LJ_UJ_L$	5	7.5	40			43		
	$B_2W_2X_3H_3V_{U2}V_LJ_UJ_L$	20	20						
	$B_2W_2X_3H_3V_{U2}V_LJ_UJ_L$	45	45						
Equivalent horizontal-tail pitch deflection	$B_2W_2X_3H_3V_{U2}V_LJ_UJ_L$	20	20				44		
Speed-brake deflection	$B_2W_2X_3H_3V_{U4}V_{L5}J_{U1}J_{L1}$	0	0	41			45		
	$B_2W_2X_3H_3V_{U4}V_{L5}J_{U1}J_{L1}$	20	20				---		
	$B_2W_2X_3H_3V_{U4}V_{L5}J_{U1}J_{L1}$	45	45				45		
Vertical-tail component deflection	$B_2W_2X_3H_3V_{U4}V_{L5}J_{U1}J_{L1}$	45	45	42					

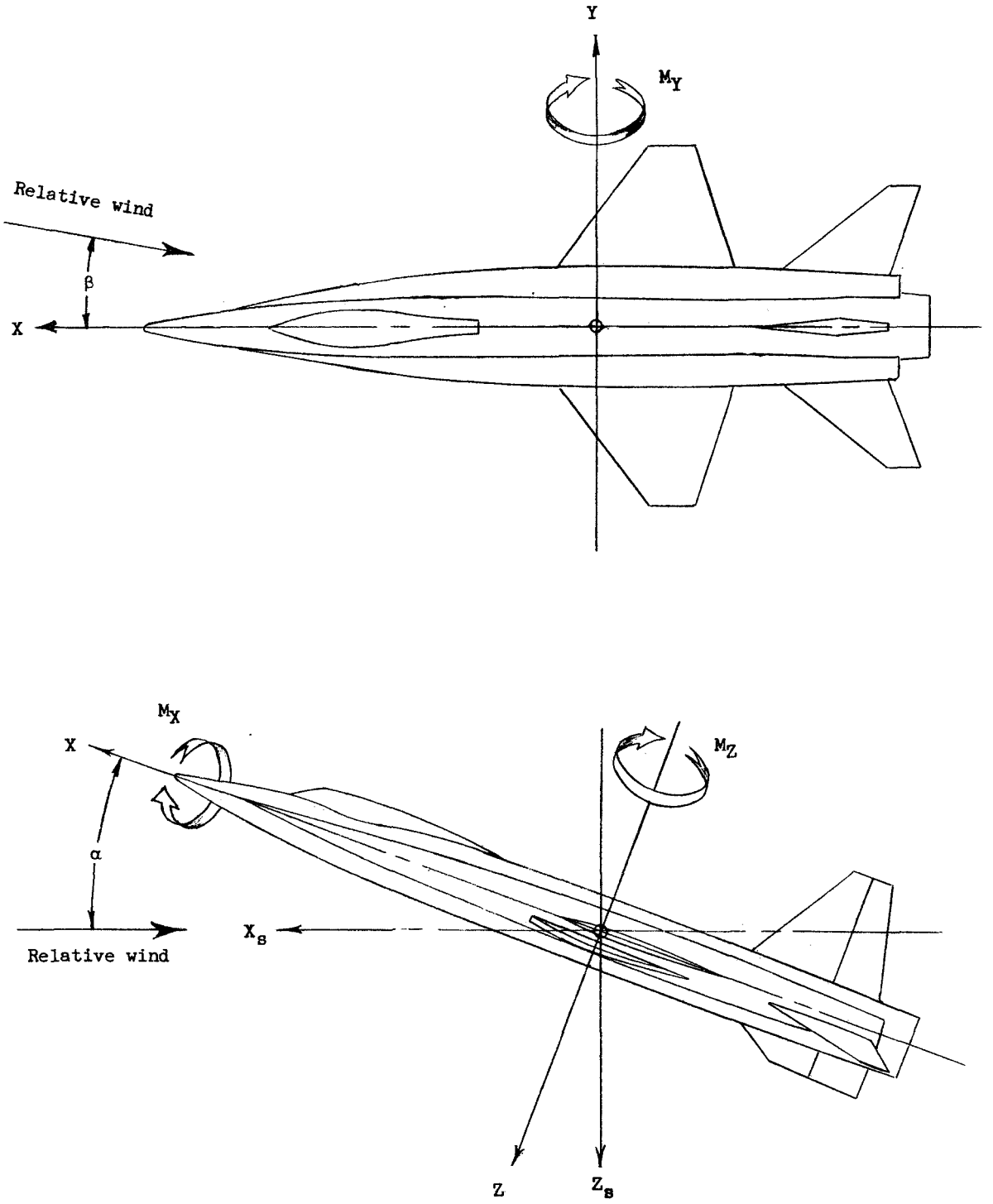

Figure 1.- Axis system.

L-740

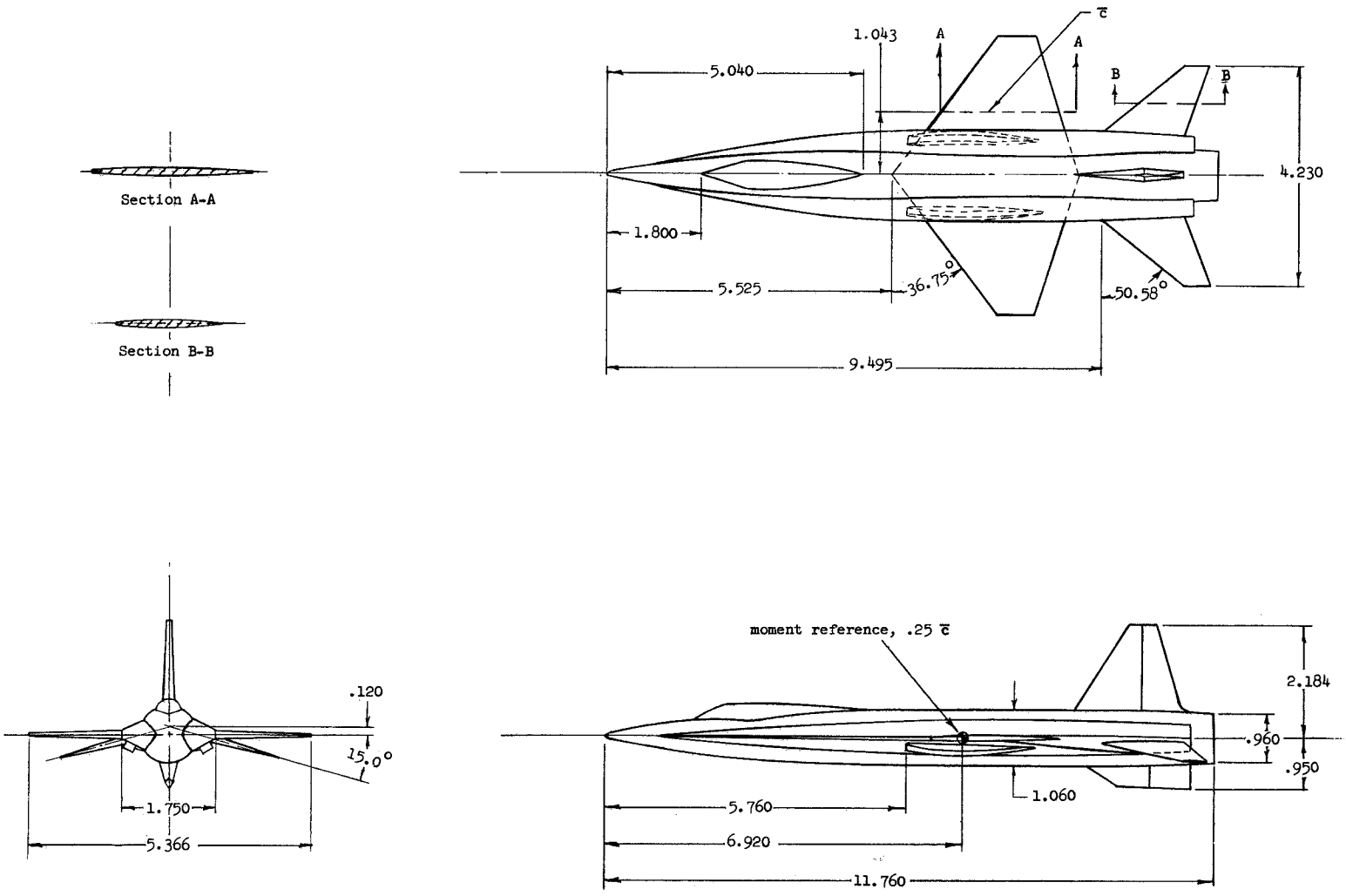

Figure 2.- Details of configuration 1, $BWXHV_UV_L$. All dimensions are in inches unless otherwise indicated.

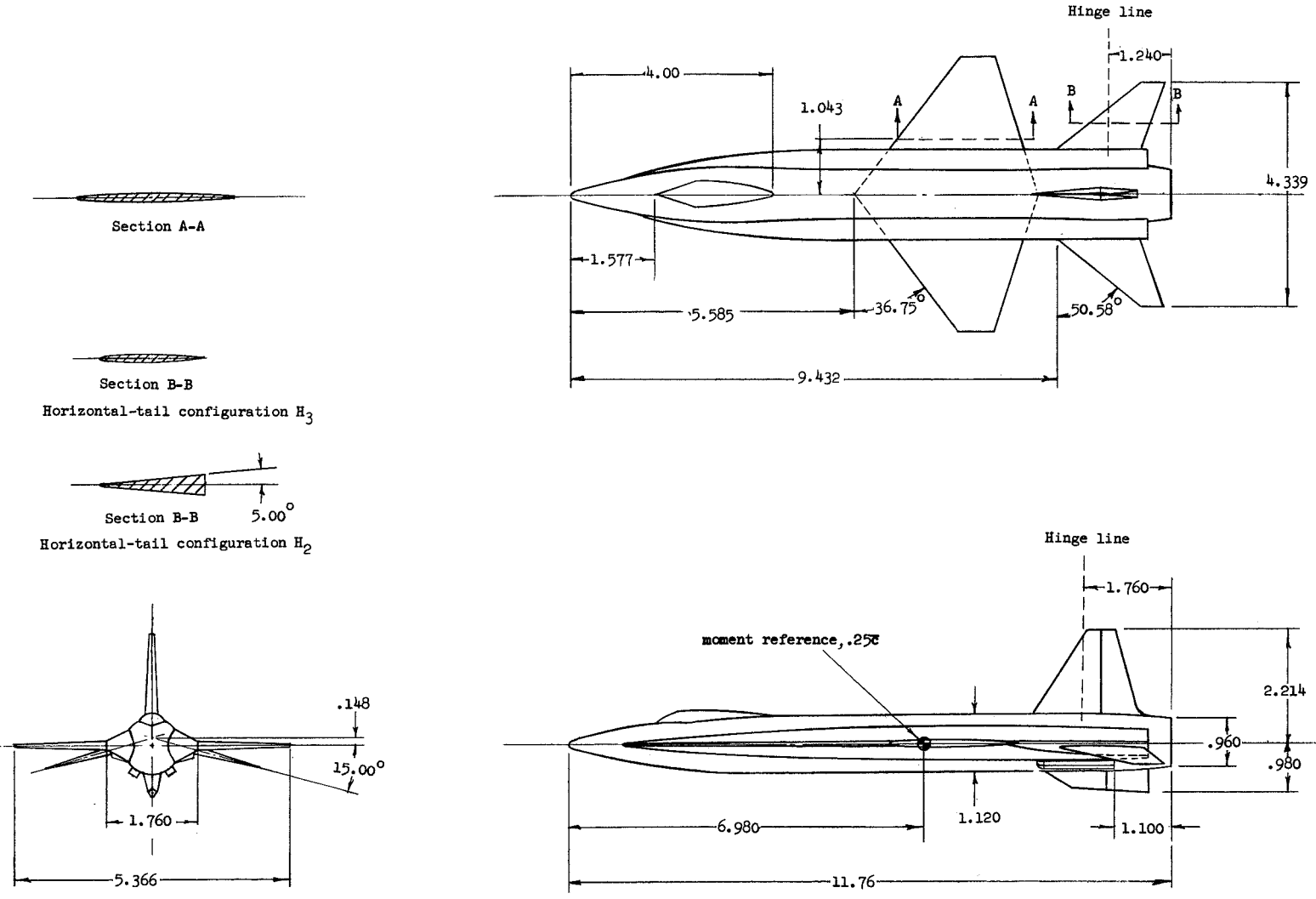

Figure 3.- Details of configuration 2, $B_2W_2X_3H_3V_{U2}V_L$. All dimensions are in inches unless otherwise indicated.

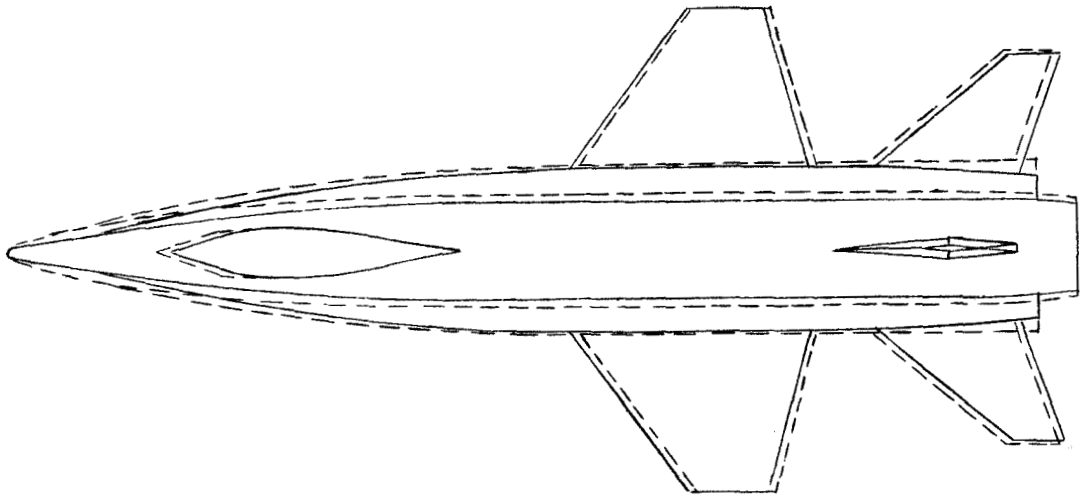

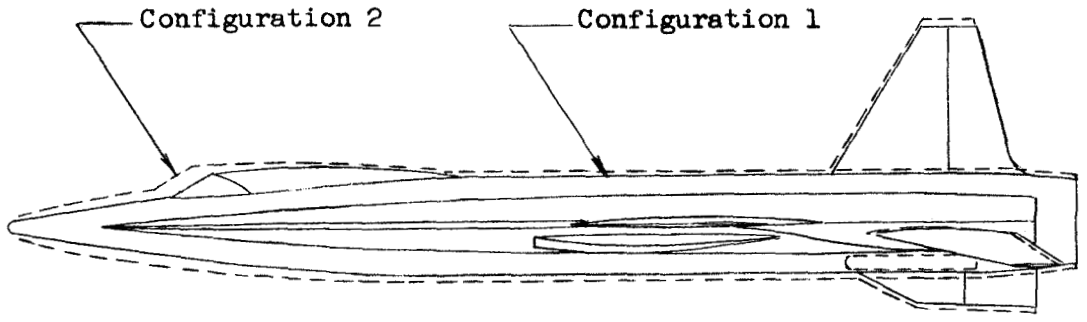

Figure 4.- Comparison of configurations 1 and 2.

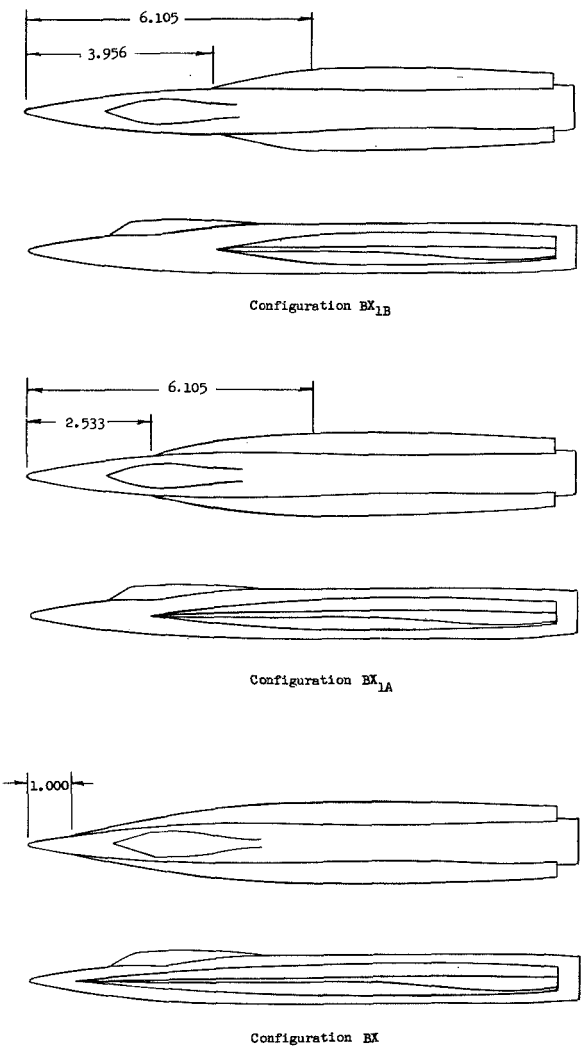

Figure 5.- Details of fuselage-fairing modifications to configuration 1. All dimensions are in inches.

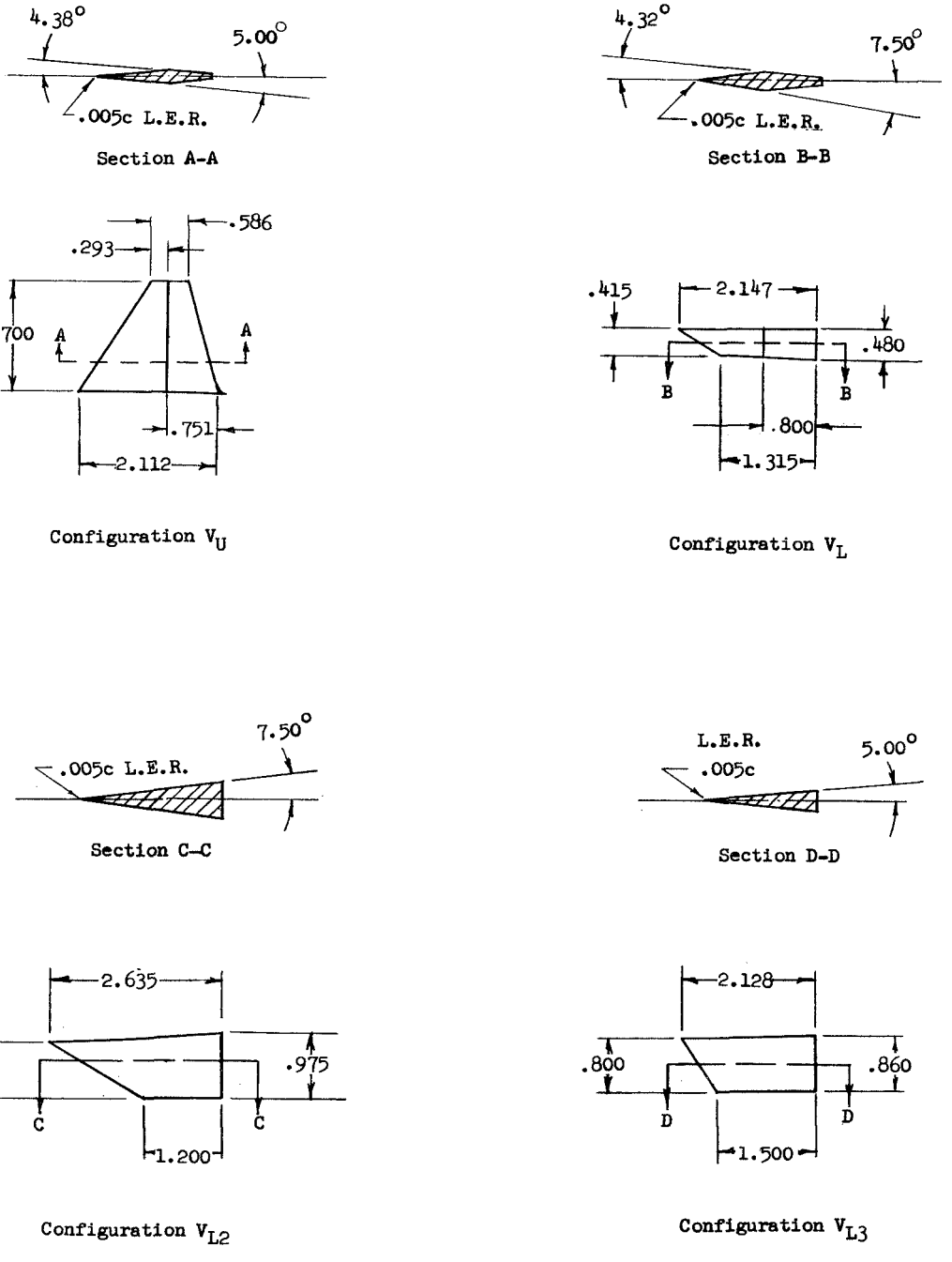

(a) Details of vertical-tail configurations.

Figure 6.- Vertical-tail modifications tested on configuration 1. All dimensions are in inches unless otherwise noted.

L-740

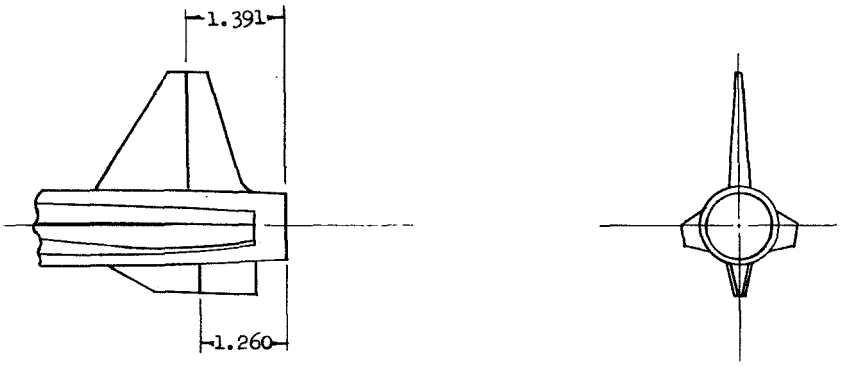

V_U V_L combination

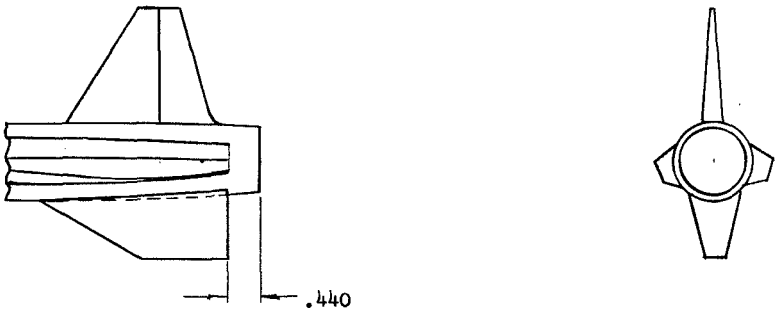

$V_U V_{L2}$ combination

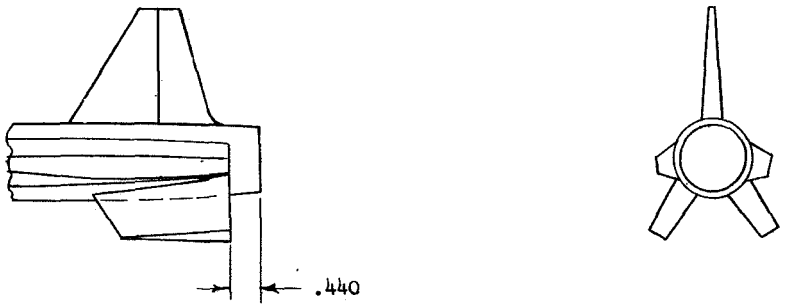

V_U V_{L3} combination

(b) Vertical-tail arrangements.

Figure 6.- Concluded.

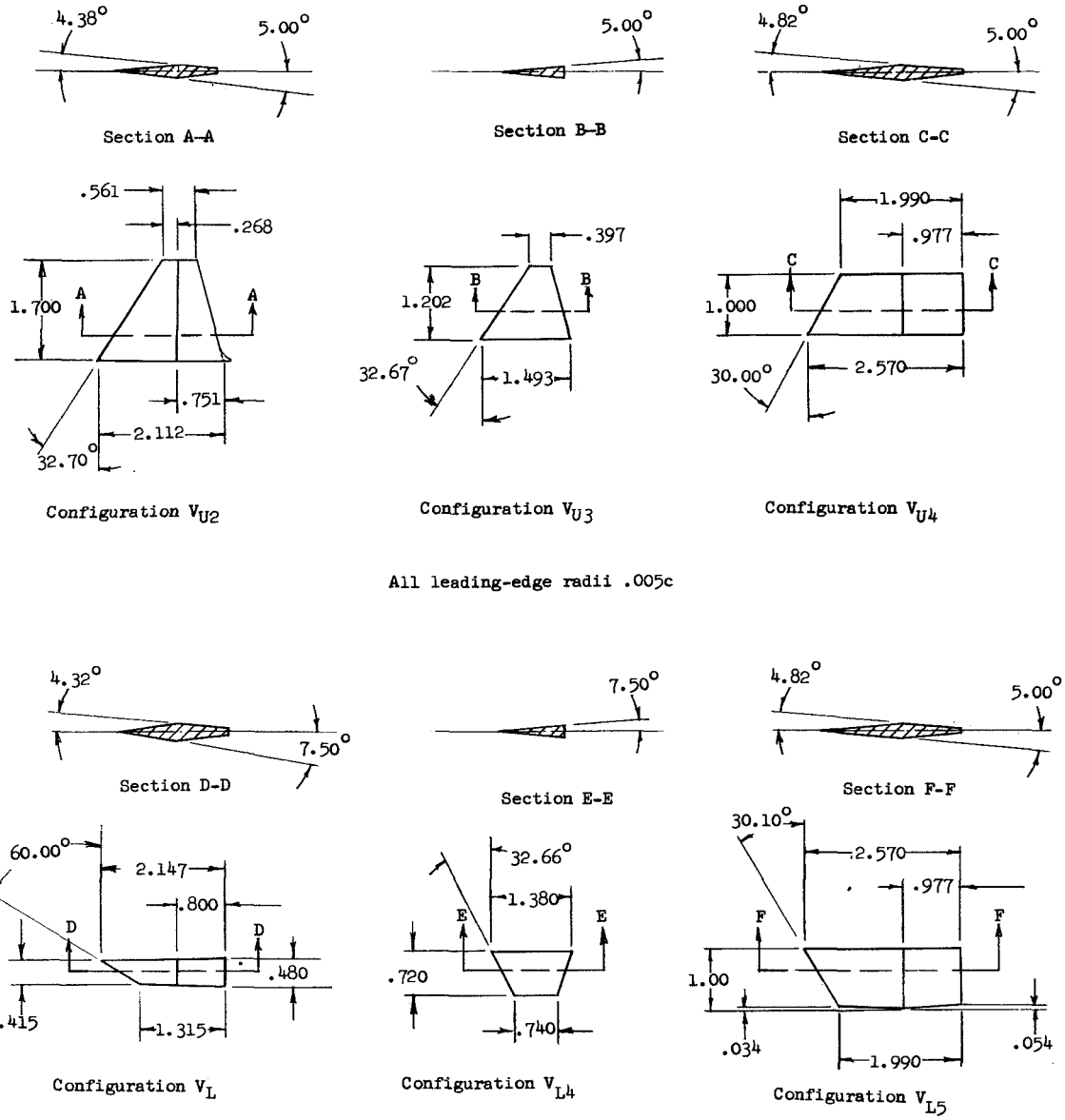

(a) Details of vertical-tail configurations.

Figure 7.- Vertical-tail modifications tested on configuration 2. All dimensions are in inches unless otherwise indicated.

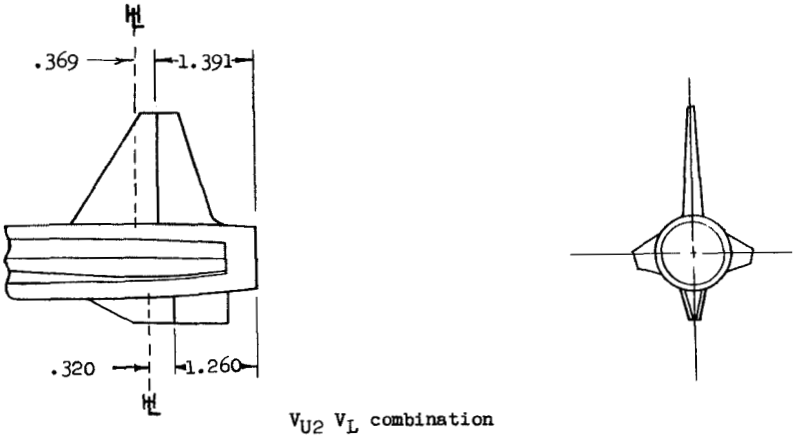

V_{U2} V_L combination

V_{U3} V_{L4} combination

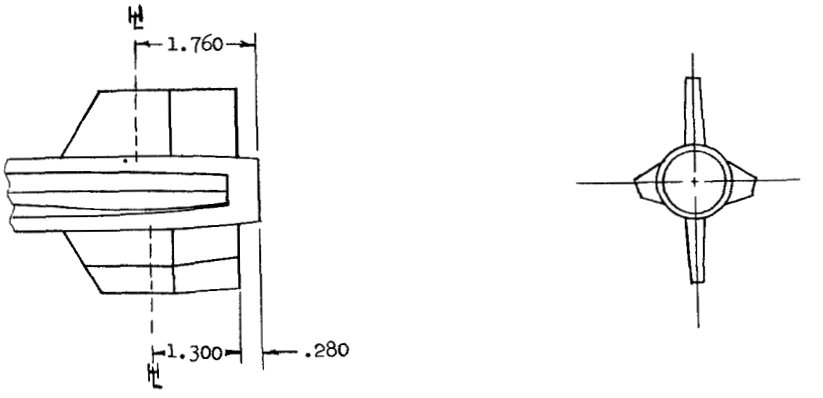

V_{U4} V_{L5} combination

(b) Vertical-tail arrangements.

Figure 7.- Concluded.

L-740

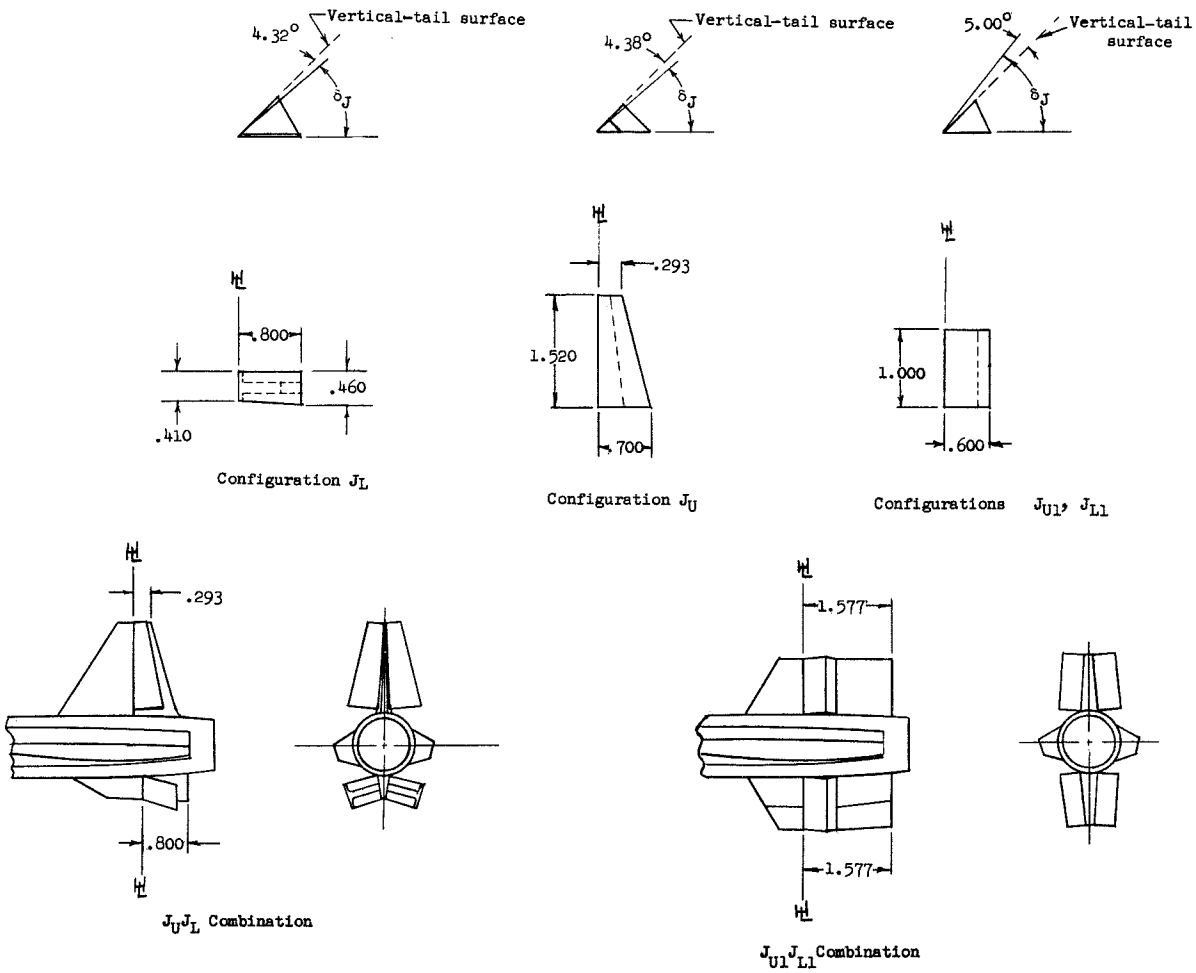

(a) Vertical-tail speed brakes.

Figure 8.- Details of speed-brake configurations. All dimensions are in inches unless otherwise indicated.

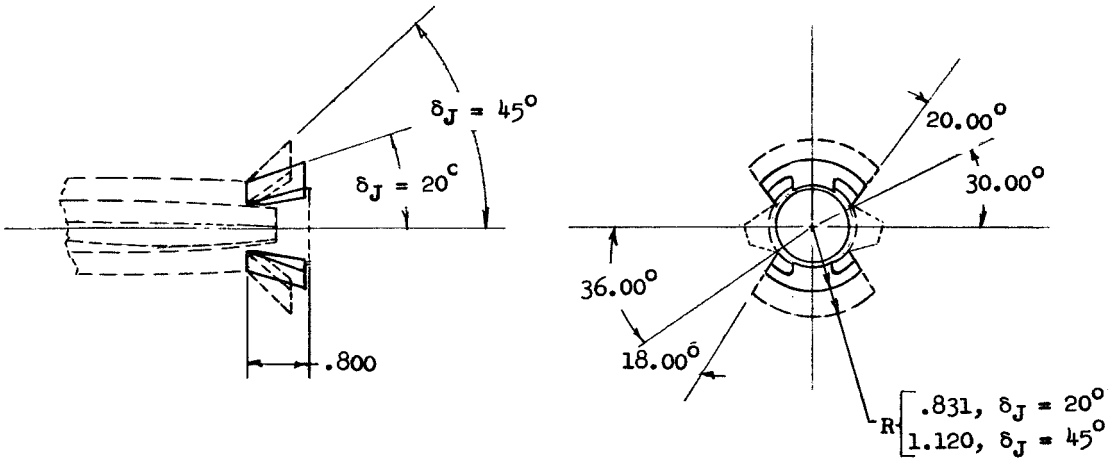

Configuration J_{B1}

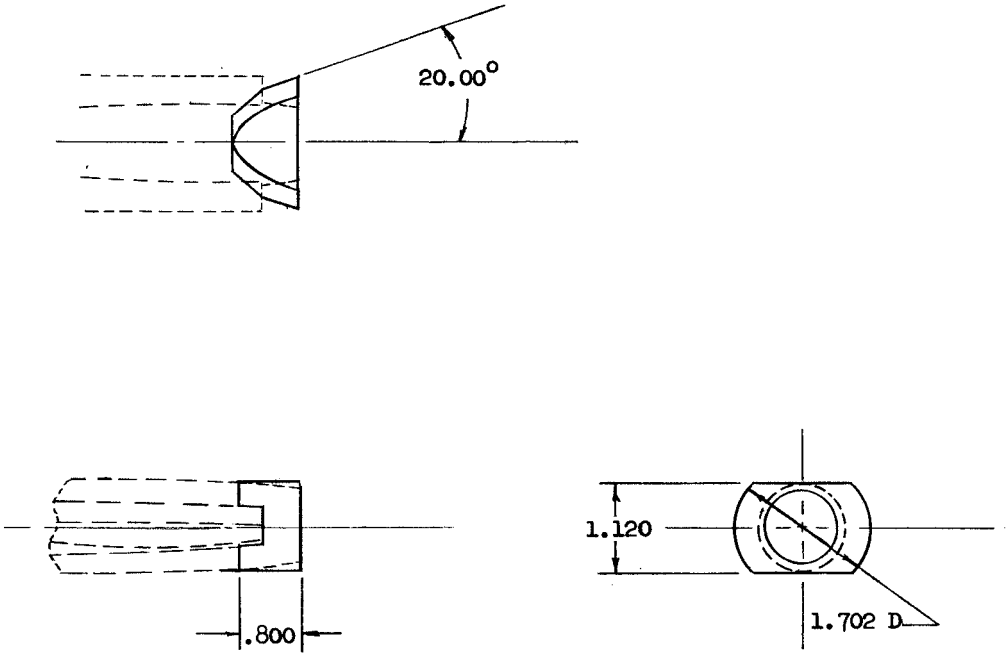

Configuration J_{B2}

(b) Fuselage speed brakes.

Figure 8.- Continued.

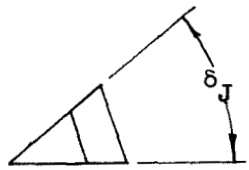

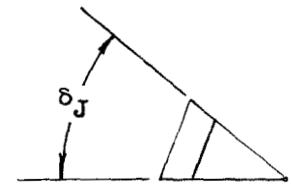

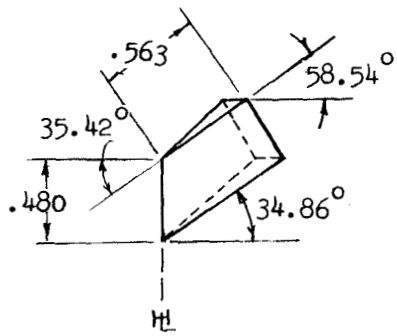

Configuration J_{FU}

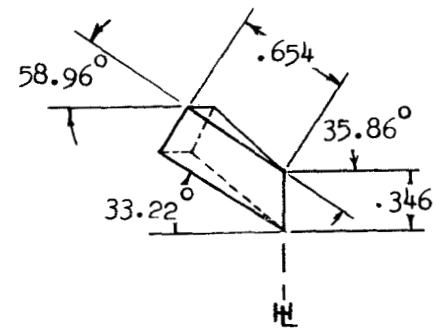

Configuration J_{FL}

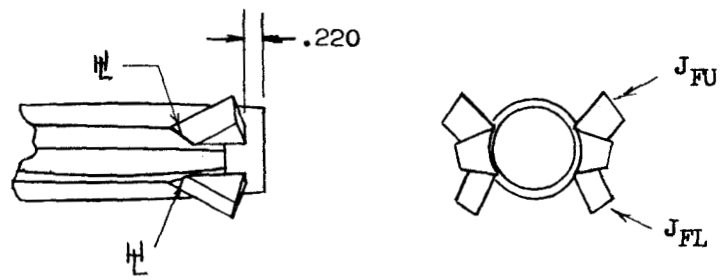

J_{FU} J_{FL} combination

(c) Fairing speed brakes.

Figure 8.- Concluded.

L-740

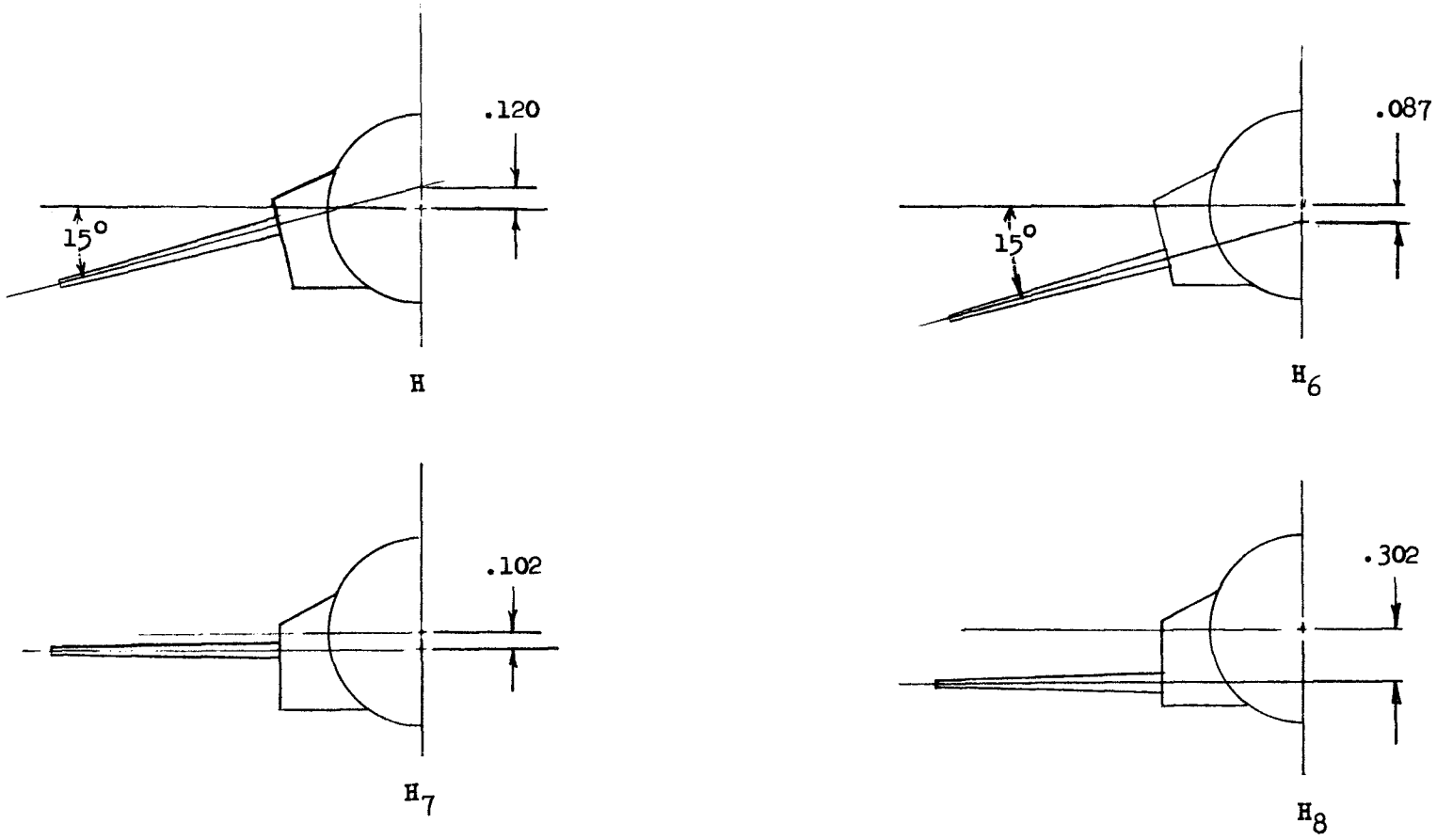

Figure 9.- Horizontal-tail modifications tested on configuration 1. Dimensions are in inches unless otherwise noted.

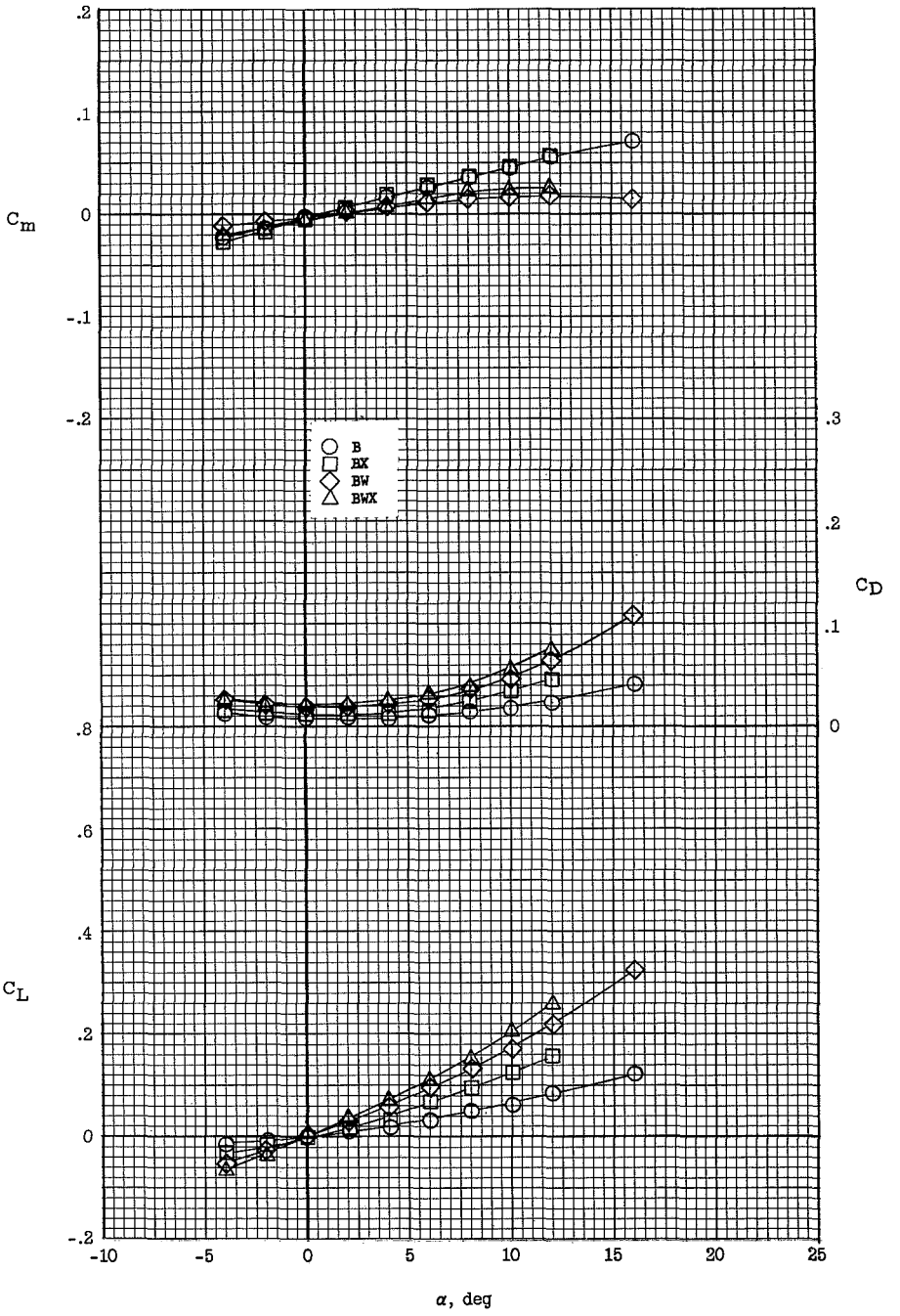

(a) Body, wing, and side fairing.

Figure 10.- Effect of component parts on the longitudinal stability characteristics of configuration 1. M = 6.83.

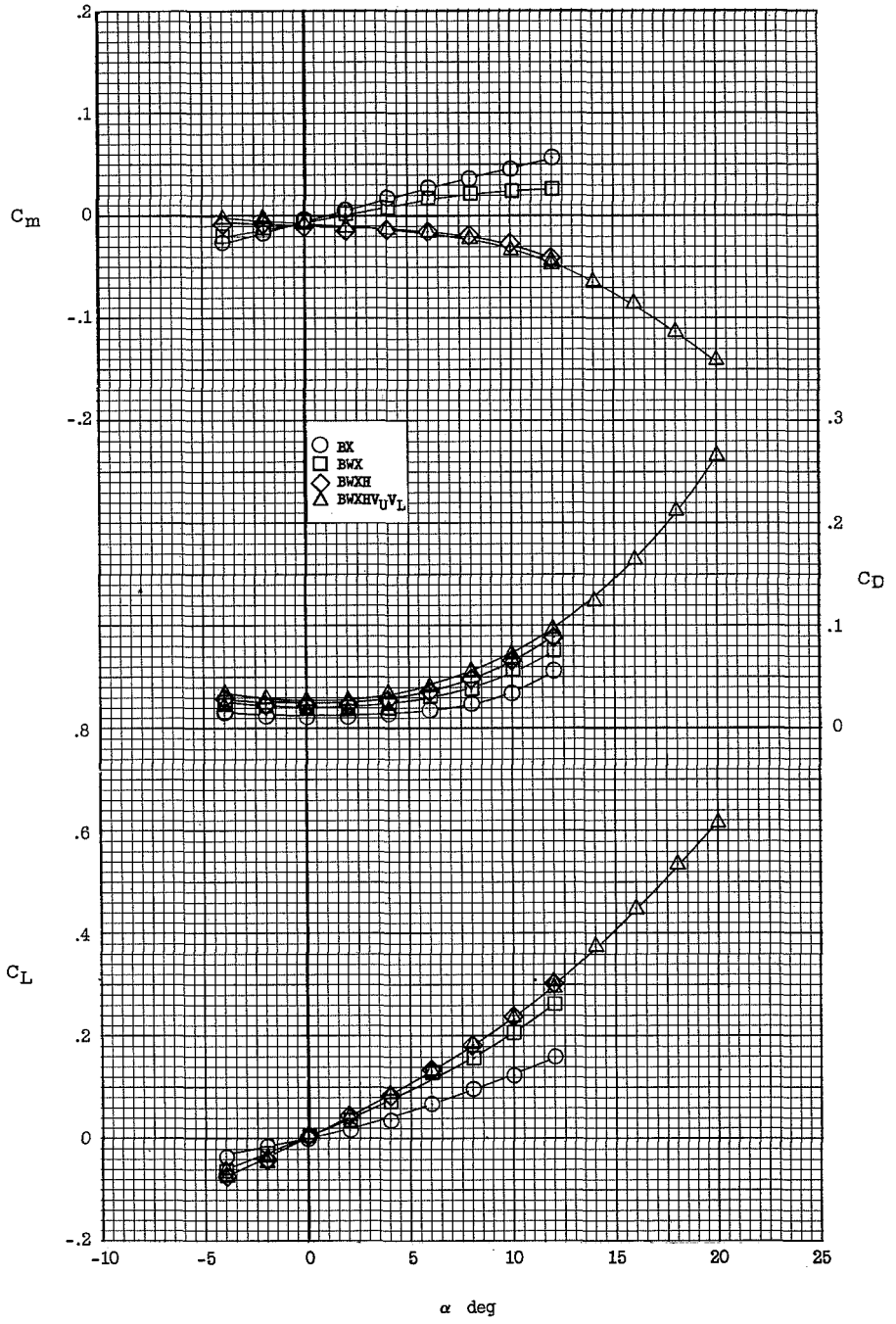

(b) Wing, horizontal tail, and vertical tails.

Figure 10.- Continued.

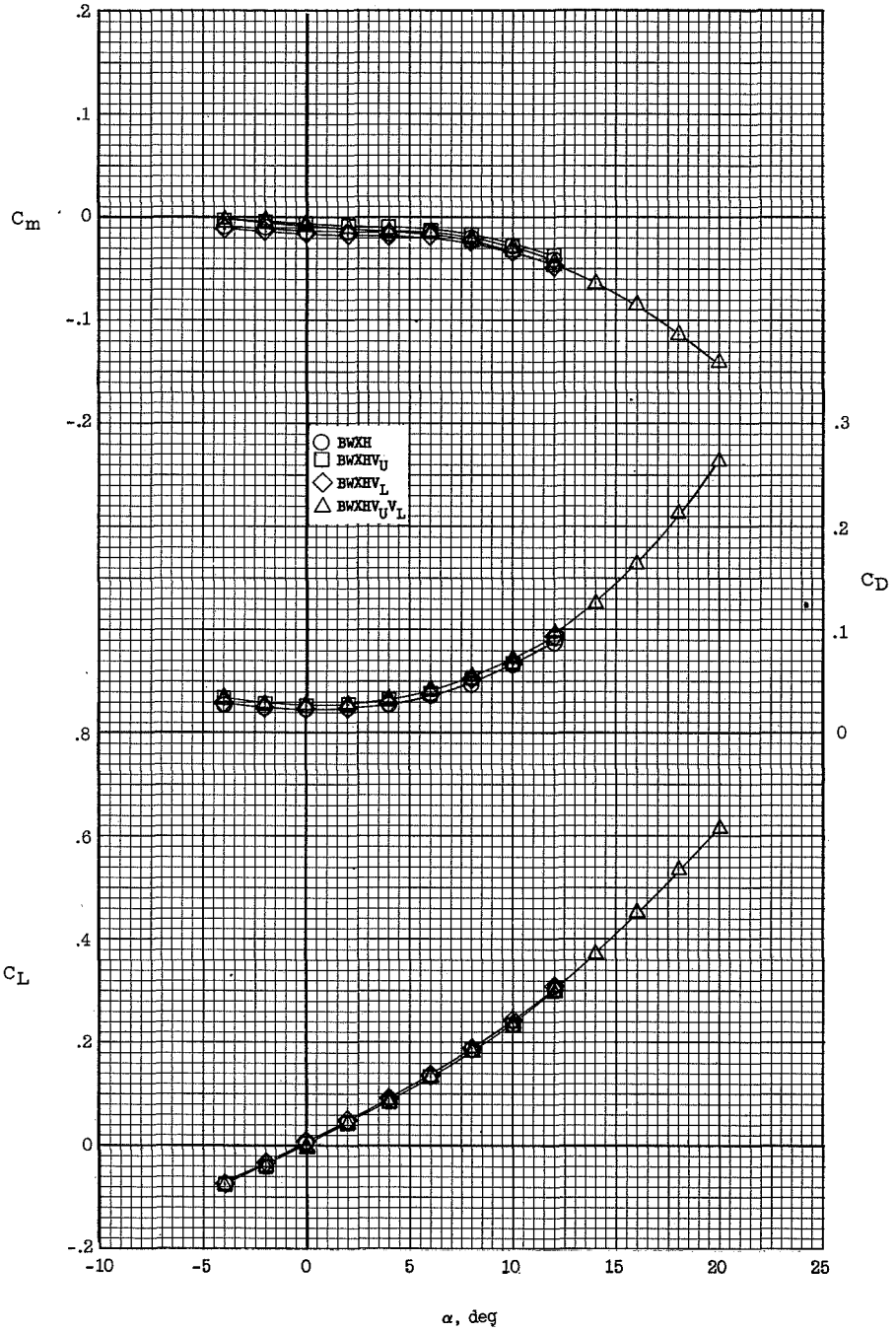

(c) Upper and lower vertical tails.

Figure 10.- Concluded.

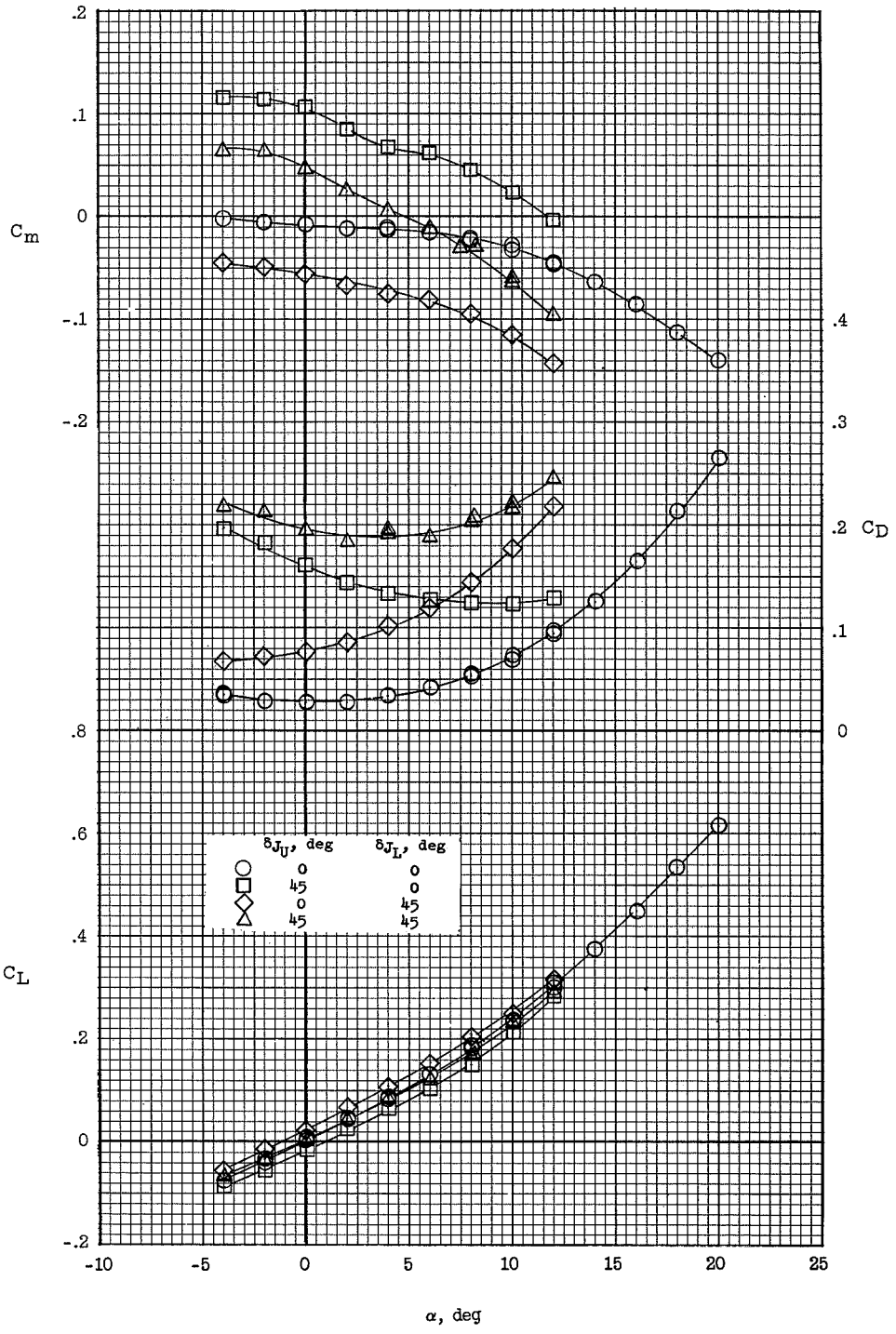

Figure 11.- Effect of speed-brake components on the longitudinal stability characteristics of configuration $BWXHV_UV_L$. M = 6.83.

L-7140

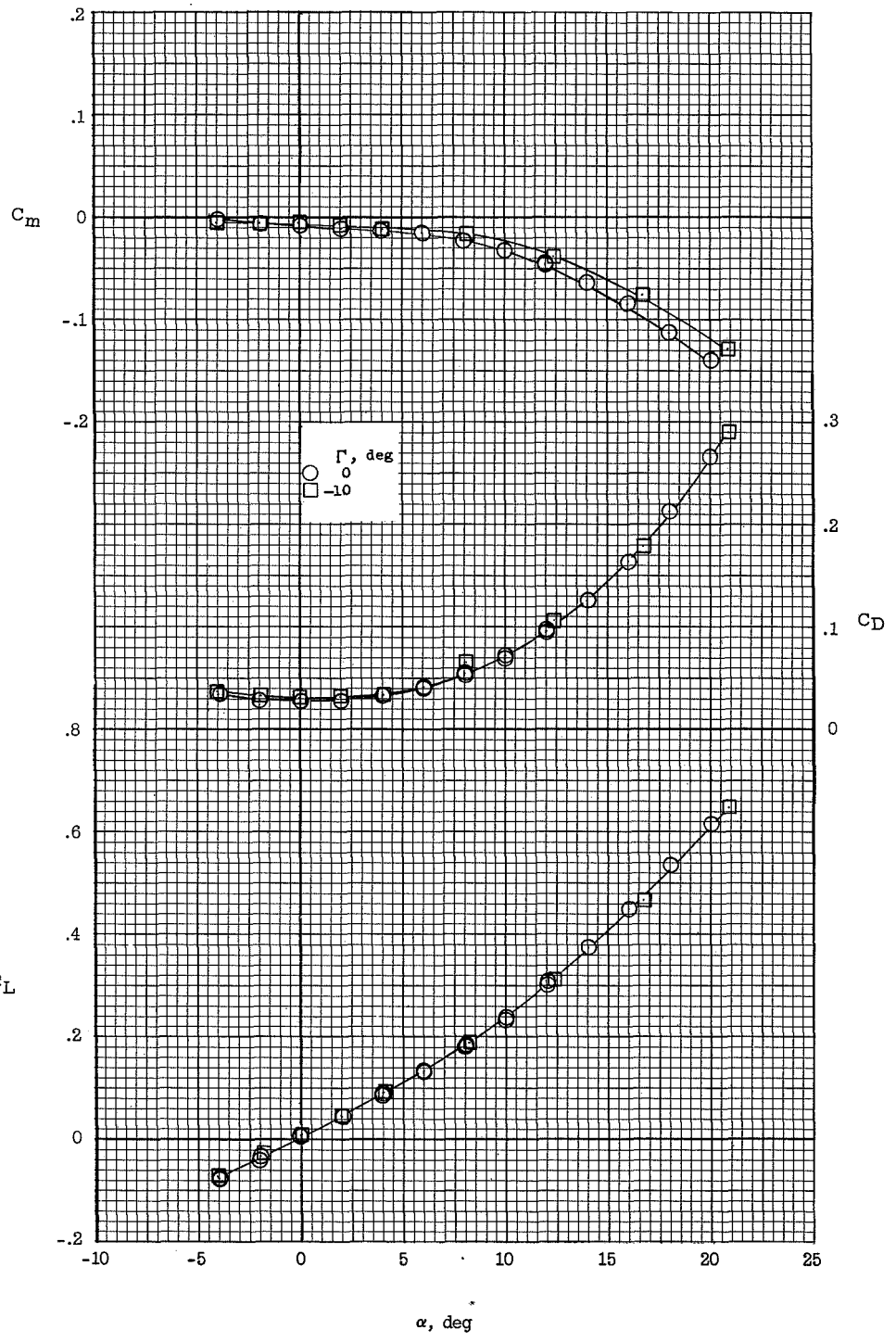

Figure 12.- Effect of wing dihedral on the longitudinal stability characteristics of configuration $BWXHV_UV_LJ_UJ_L$. M = 6.83.

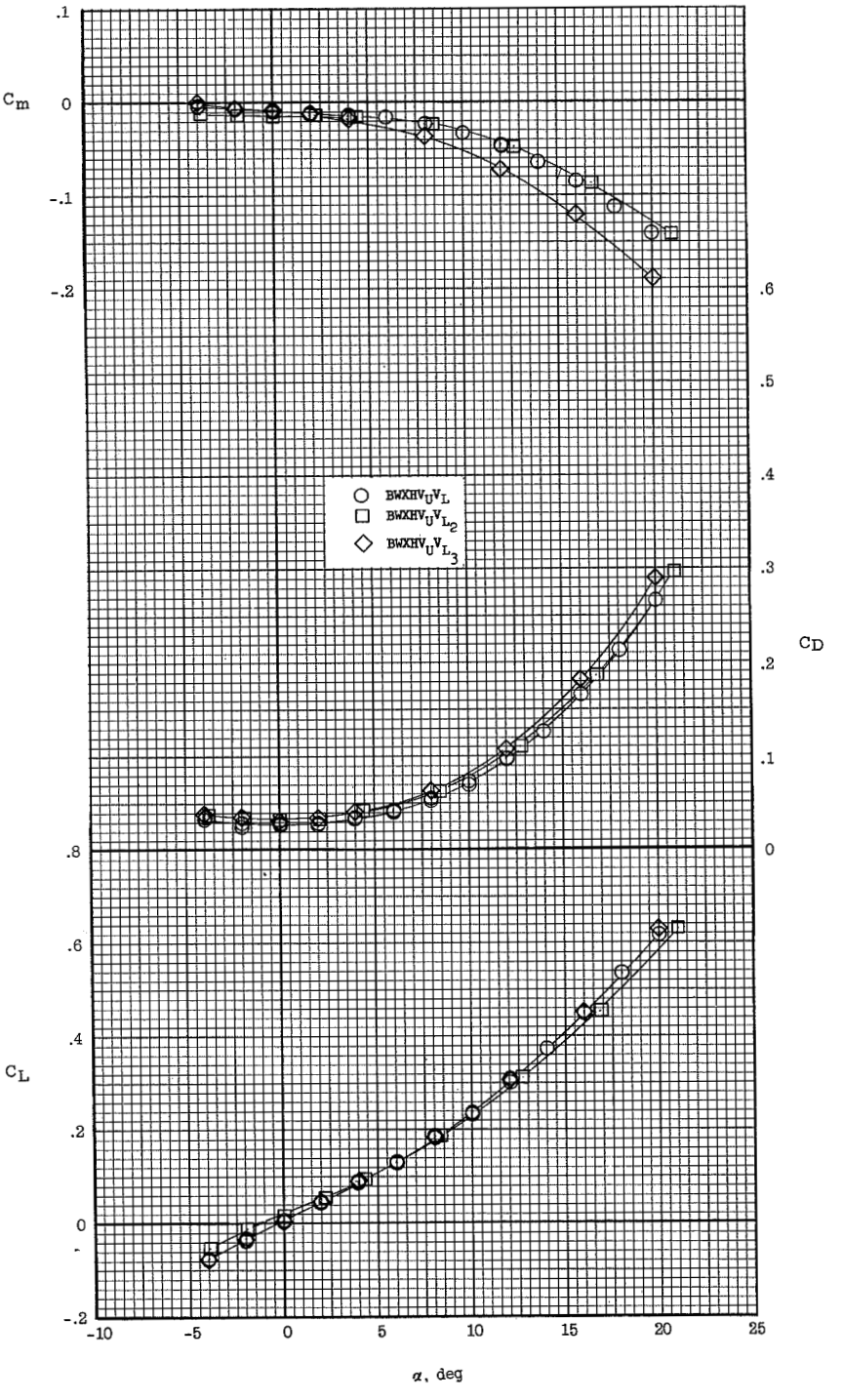

Figure 13.- Effect of lower vertical-tail modifications on the longitudinal stability characteristics of configuration 1. M = 6.83.

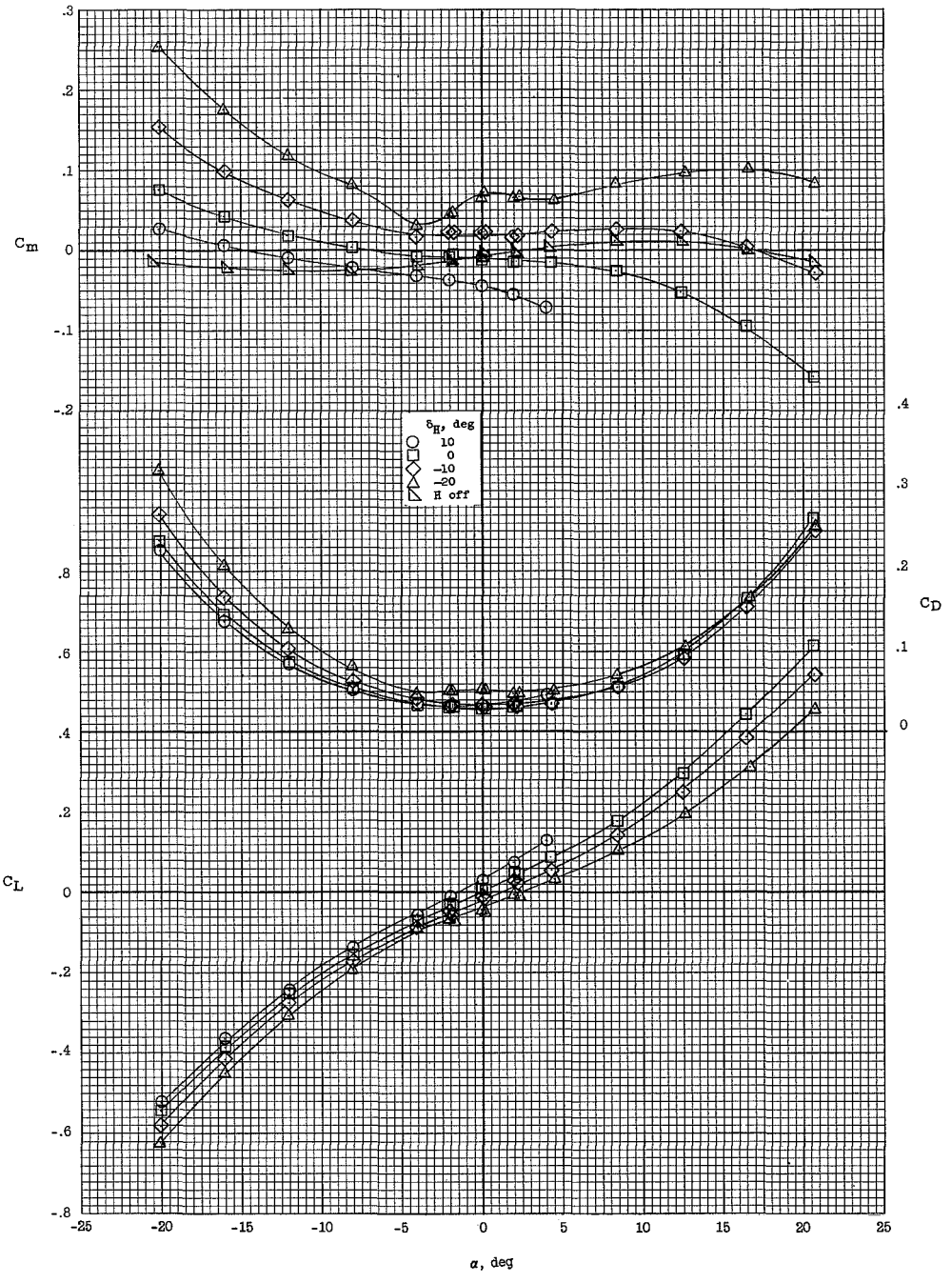

(a) Configuration $BWXHV_UV_L$.

Figure 14.- Effect of horizontal-tail deflection on the longitudinal stability characteristics of configuration 1 with various horizontal-tail locations and dihedral angles. M = 6.83.

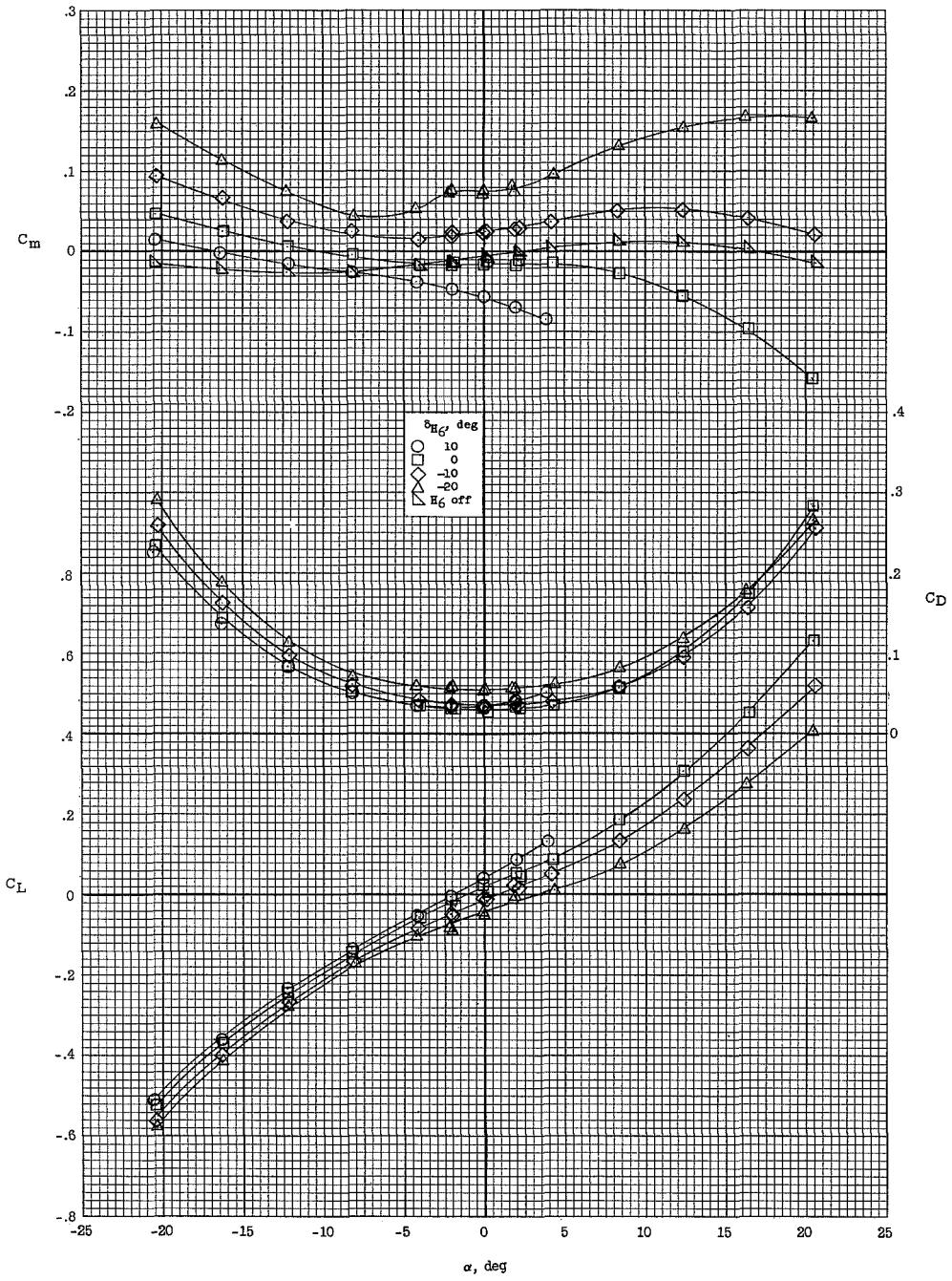

(b) Configuration $BWXH_6V_UV_L$.

Figure 14.- Continued.

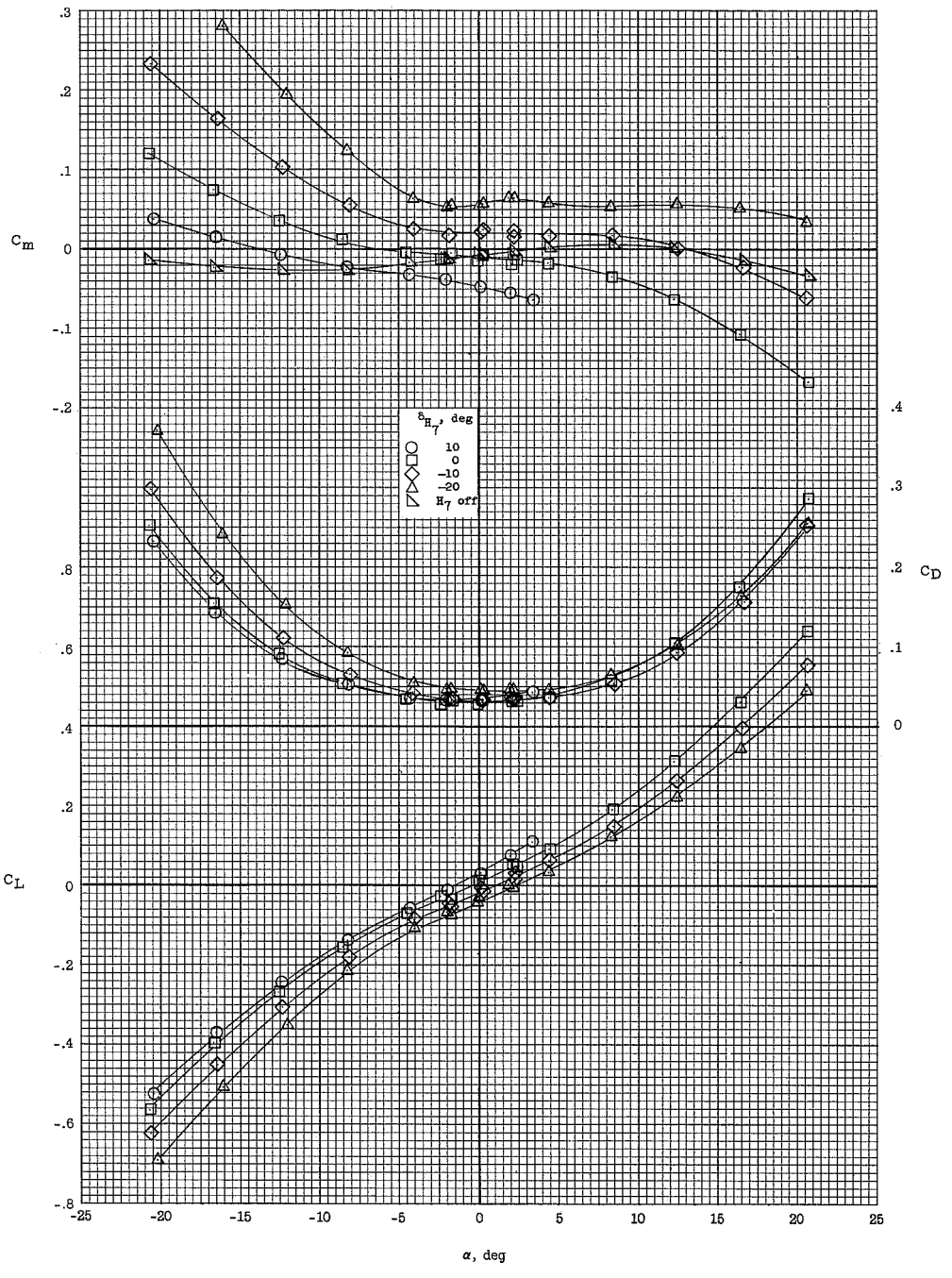

(c) Configuration $BWXH_7V_UV_L$.

Figure 14.- Continued.

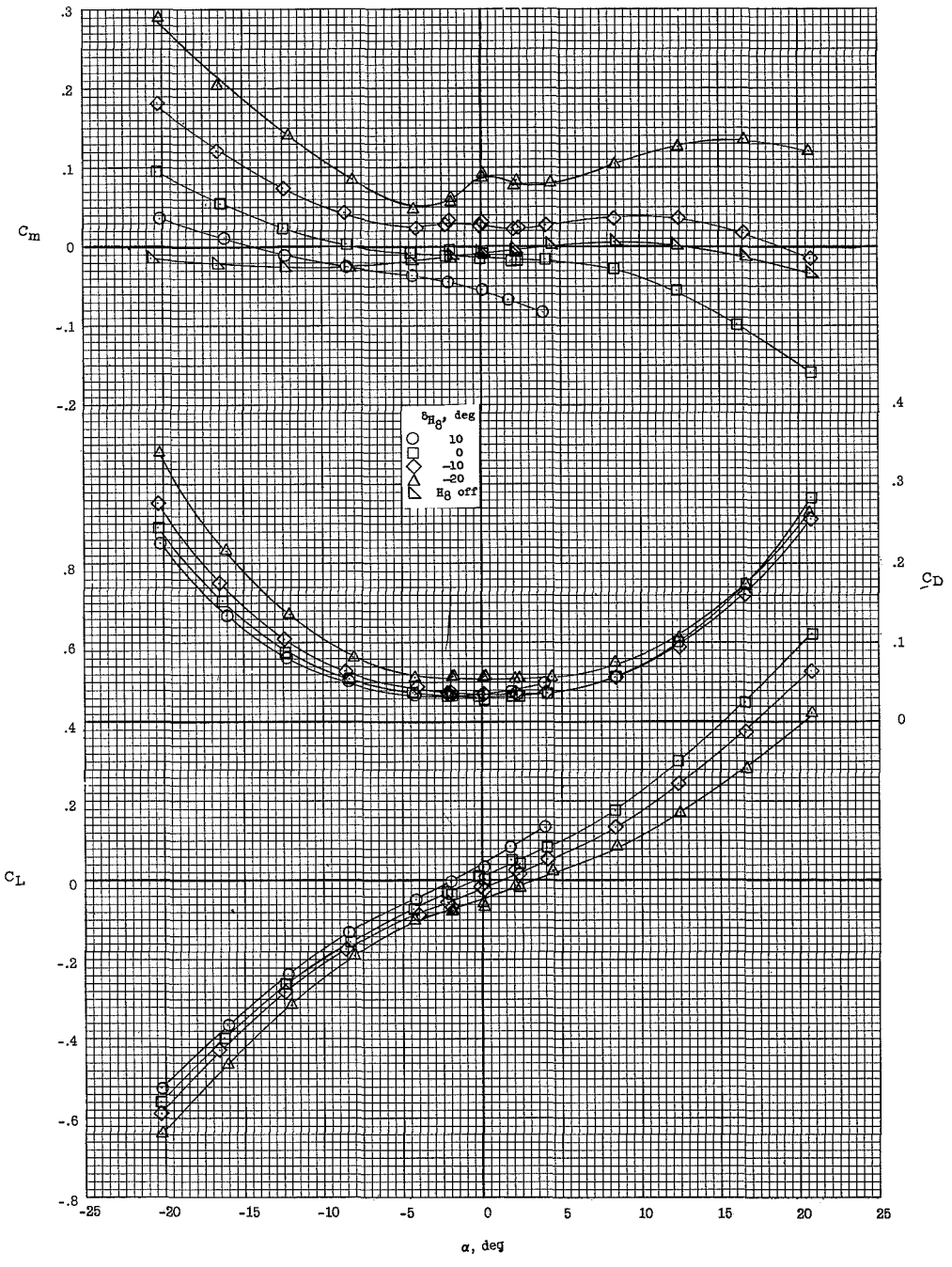

(d) Configuration $BWXH_8V_UV_L$.

Figure 14.- Concluded.

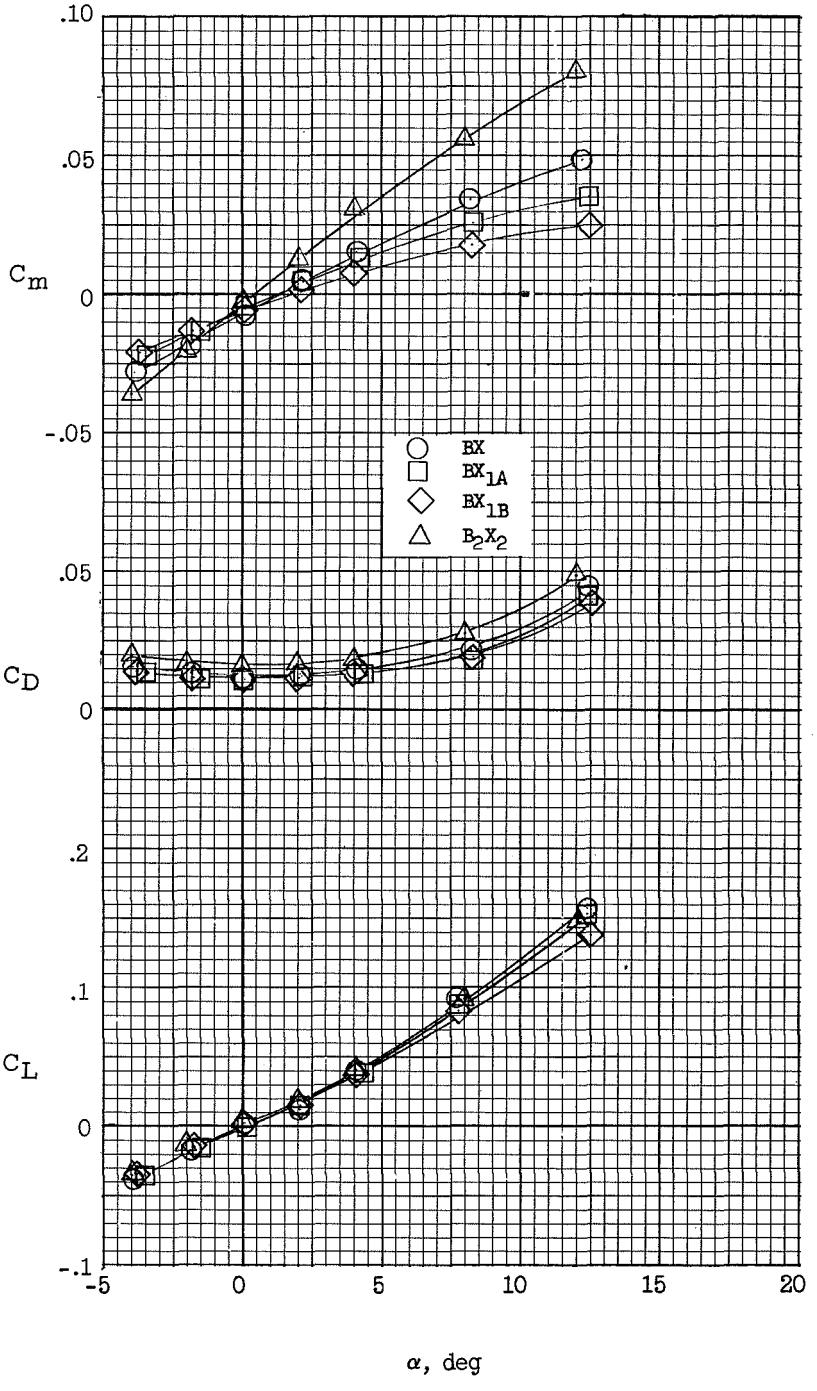

Figure 15.- Effect of fuselage fairing modifications on the longitudinal stability characteristics of the body-fairing configuration. M = 6.83.

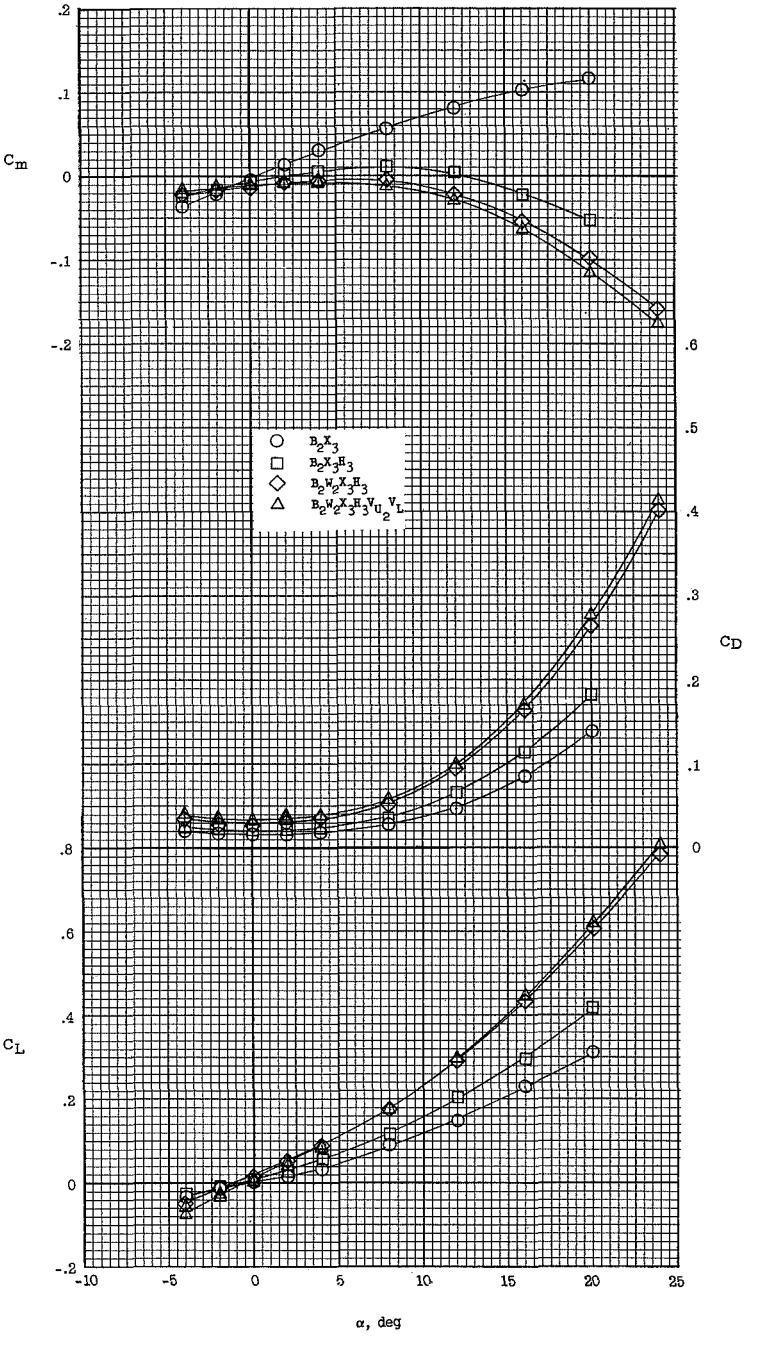

Figure 16.- Effect of the various components on the longitudinal stability characteristics of configuration 2. M = 6.83.

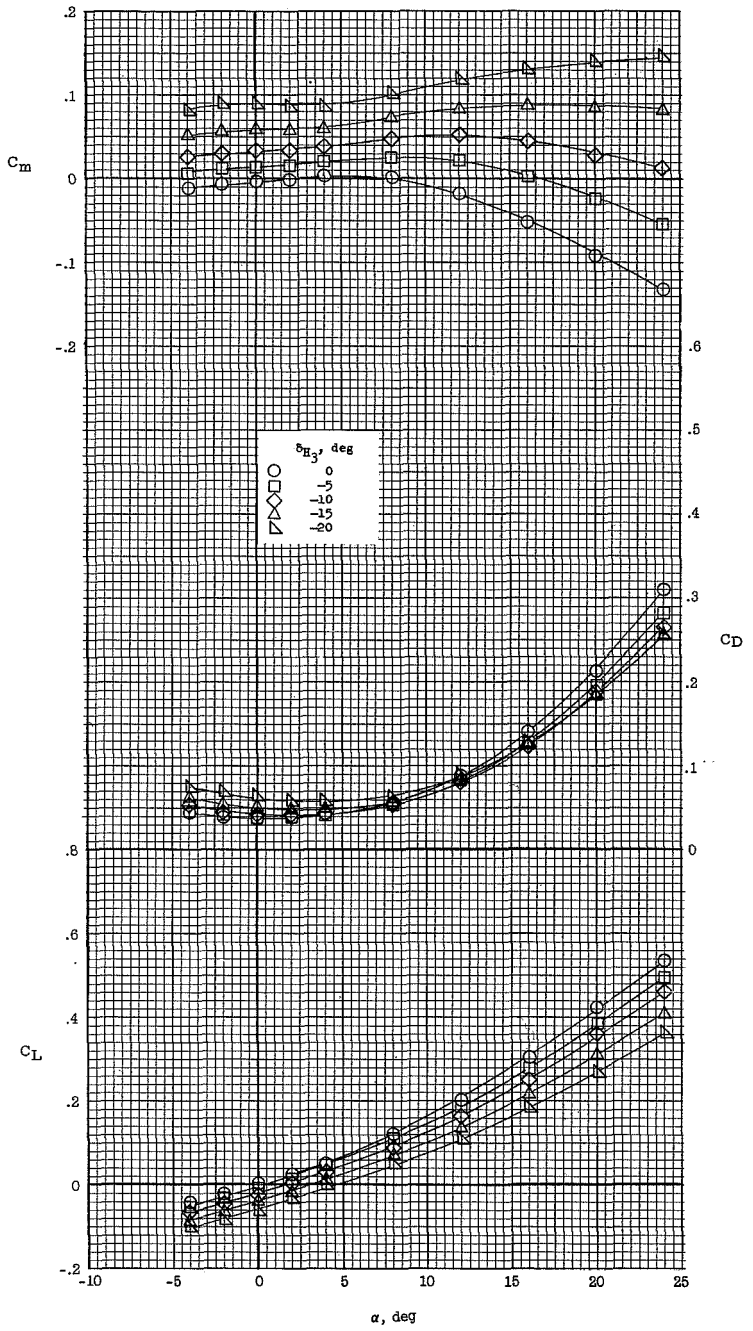

Figure 17.- Effect of horizontal-tail deflection on the longitudinal stability characteristics of configuration $B_2X_3H_3V_{U2}V_LJ_UJ_L$. M = 6.83; $\delta_{J_U} = \delta_{J_L} = 20^\circ$.

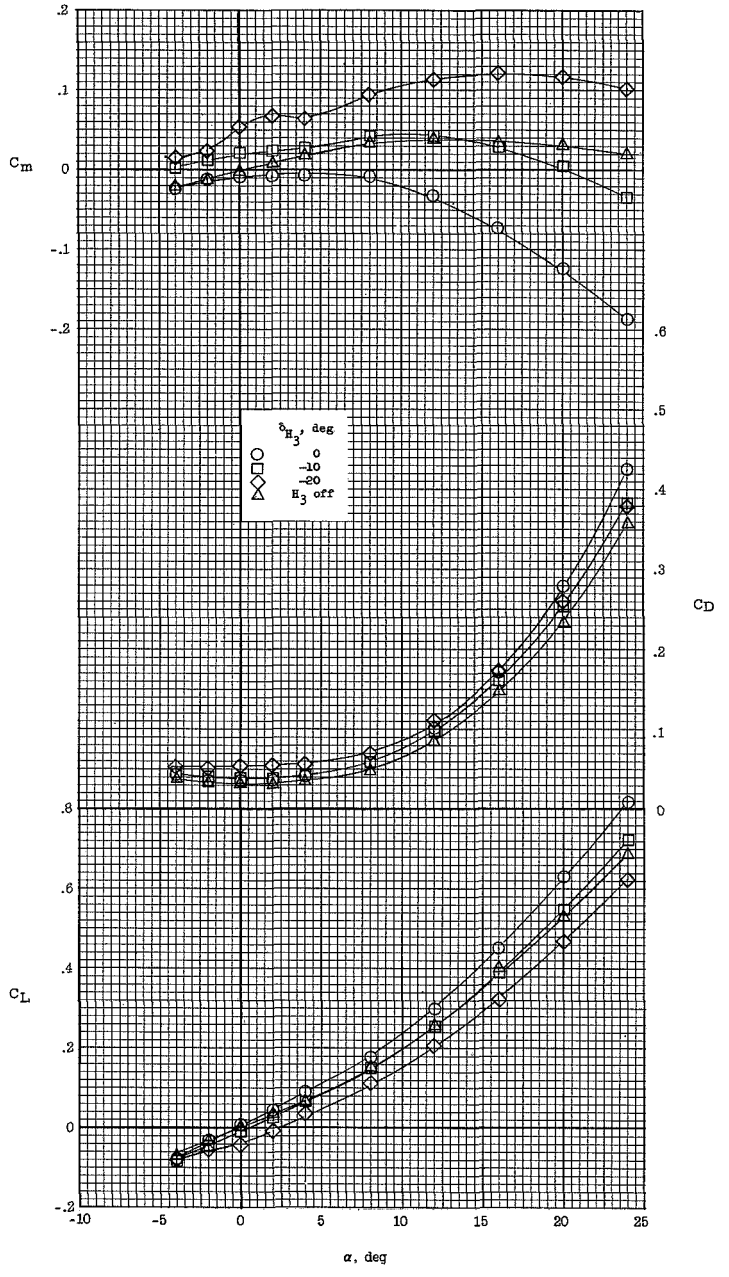

(a) $\delta_{J_U} = 5°$; $\delta_{J_L} = 7.5°$.

Figure 18.- Effect of horizontal-tail deflection on the longitudinal stability characteristics of configuration $B_2W_2X_3H_3V_{U2}V_LJ_UJ_L$ with various speed-brake deflections. M = 6.83.

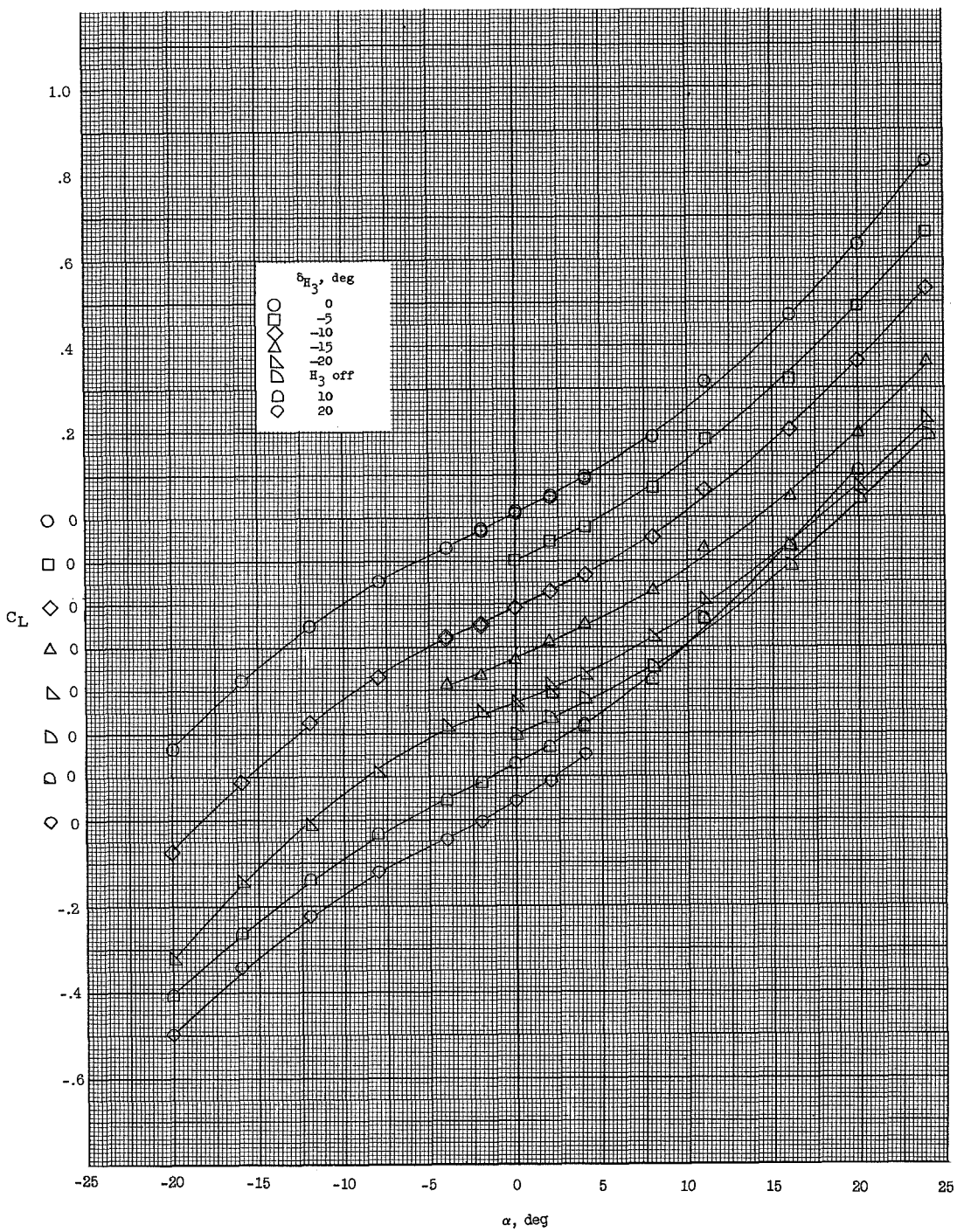

(b) Variation of C_L with α. $\delta_{J_U} = \delta_{J_L} = 20^\circ$.

Figure 18.- Continued.

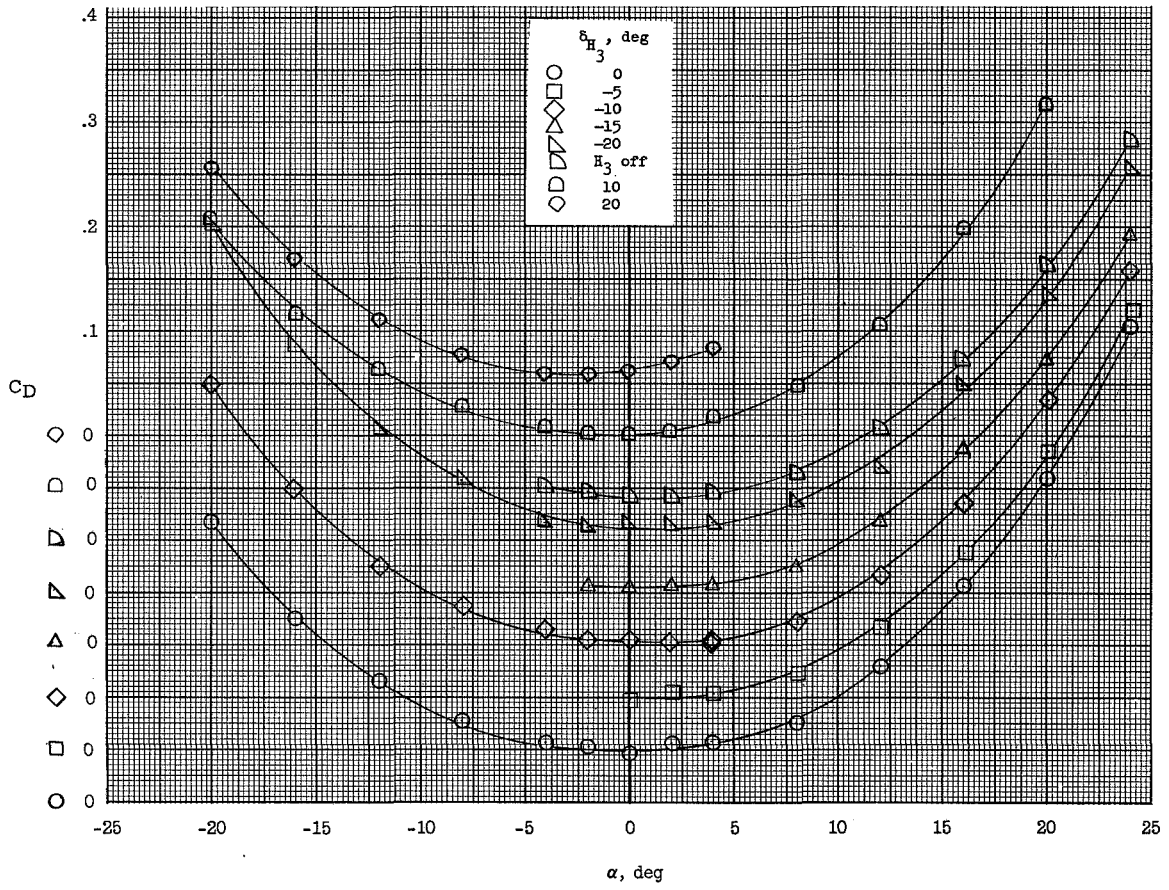

(c) Variation of C_D with α. $\delta_{J_U} = \delta_{J_L} = 20^\circ$.

Figure 18.- Continued.

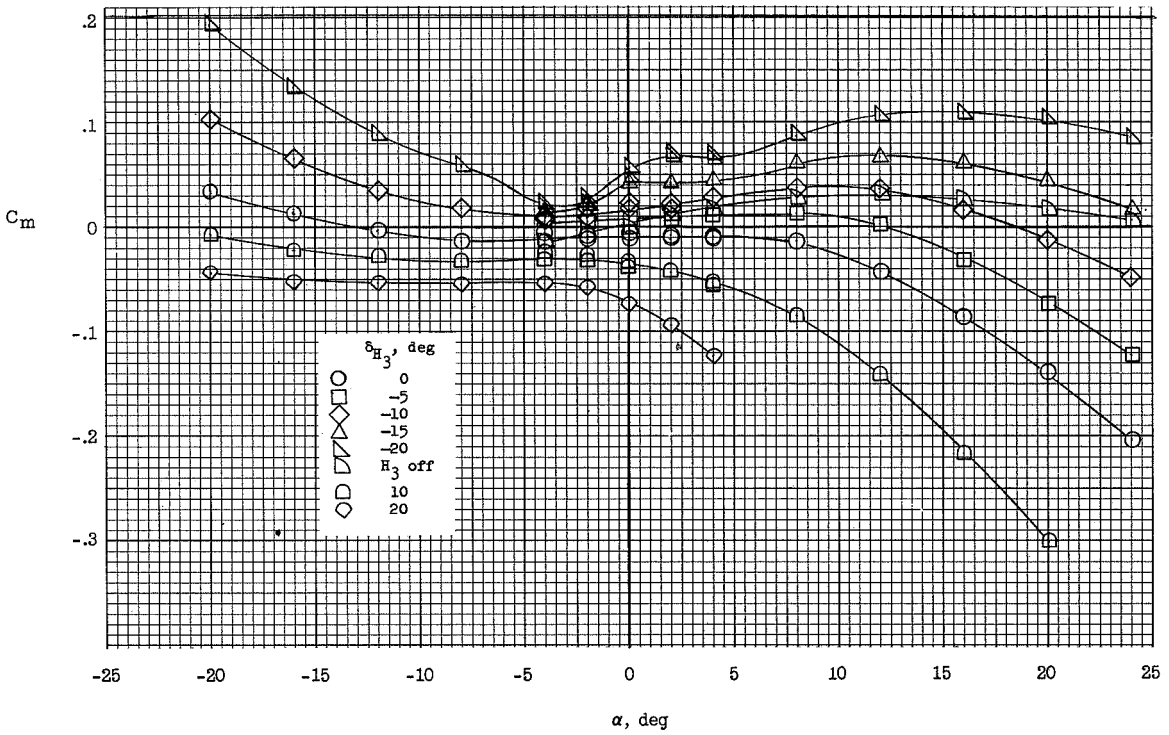

(d) Variation of C_m with α. $\delta_{J_U} = \delta_{J_L} = 20^\circ$.

Figure 18.- Continued.

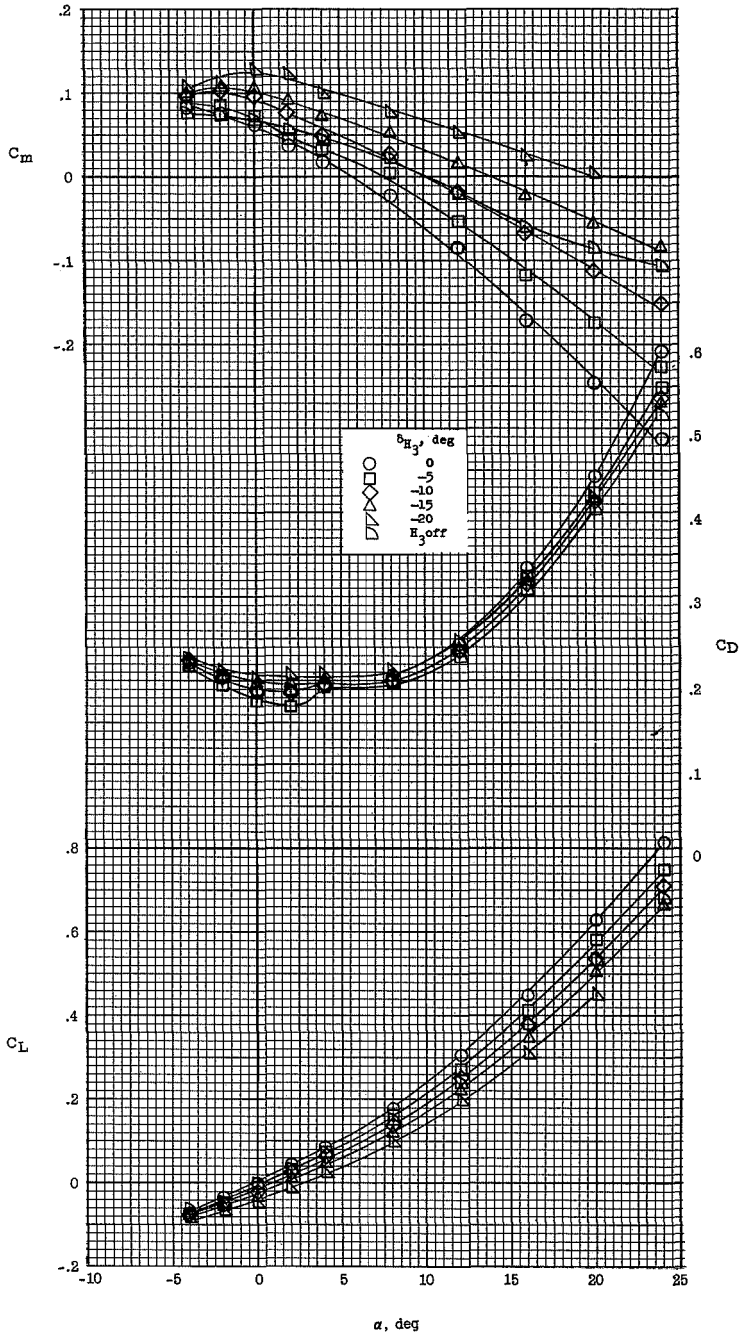

(e) $\delta_{J_U} = \delta_{J_L} = 45^\circ$.

Figure 18.- Concluded.

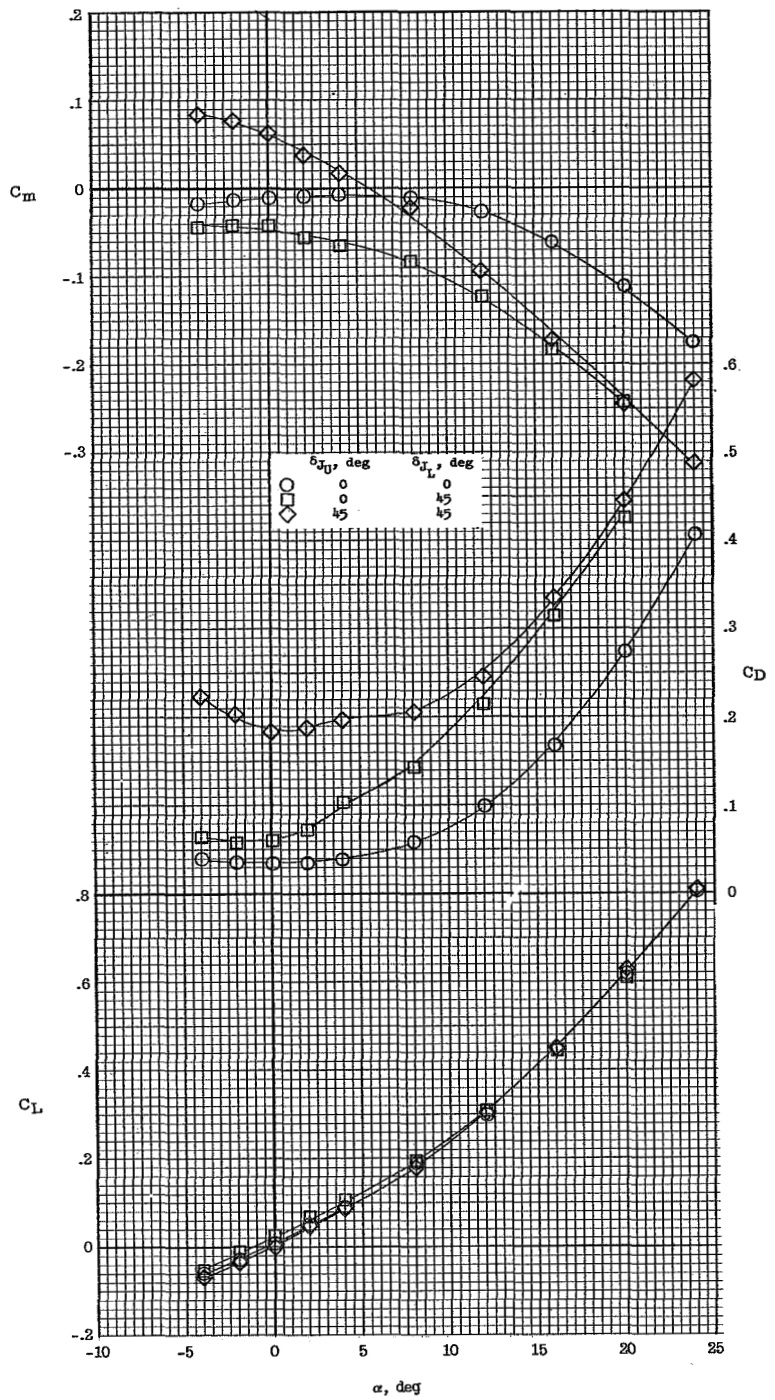

Figure 19.- Effect of speed-brake components on the longitudinal stability characteristics of configuration $B_2W_2X_3H_3V_{U2}V_LJ_UJ_L$. M = 6.83.

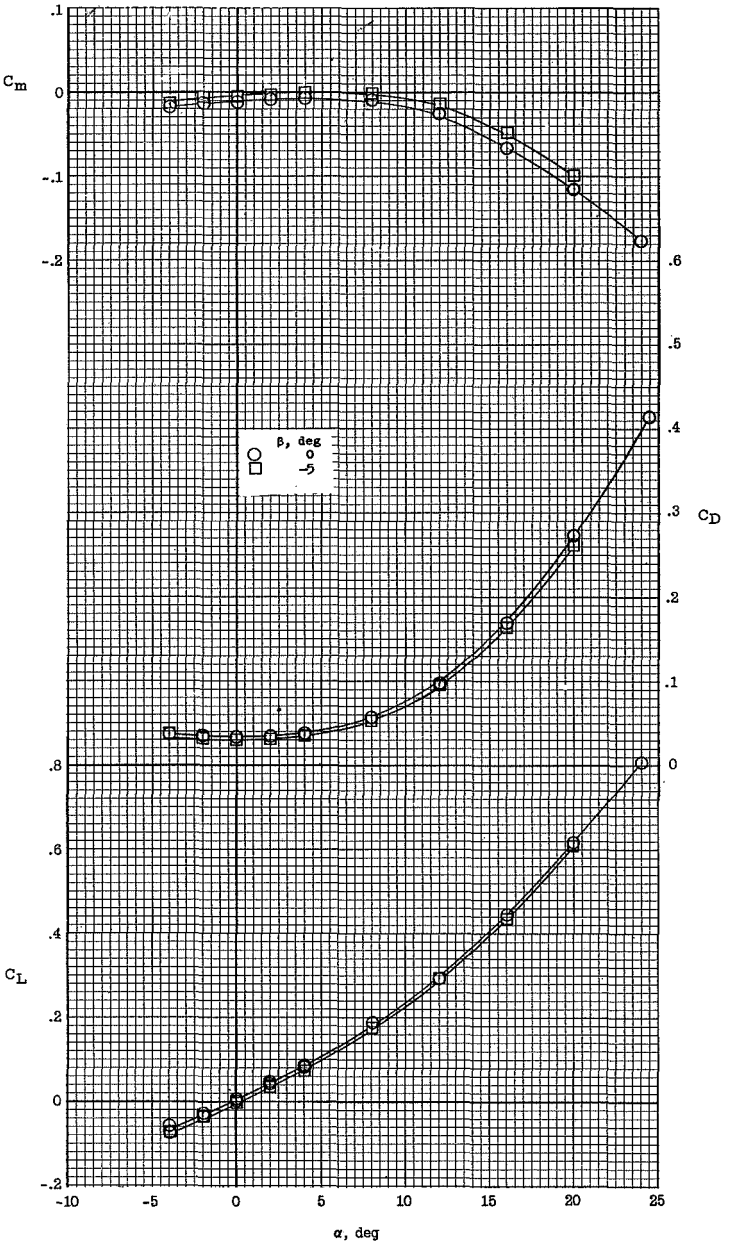

(a) $\delta_{J_U} = \delta_{J_L} = 0^\circ$.

Figure 20.- Effect of sideslip on the longitudinal stability characteristics of configuration $B_2W_2X_3H_3V_{U2}V_LJ_UJ_L$ with various speed-brake deflections. M = 6.83.

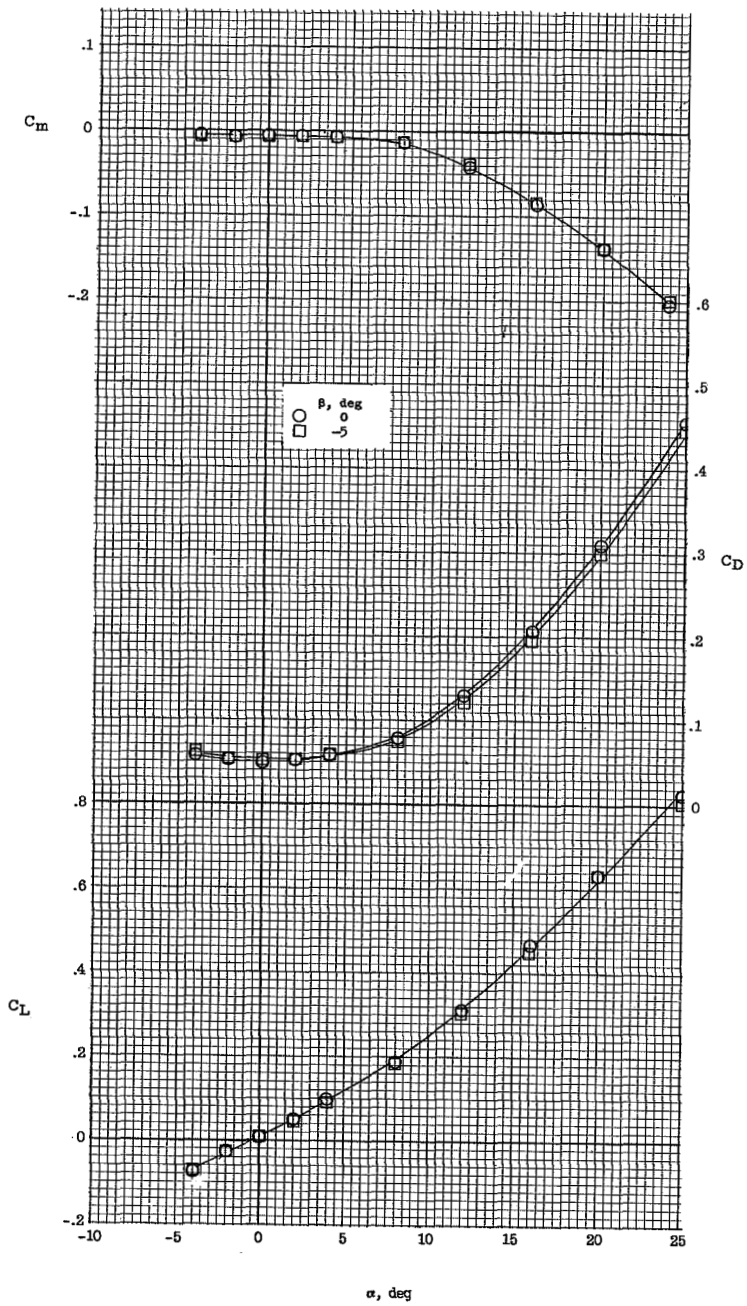

(b) $\delta_{J_U} = \delta_{J_L} = 20^\circ$.

Figure 20.- Continued.

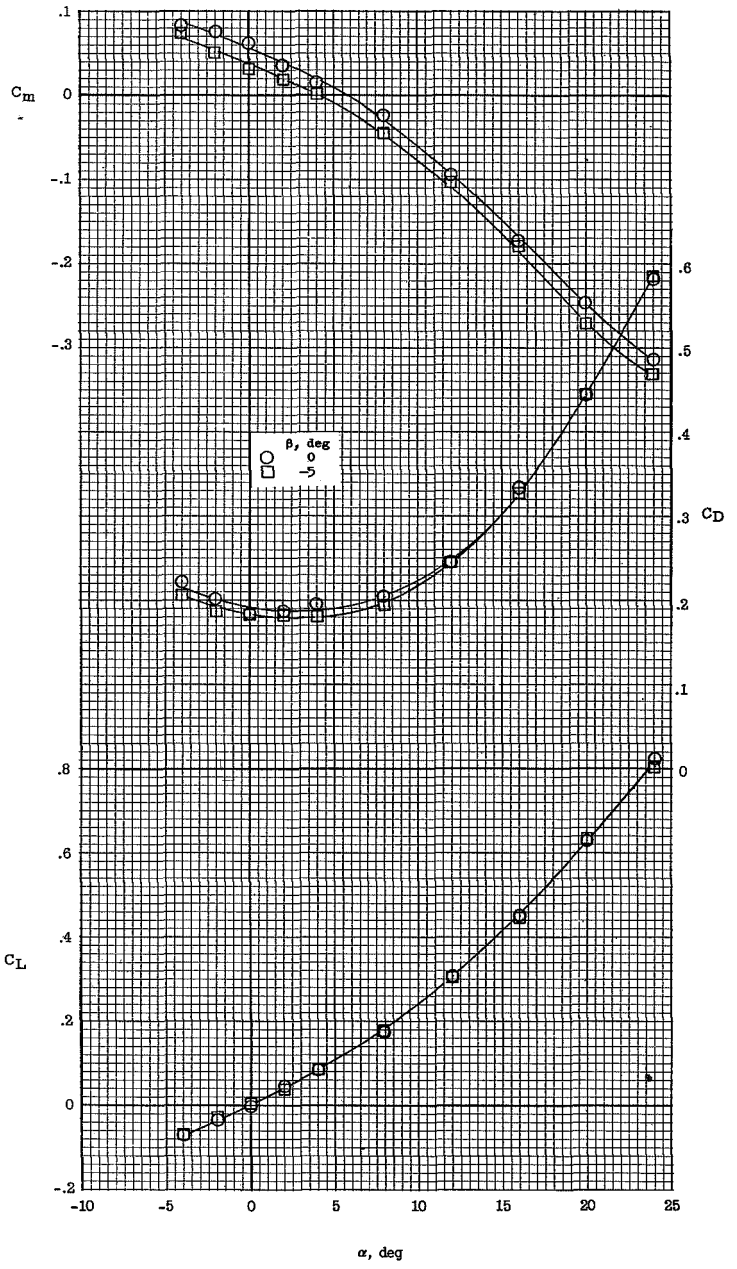

(c) $\delta_{J_U} = \delta_{J_L} = 45^\circ$.

Figure 20.- Concluded.

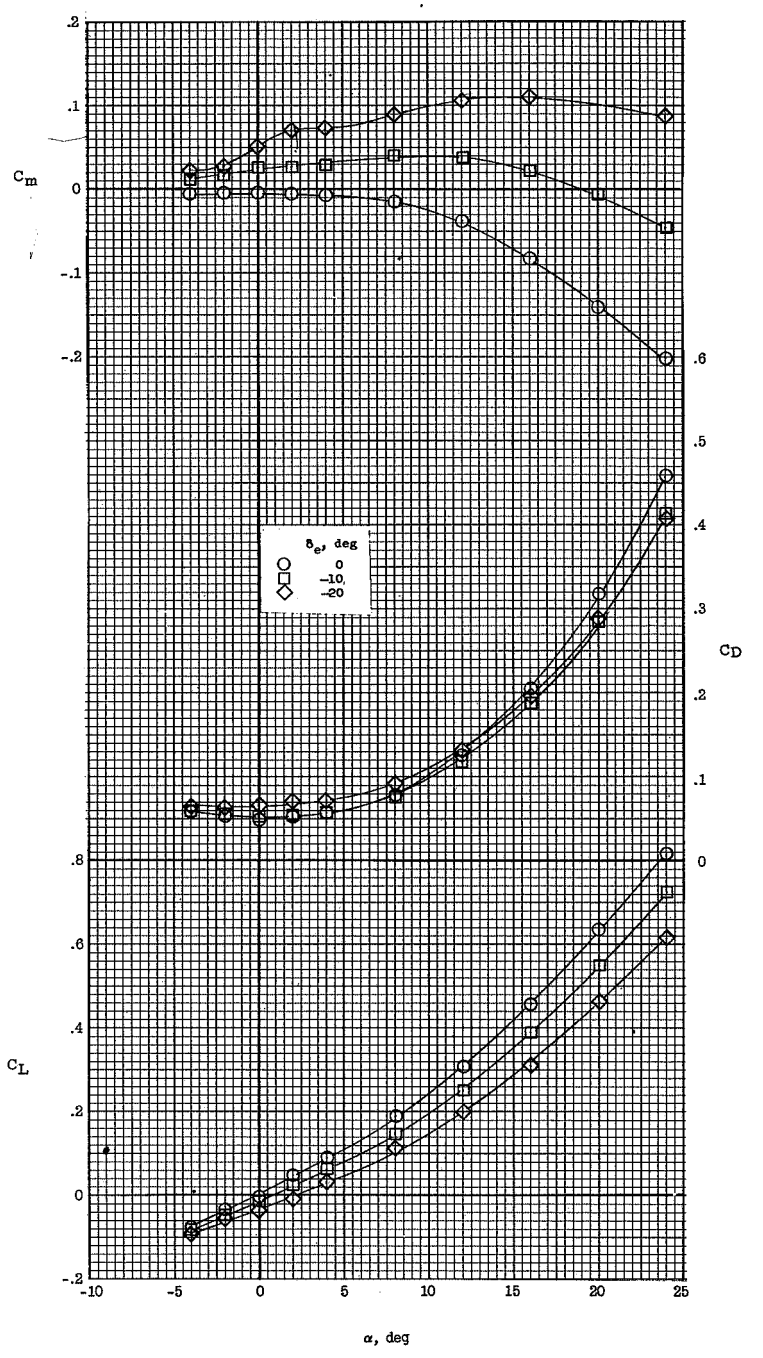

Figure 21.- Effect of differential horizontal-tail deflection on the longitudinal stability characteristics of configuration $B_2W_2X_3H_3V_{U2}V_LJ_UJ_L$. $M = 6.83$; $\delta_{h'} = 10^\circ$; $\delta_{J_U} = \delta_{J_L} = 20^\circ$.

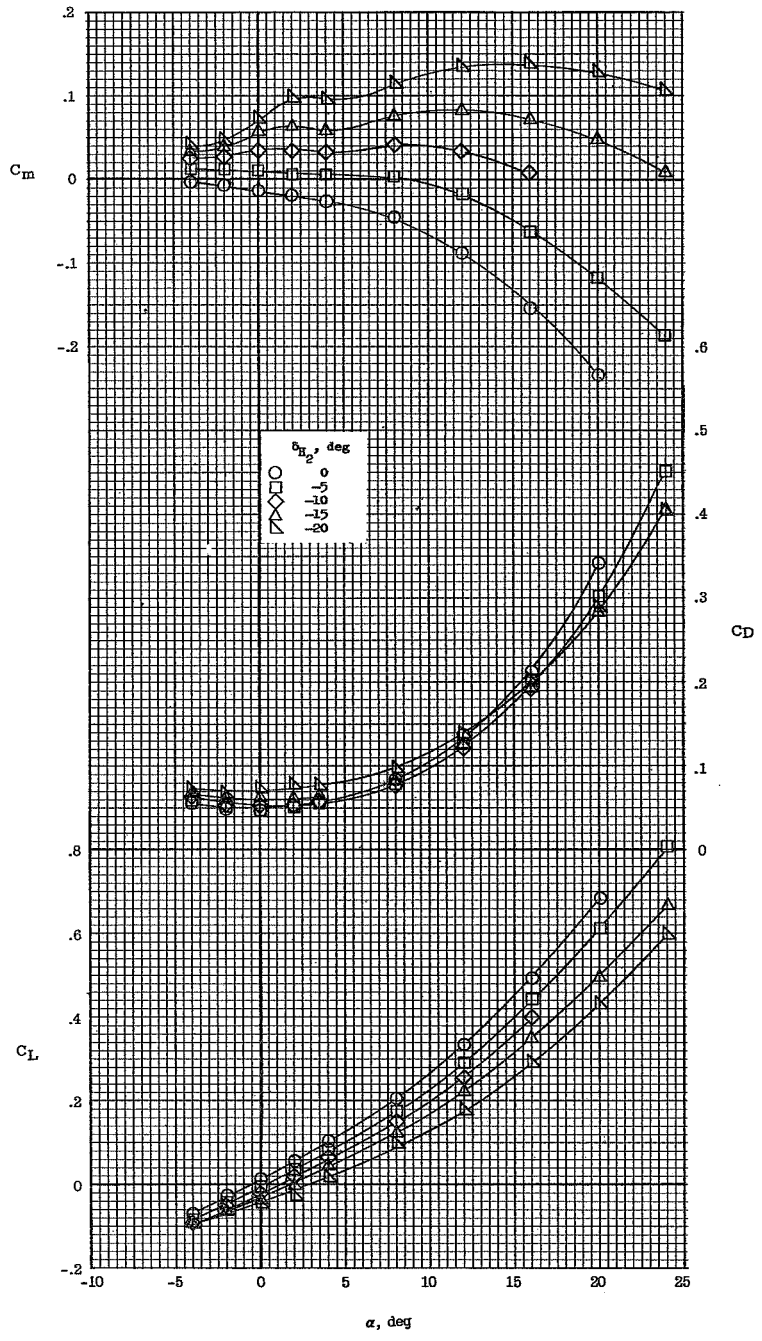

Figure 22.- Effect of horizontal-tail deflection on longitudinal stability characteristics of configuration $B_2W_2X_3H_2V_{U2}V_LJ_UJ_L$. M = 6.83; $\delta_{J_U} = \delta_{J_L} = 20^\circ$.

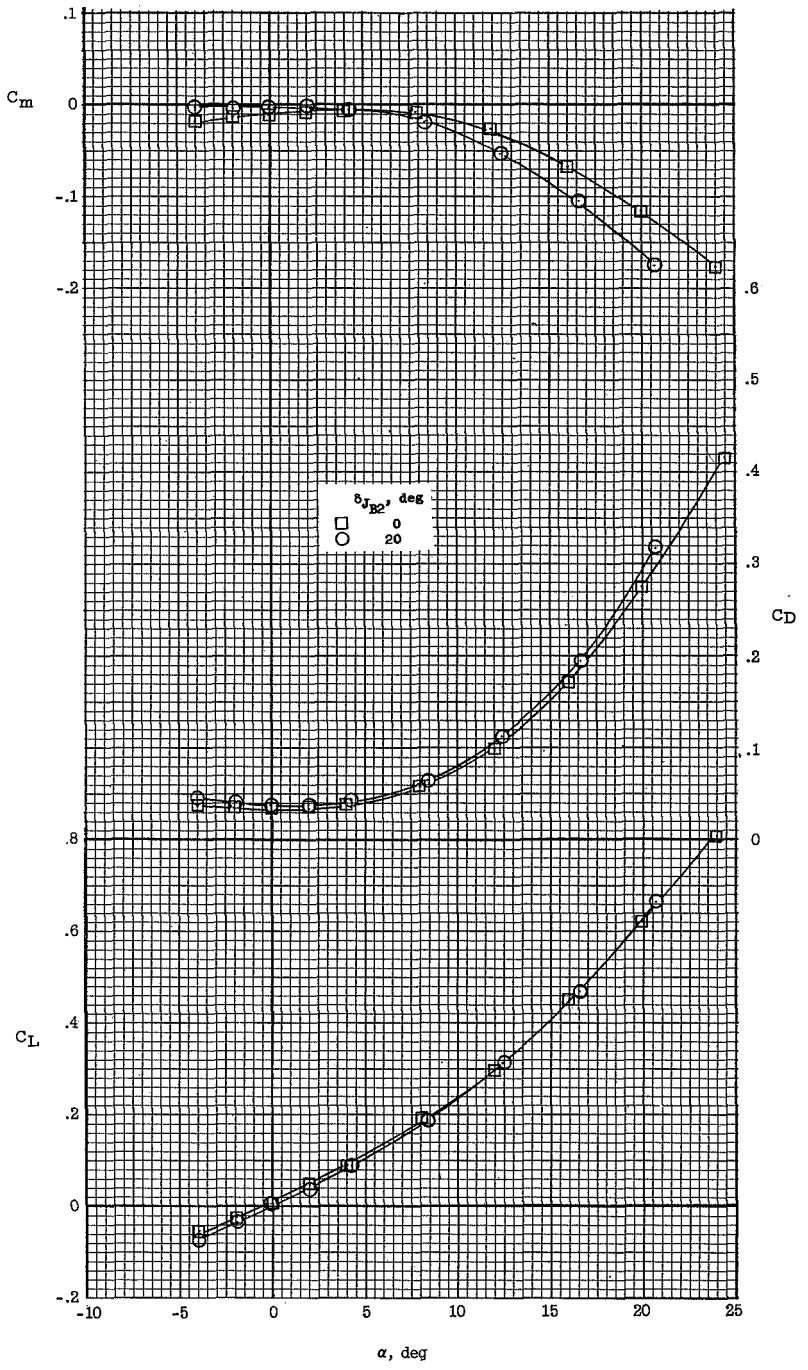

Figure 23.- Effect of fuselage conical speed-brake deflection $\delta_{J_{B2}}$ on the longitudinal stability characteristics of configuration $B_2W_2X_3H_3V_{U2}V_LJ_{B2}$. M = 6.83.

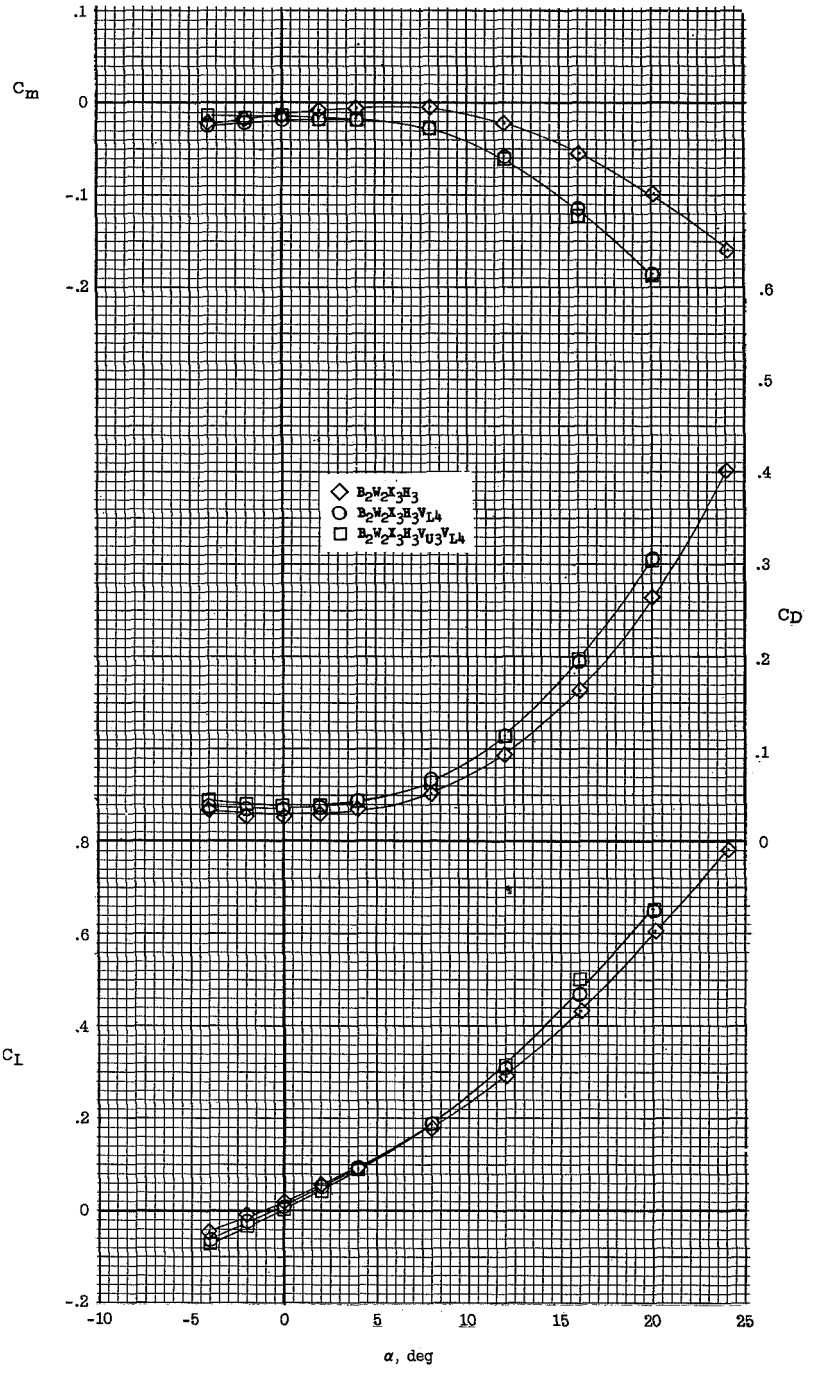

Figure 24.- Effect of twin upper and lower vertical-tail components on the longitudinal stability characteristics of configuration $B_2W_2X_3H_3V_{U3}V_{L4}$. M = 6.83.

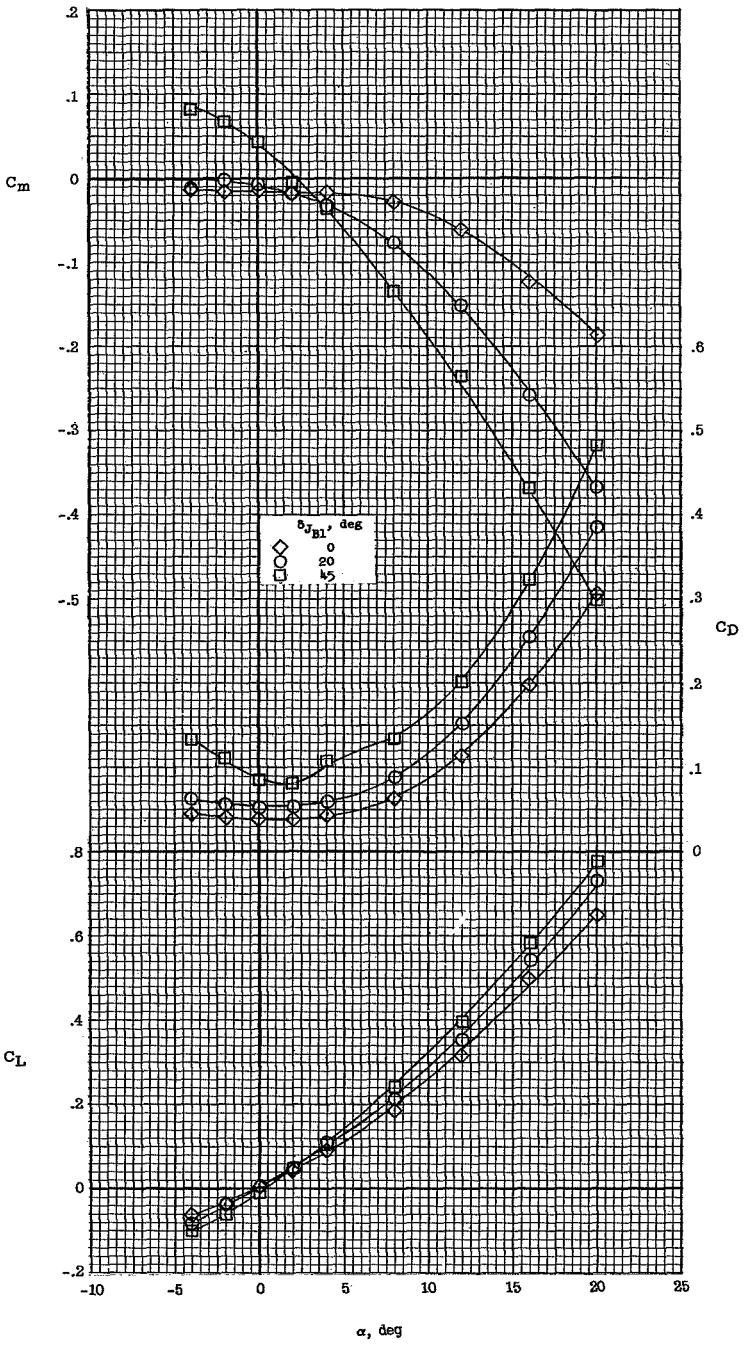

Figure 25.- Effect of fuselage conical speed-brake deflection $\delta_{J_{B1}}$ the longitudinal stability characteristics of configuration $B_2W_2X_3H_3V_{U3}V_{L4}J_{B1}$. M = 6.83.

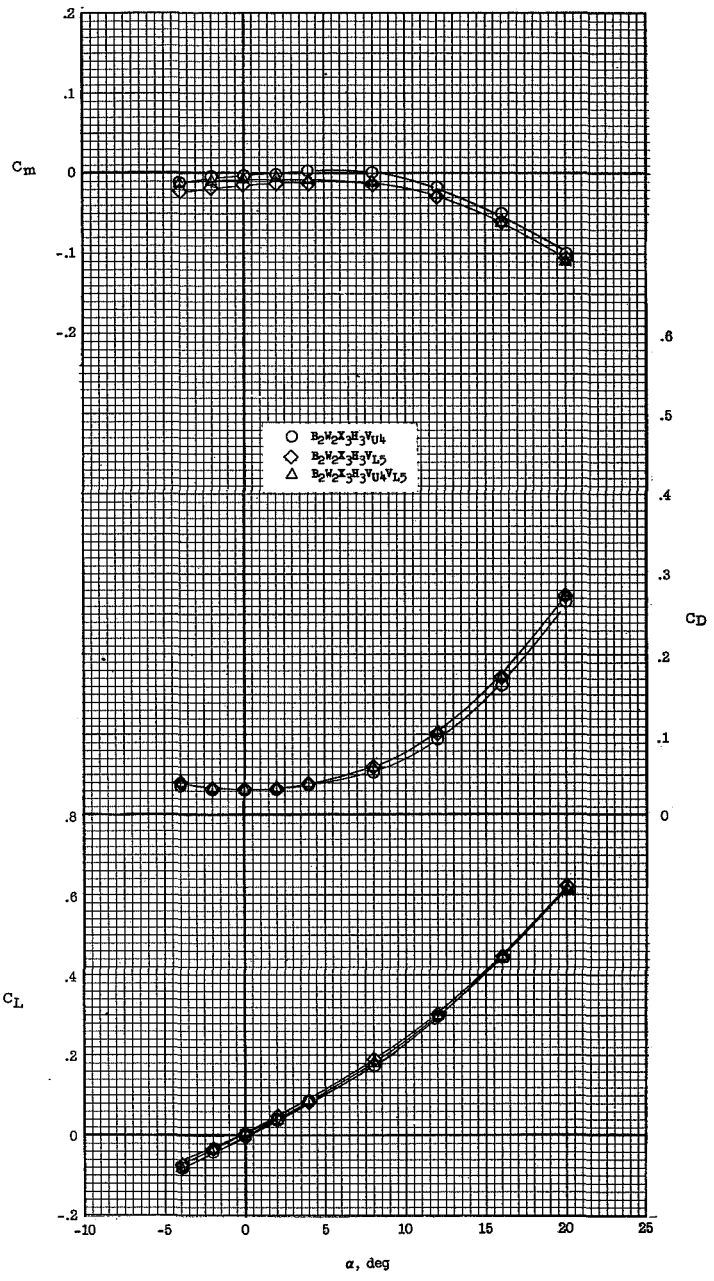

(a) $\delta_{J_{U1}} = \delta_{J_{L1}} = 0^{\circ}$.

Figure 26.- Effect of vertical tail and speed-brake components on the longitudinal stability characteristics of configuration $B_2W_2X_3H_3V_{U4}V_{L5}J_{U1}J_{L1}$. M = 6.83.

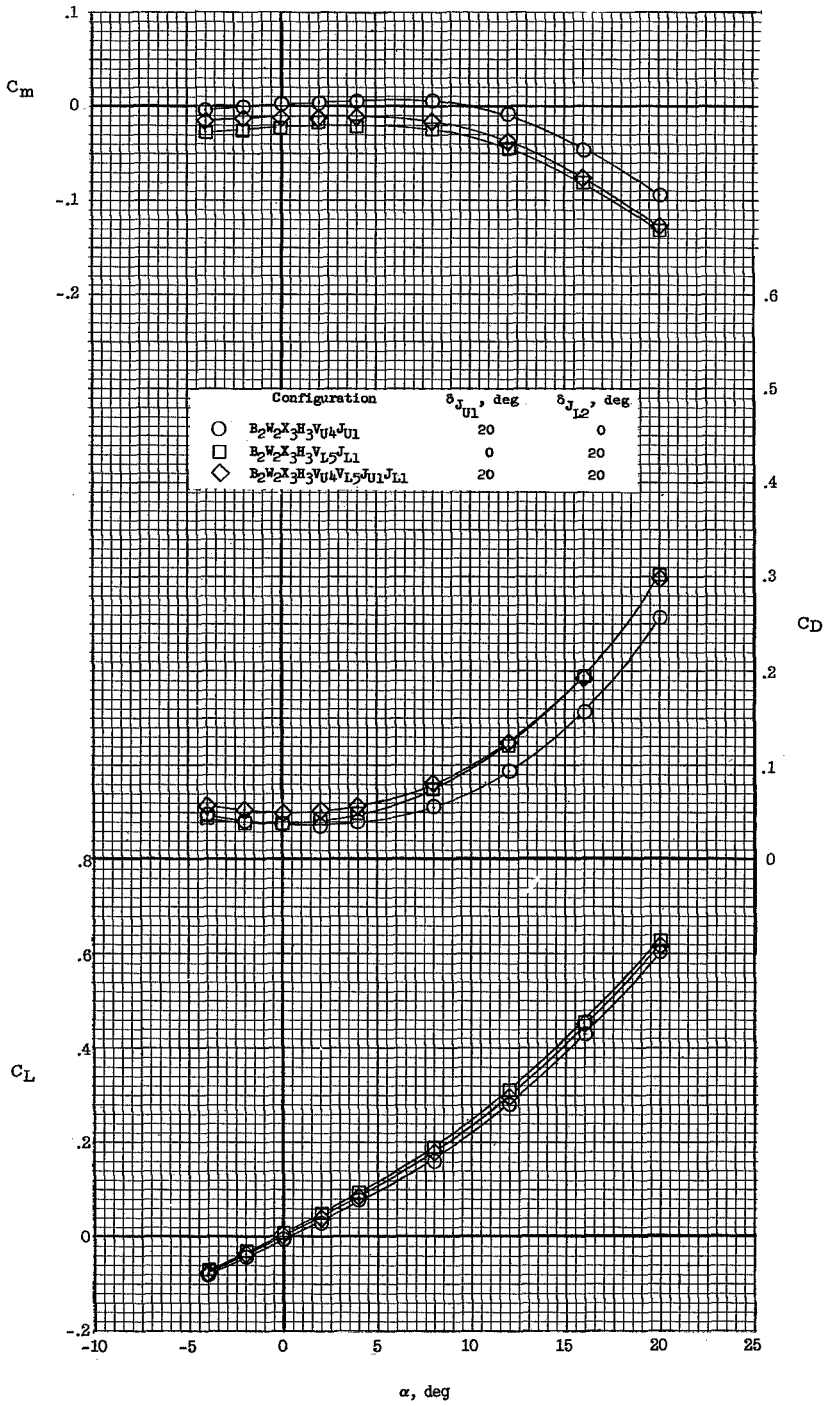

(b) $\delta_J = 20^o$.

Figure 26.- Continued.

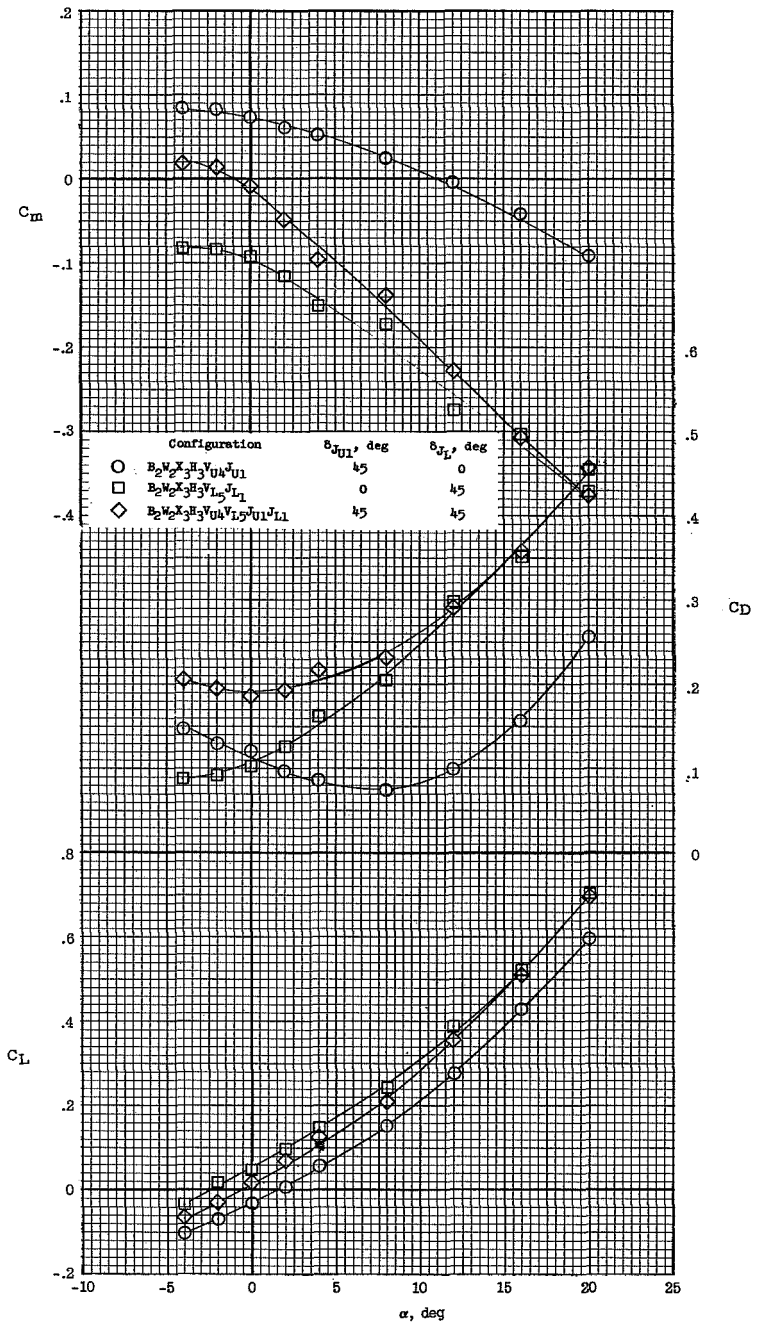

(c) $\delta_J = 45°$.

Figure 26.- Concluded.

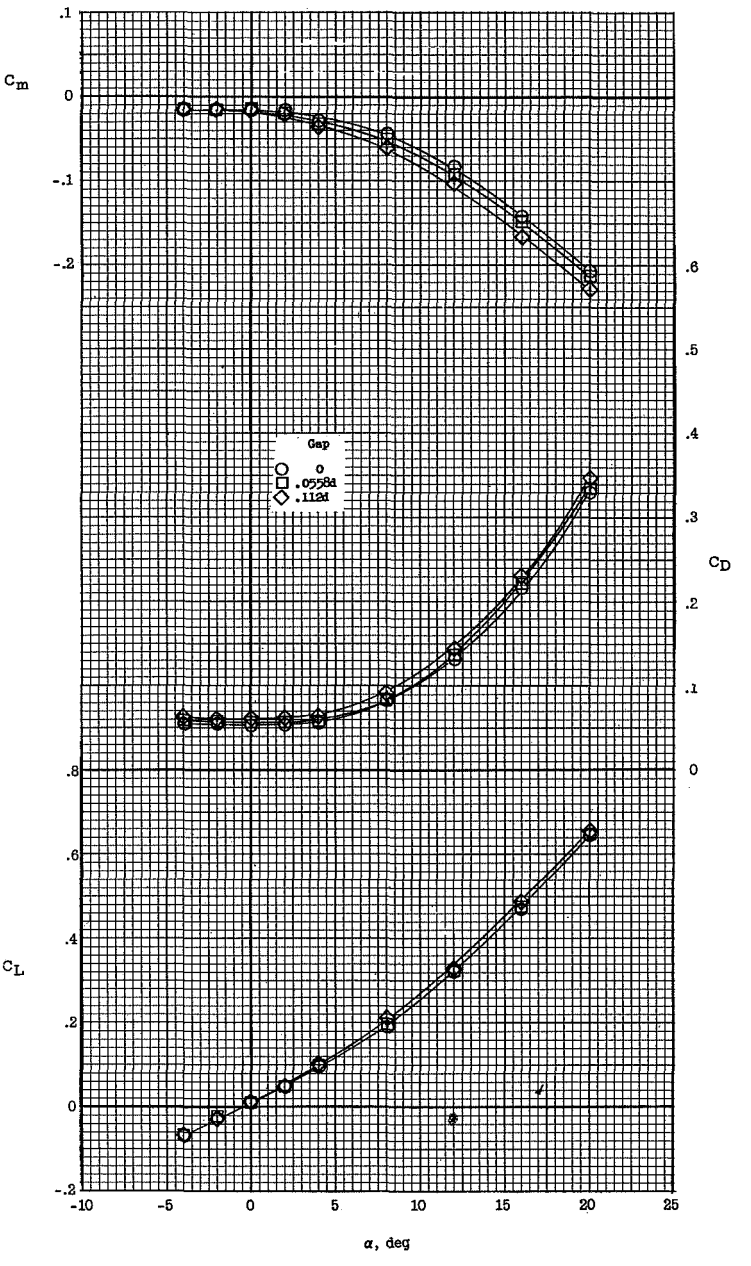

(a) $\delta_{J_F} = 40^\circ$.

Figure 27.- Effect of boundary-layer gap on the longitudinal stability characteristics of configuration $B_2W_2X_3H_3V_{U4}V_{L5}J_F$ with various fairing speed-brake deflections. M = 6.83.

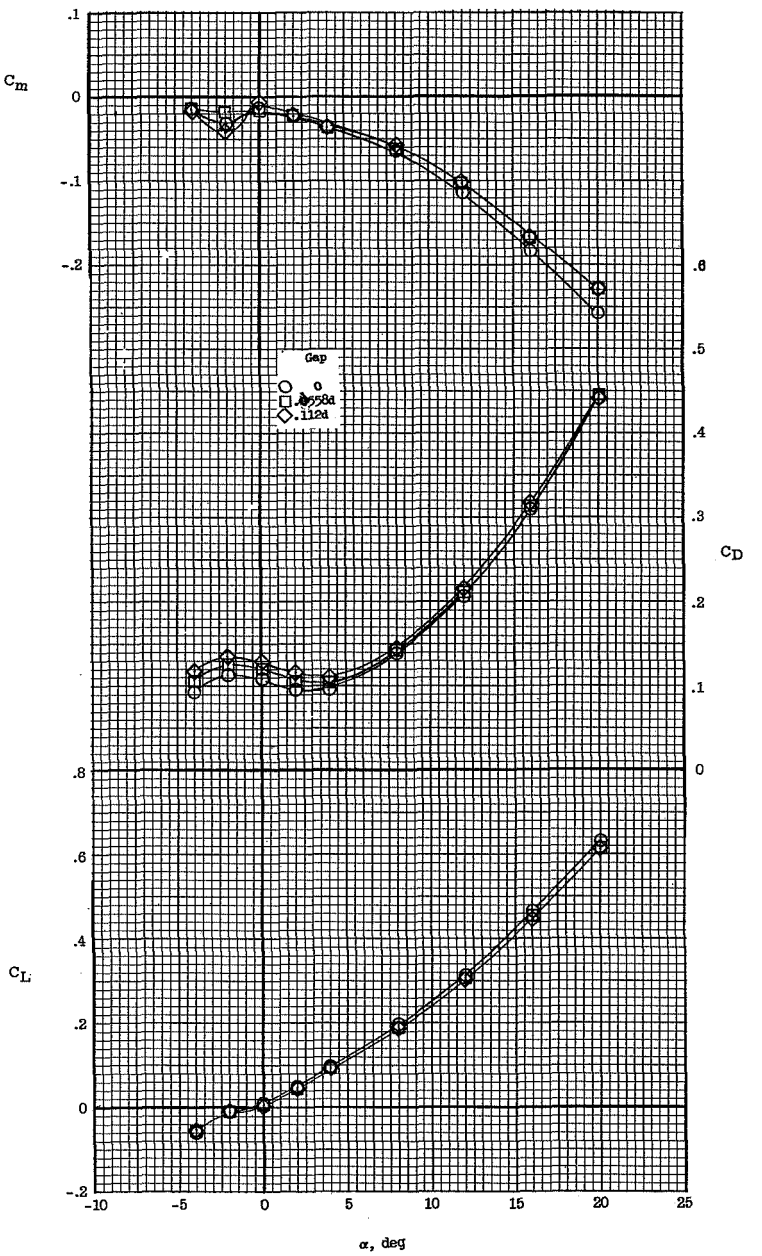

(b) $\delta_{J_F} = 75^\circ$.

Figure 27.- Concluded.

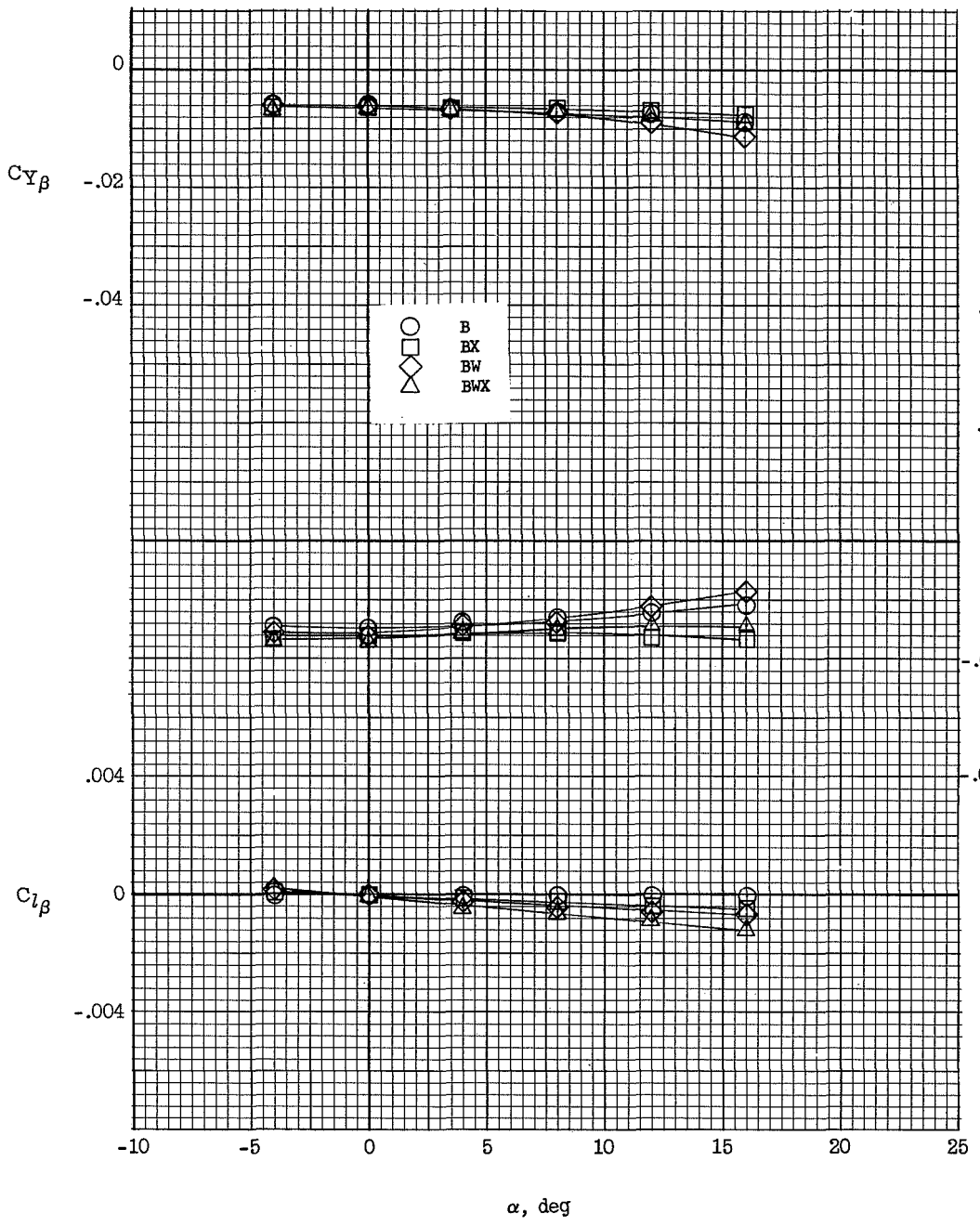

(a) Body, wing, and side fairing.

Figure 28.- Effect of component parts on the lateral and directional stability derivatives of configuration 1. M = 6.83.

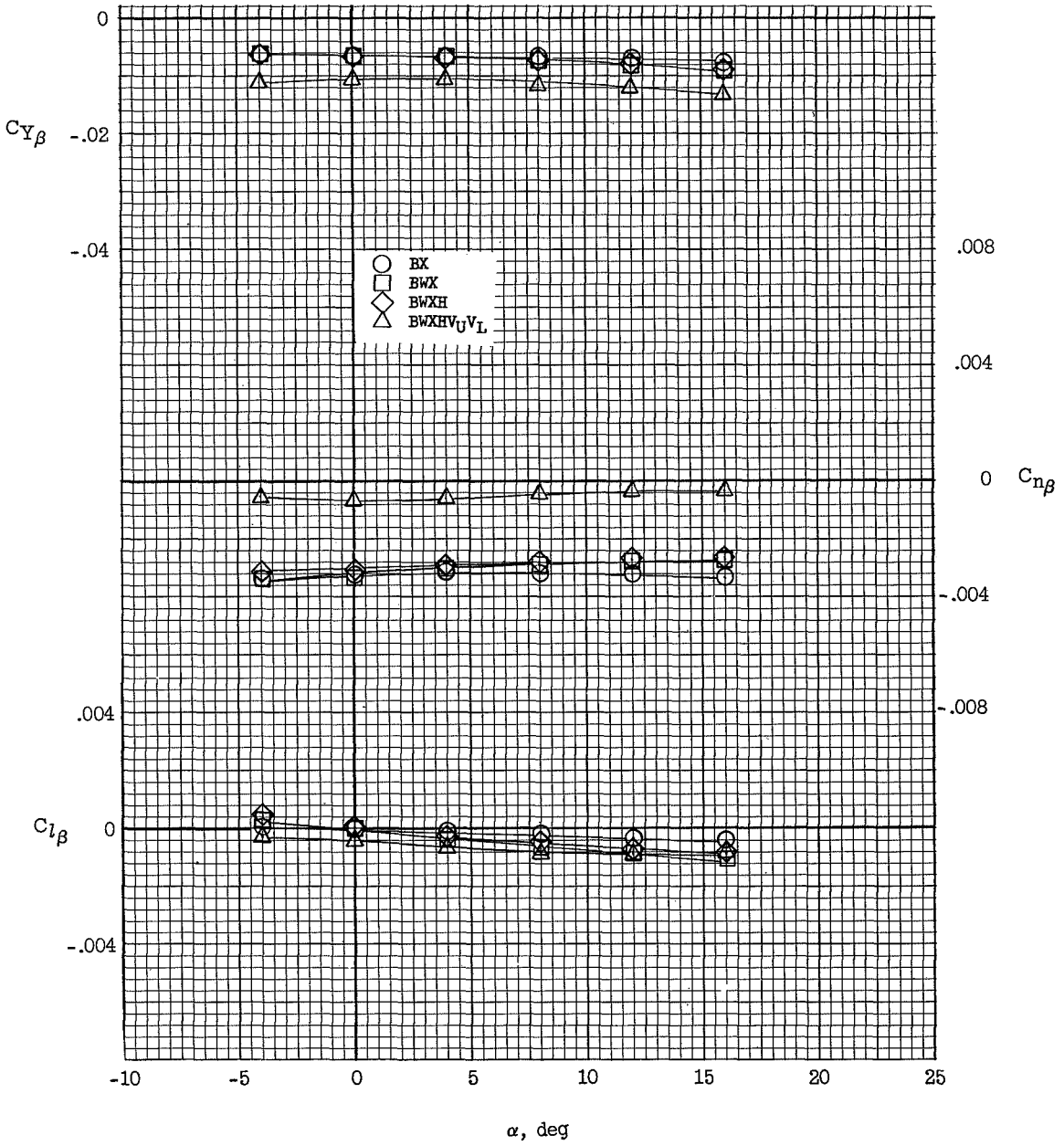

(b) Wing, horizontal tail, and vertical tails.

Figure 28.- Continued.

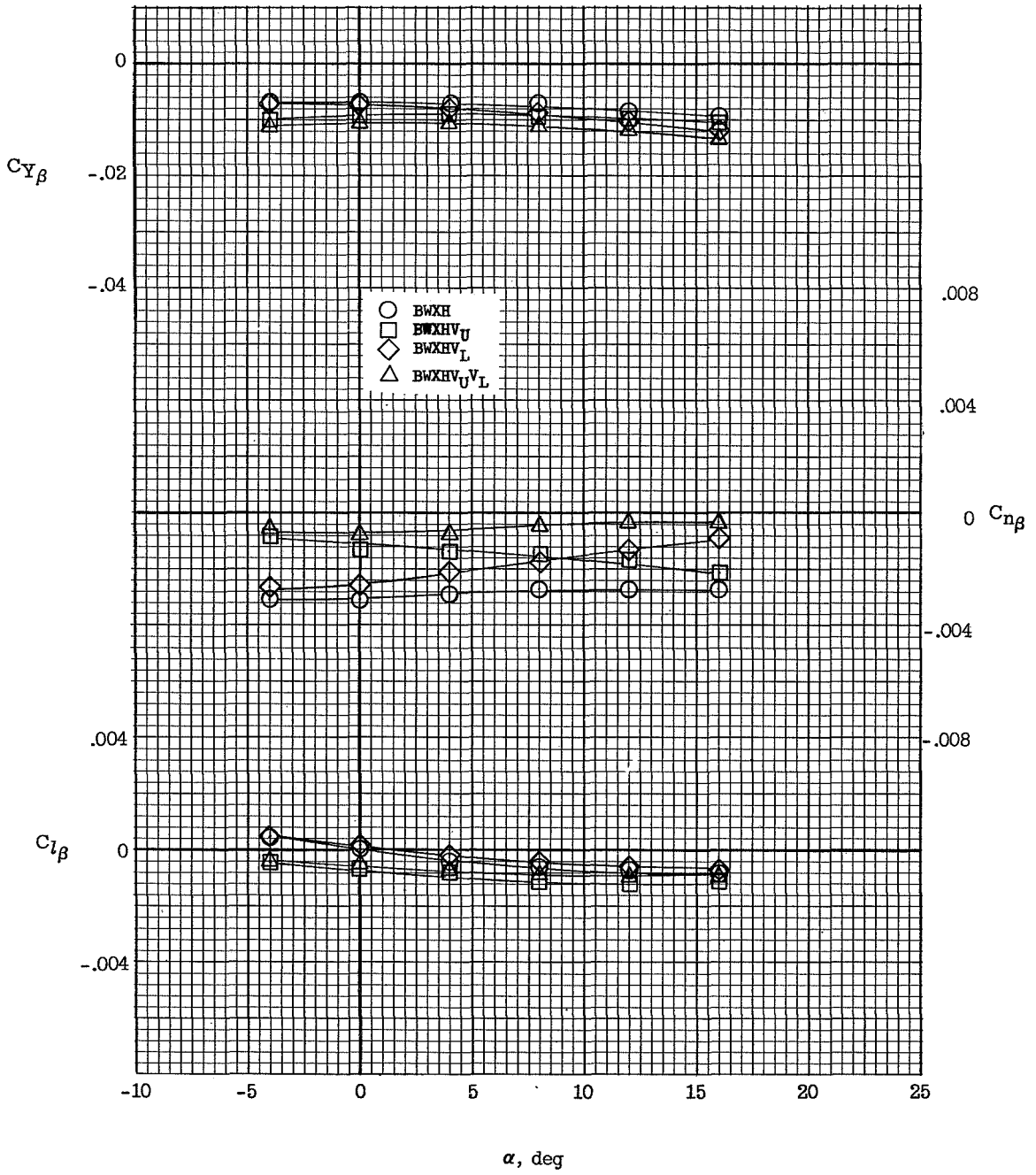

(c) Upper and lower vertical tails.

Figure 28.- Concluded.

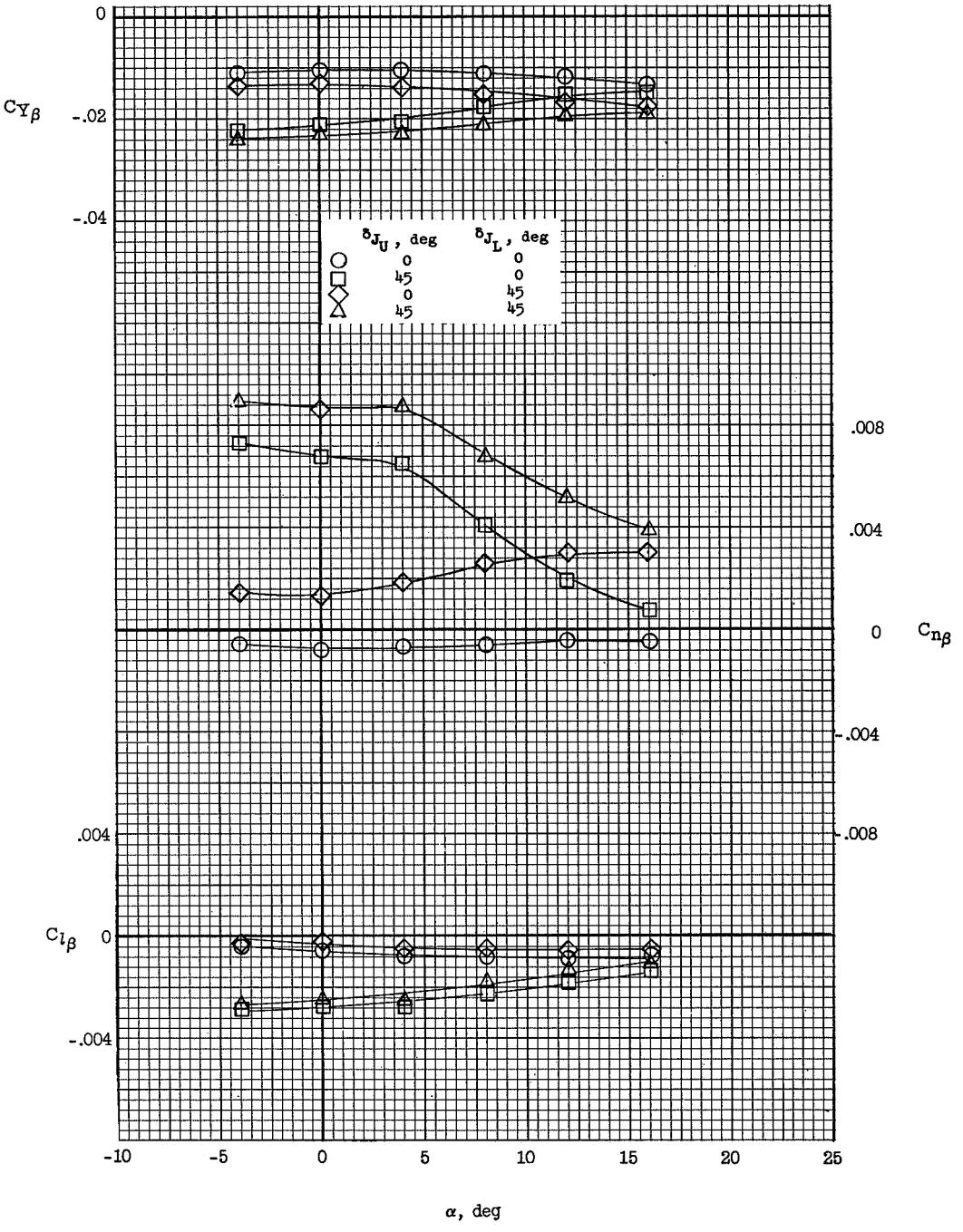

L-740

Figure 29.- Effect of speed-brake components on the directional and lateral stability derivatives of configuration $BWXHV_UV_LJ_UJ_L$. M = 6.83.

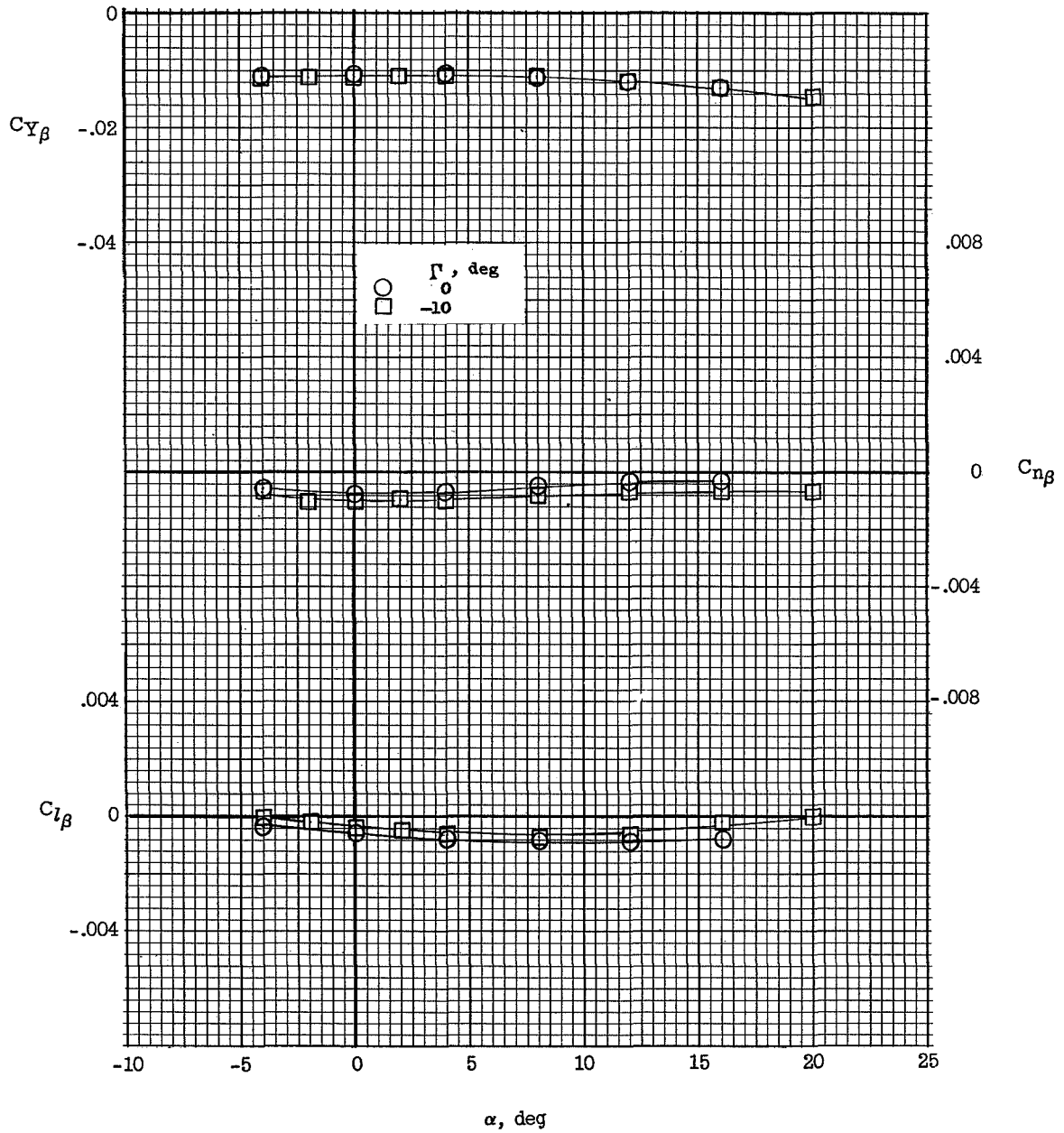

Figure 30.- Effect of wing dihedral on the lateral and directional stability derivatives of configuration 1. M = 6.83.

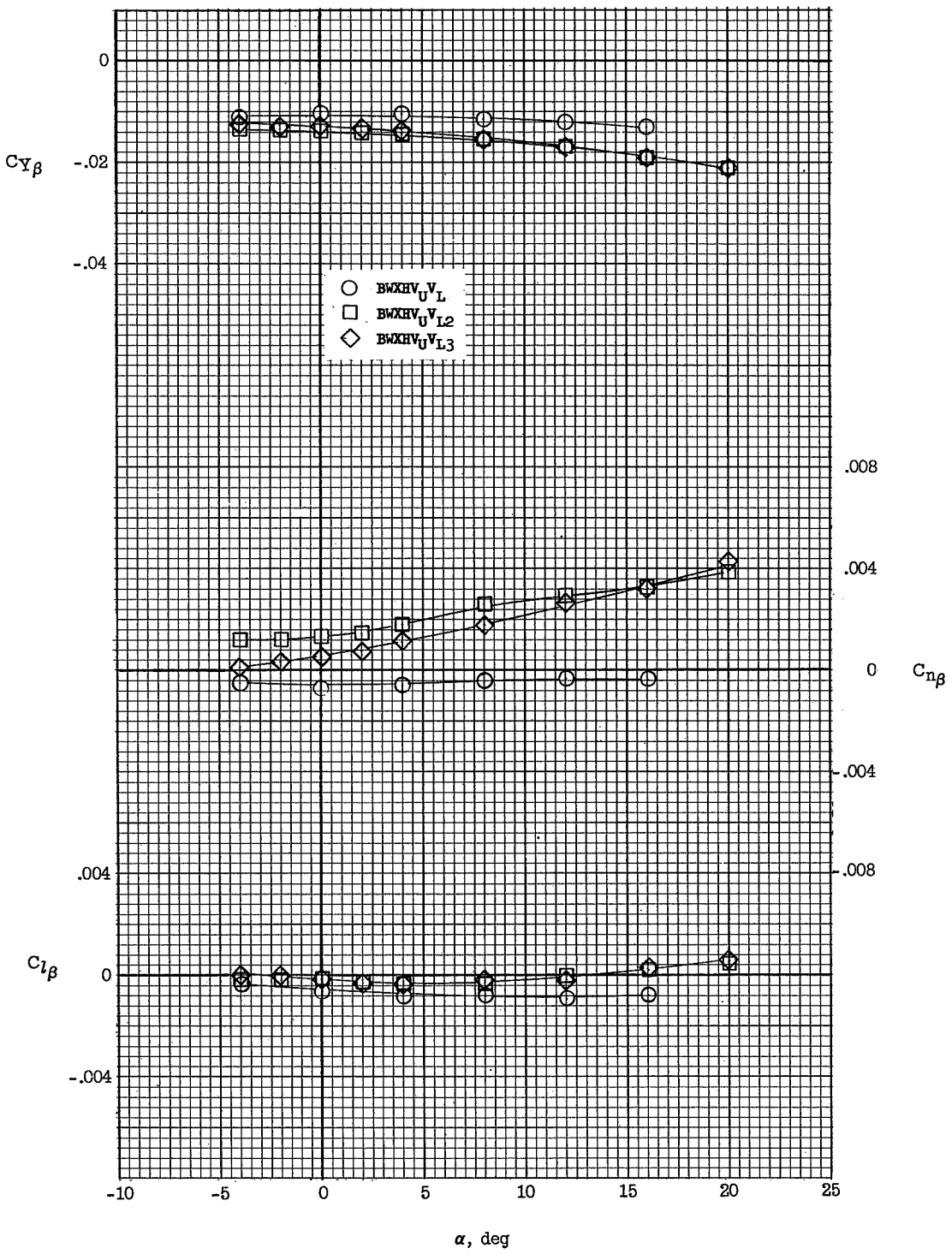

L-740

Figure 31.- Effect of lower vertical-tail modifications on the lateral and directional stability derivatives of configuration 1. M = 6.83.

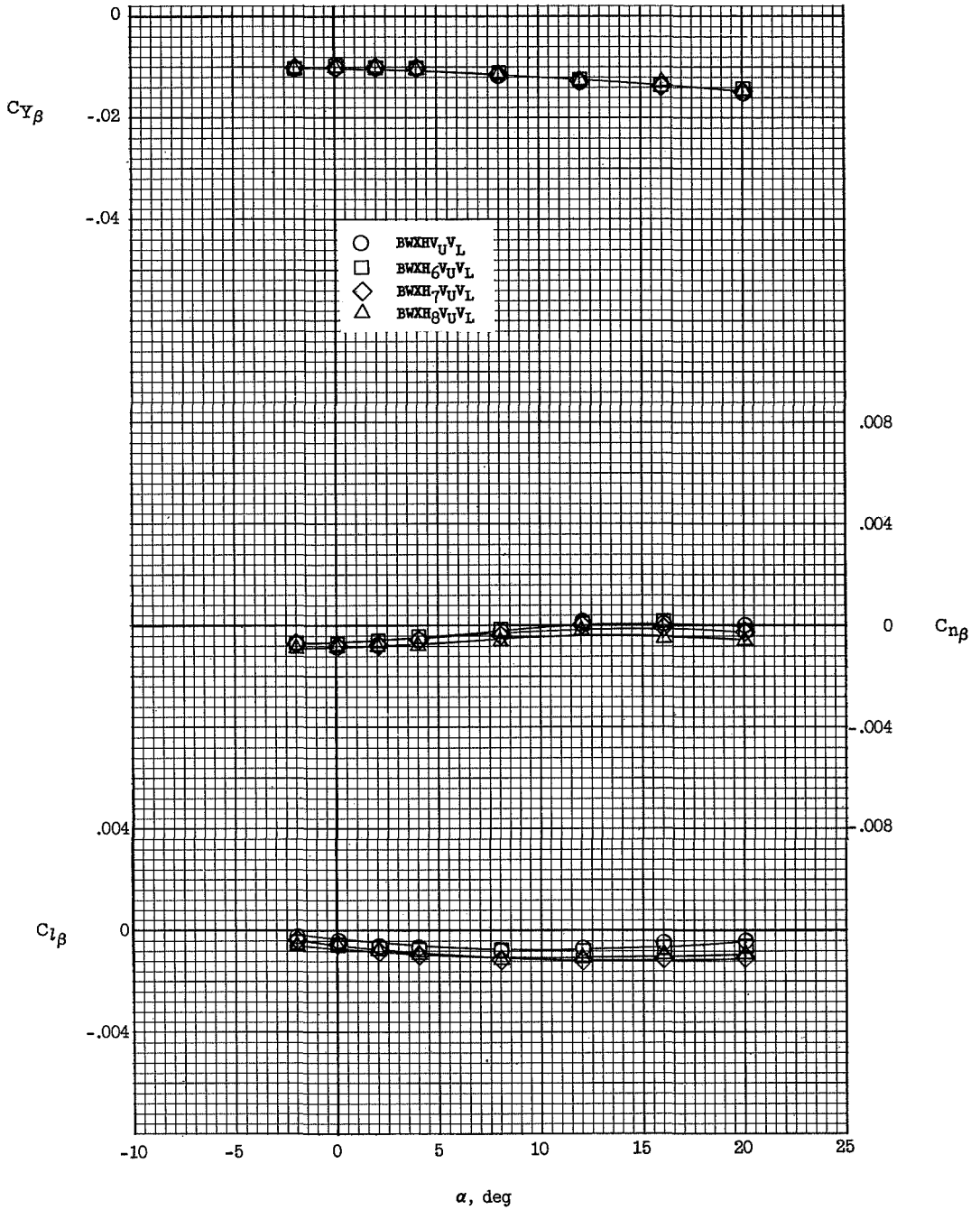

Figure 32.- Effect of horizontal-tail location and dihedral on the lateral and directional stability derivatives of configuration 1. M = 6.83.

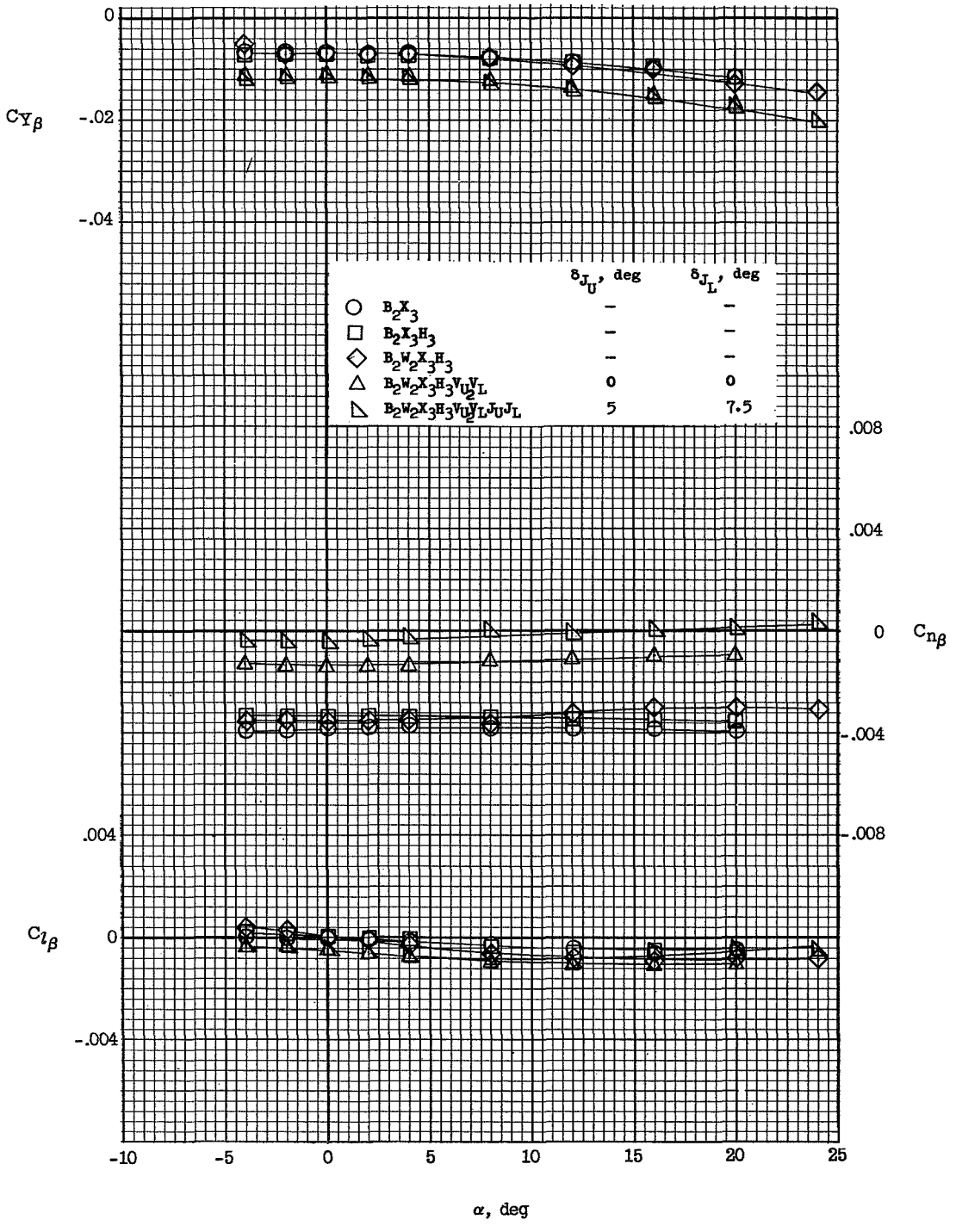

Figure 33.- Effect of various components on the lateral and directional stability derivatives of configuration 2. M = 6.83.

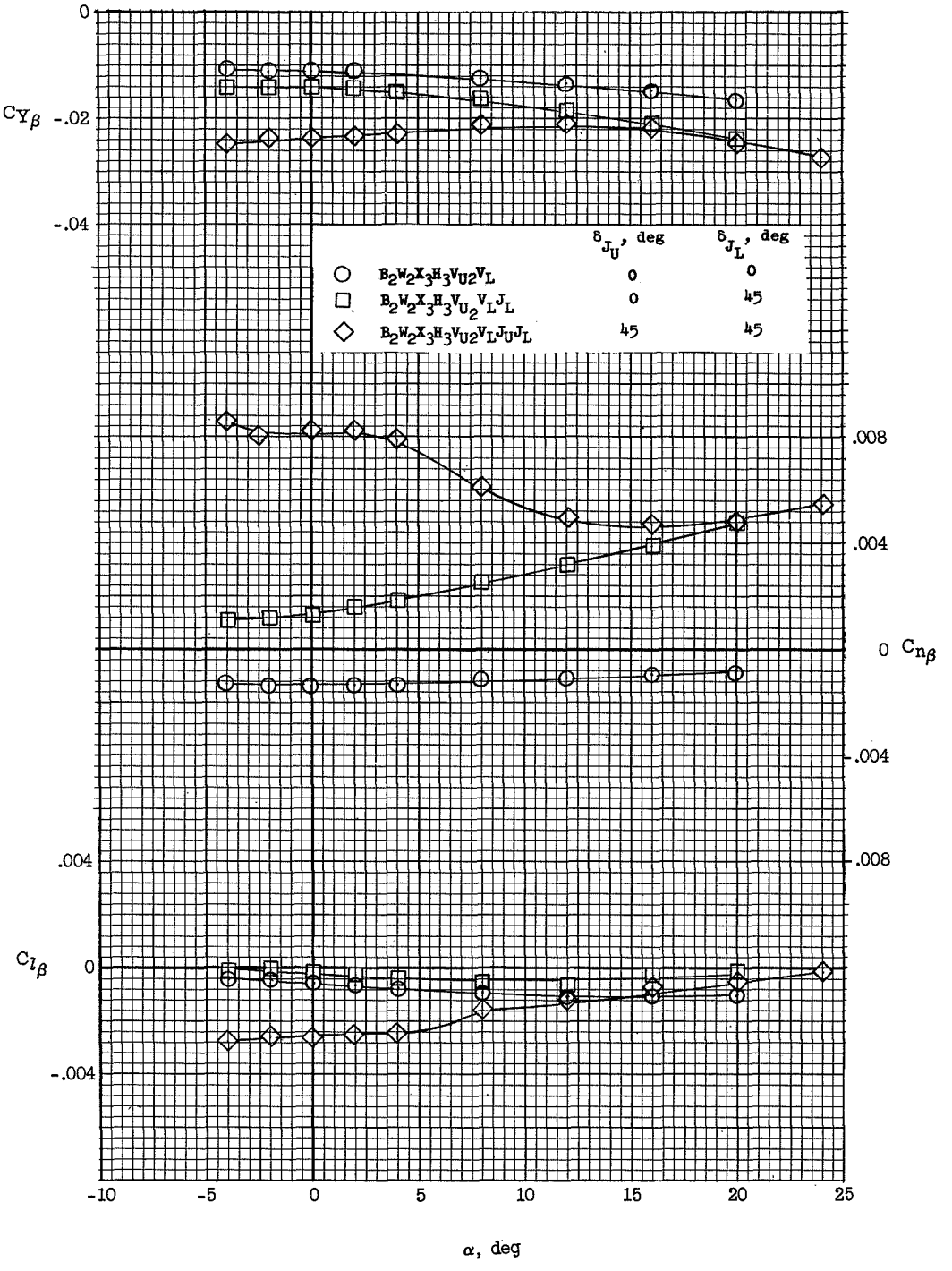

Figure 34.- Effect of speed-brake components on the lateral and directional stability derivatives of configuration 2. M = 6.83.

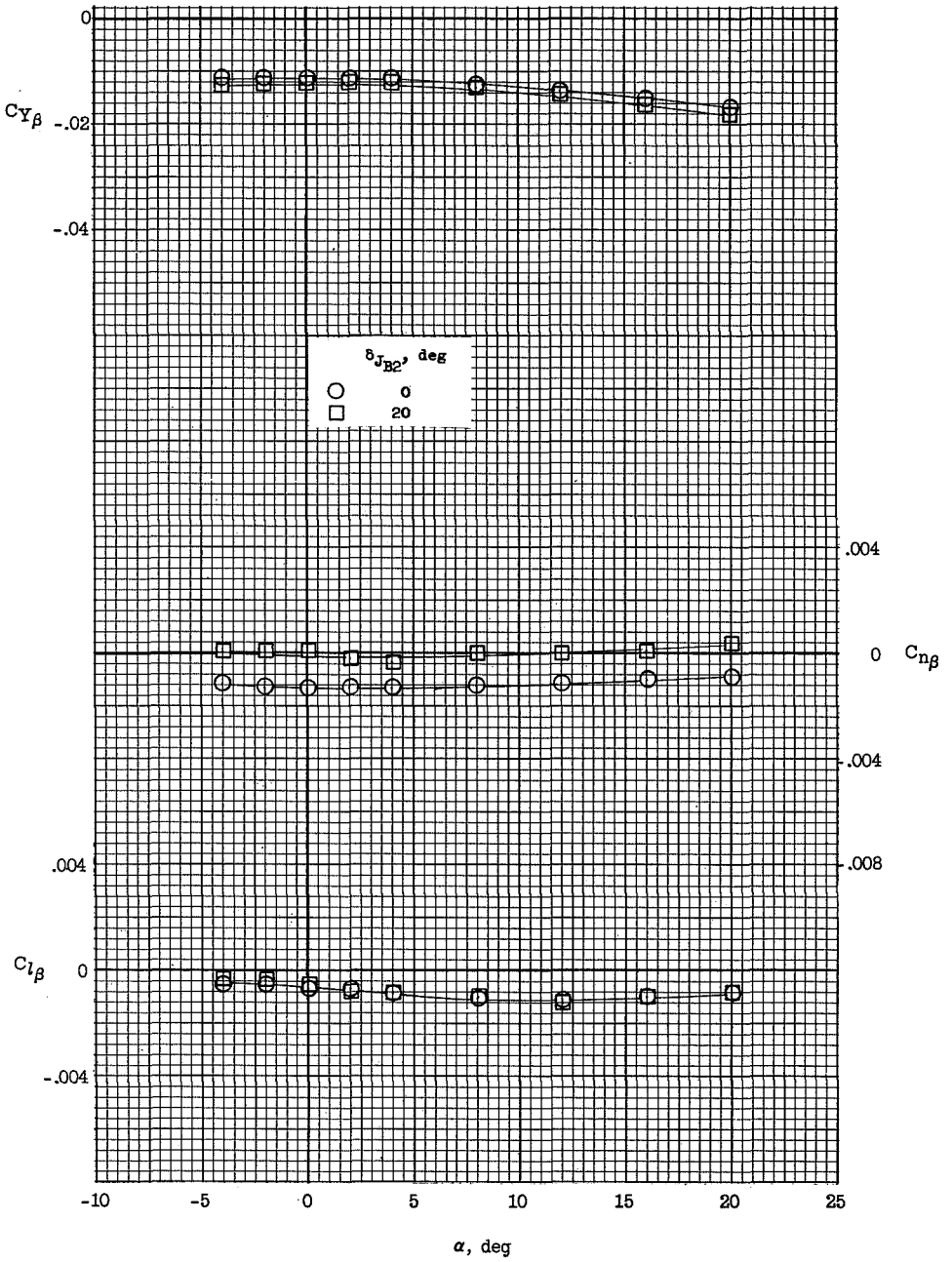

Figure 35.- Effect of fuselage conical speed-brake deflection $\delta_{J_{B2}}$ on the lateral and directional stability derivatives of configuration $B_2W_2X_3H_3V_{U2}V_LJ_{B2}$. M = 6.83.

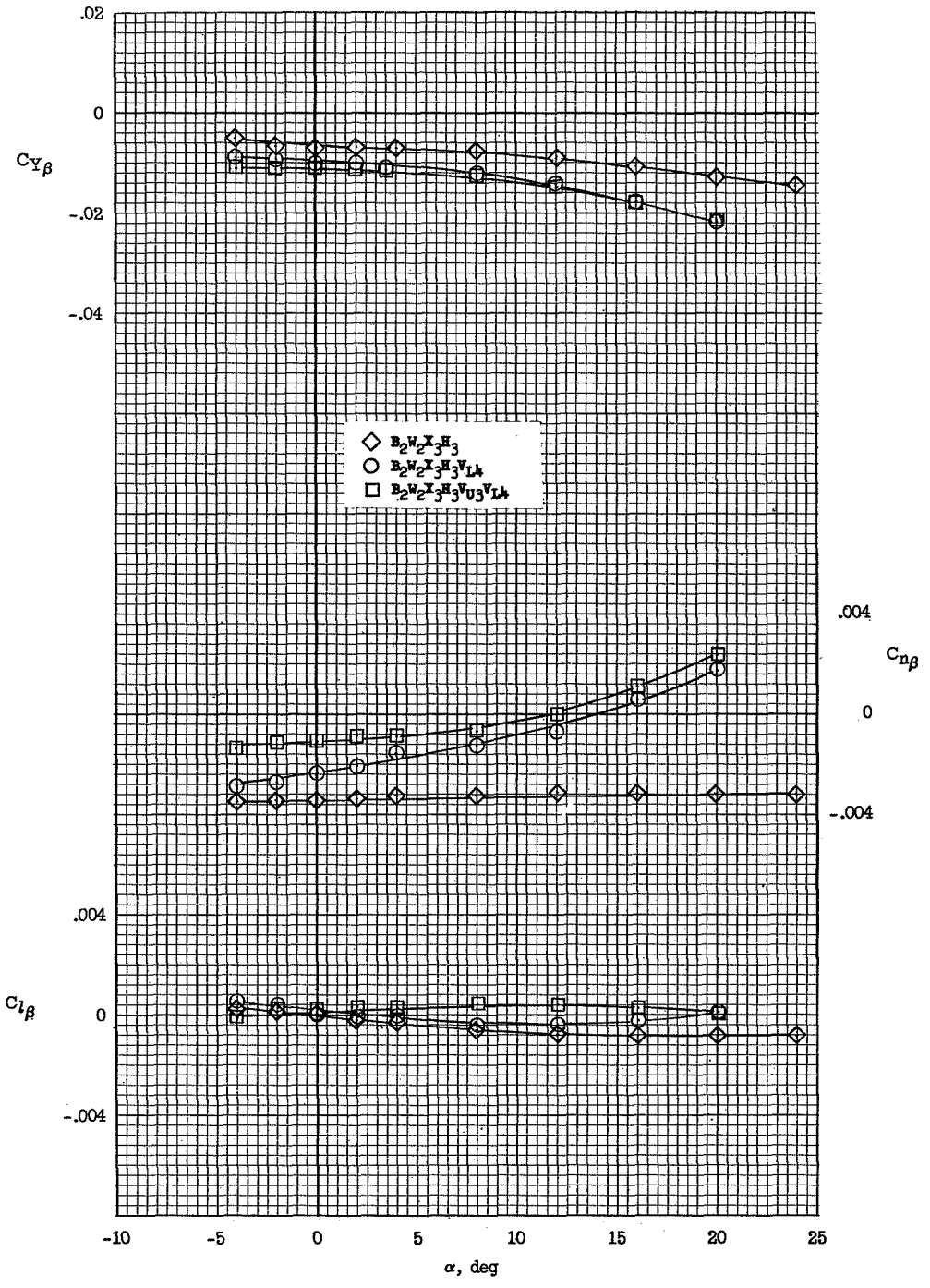

Figure 36.- Effect of twin upper and lower vertical-tail components on the lateral and directional stability derivatives of configuration $B_2W_2X_3H_3V_{U3}V_{L4}$. M = 6.83.

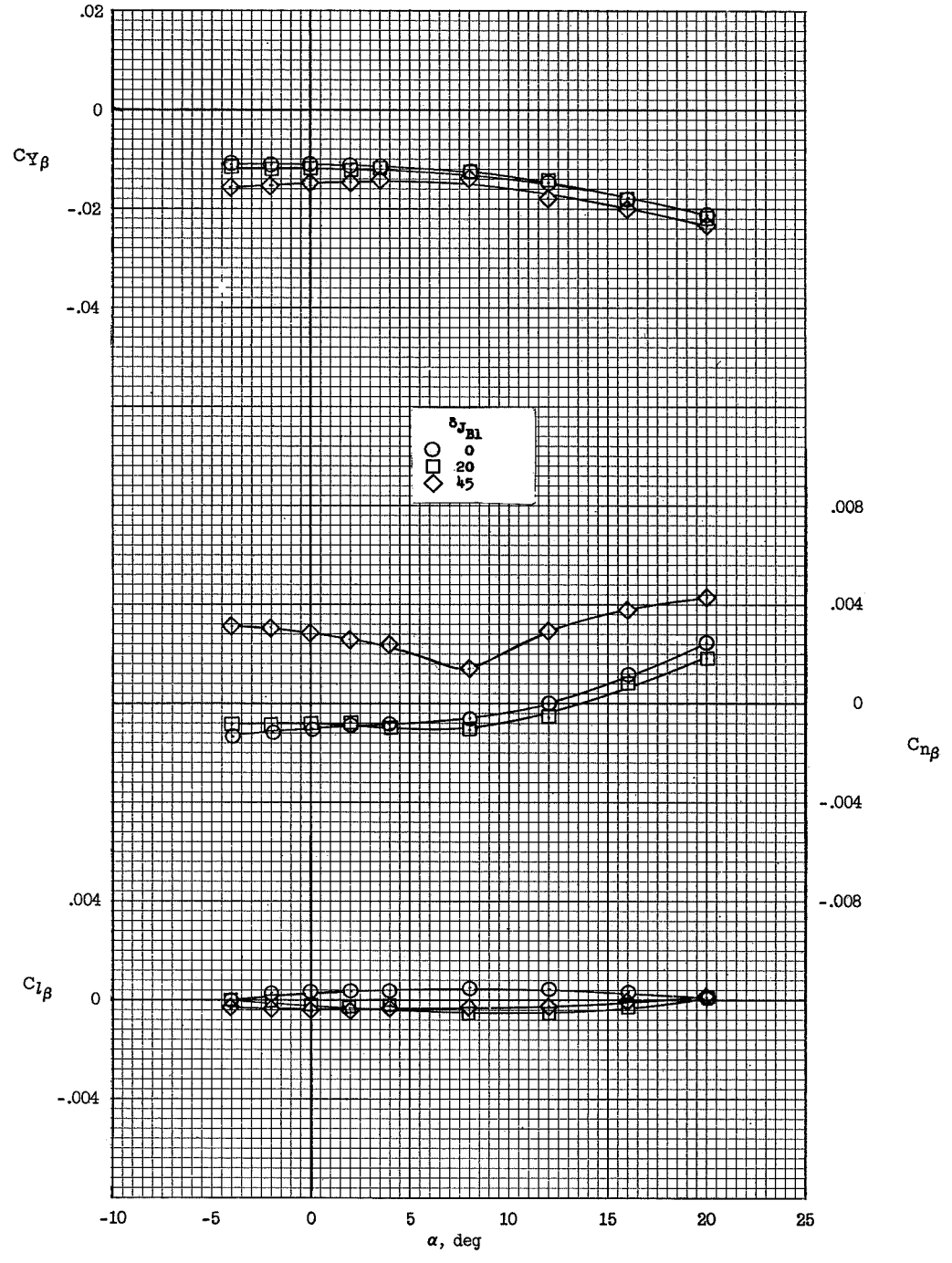

Figure 37.- Effect of fuselage conical speed-brake deflection $\delta_{J_{B1}}$ on the lateral and directional stability derivatives of configuration $B_2W_2X_3H_3V_{U3}V_{L4}J_{B1}$. M = 6.83.

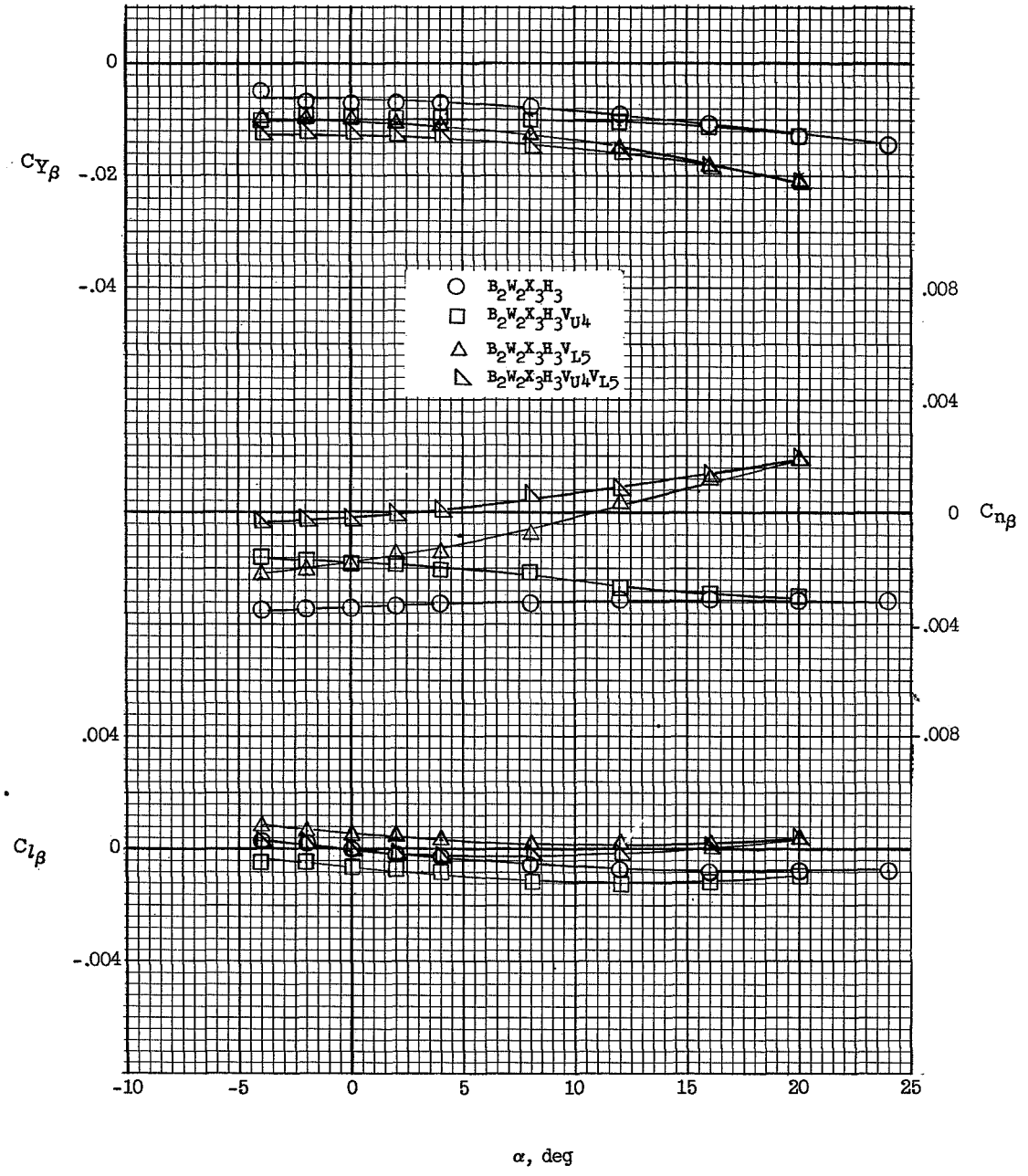

(a) $\delta_{J_{U1}} = \delta_{J_{L1}} = 0^\circ$.

Figure 38.- Effect of vertical-tail components and speed-brake components on the lateral and directional stability derivatives of configuration $B_2W_2X_3H_3V_{U4}V_{L5}J_{U1}J_{L1}$. M = 6.83.

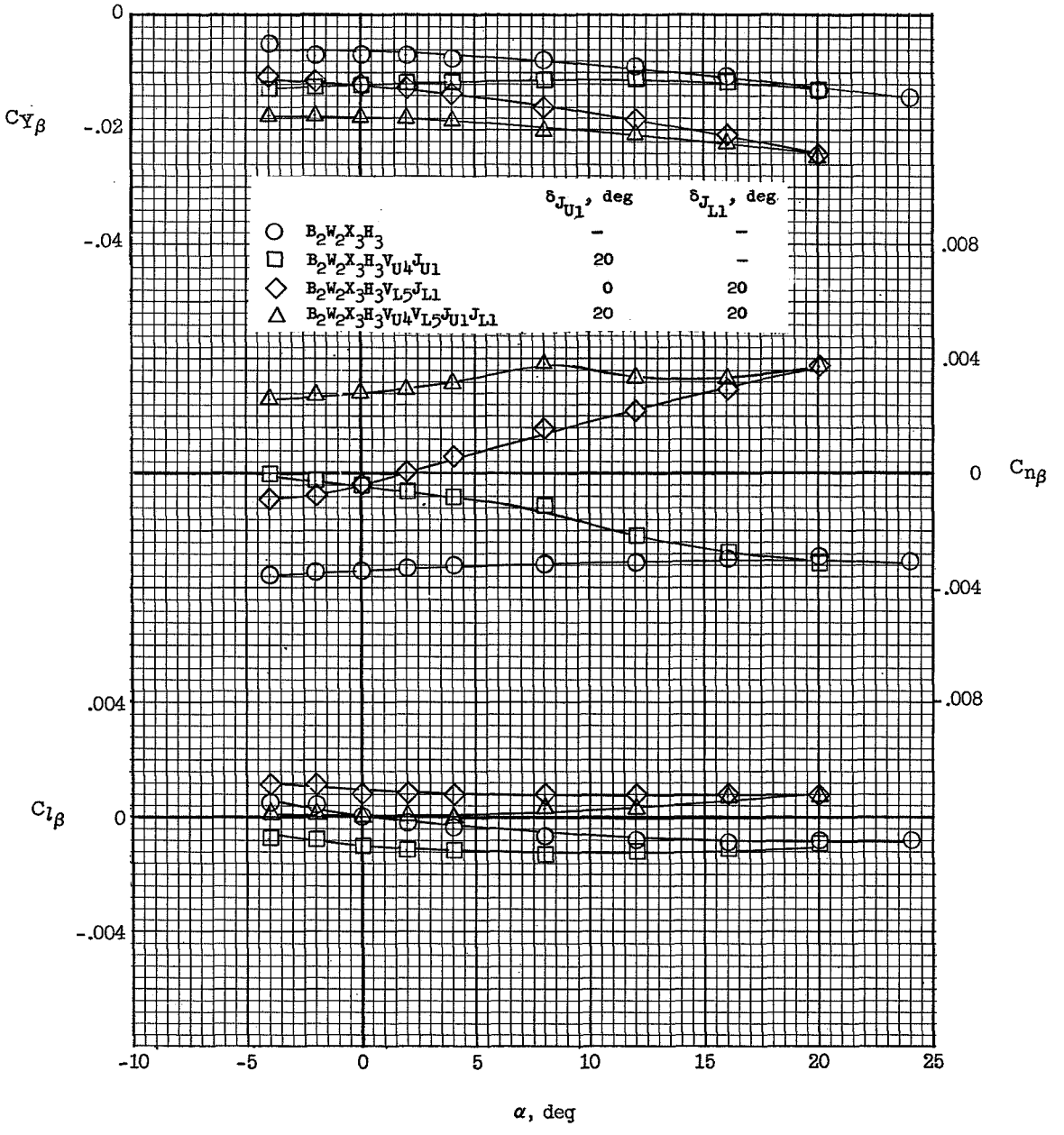

(b) $\delta_J = 20^\circ$.

Figure 38.- Continued.

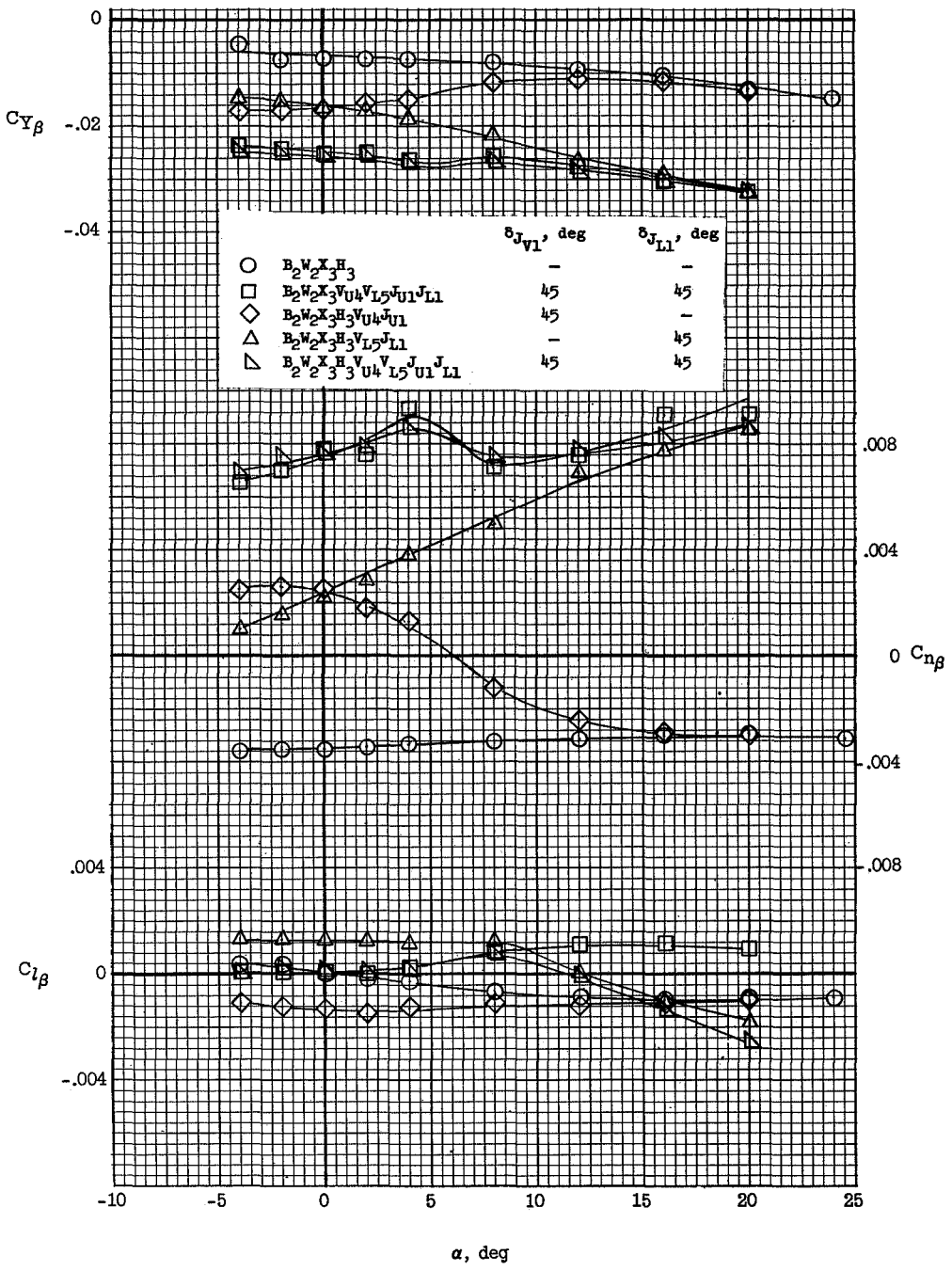

(c) $\delta_J = 45^\circ$.

Figure 38.- Concluded.

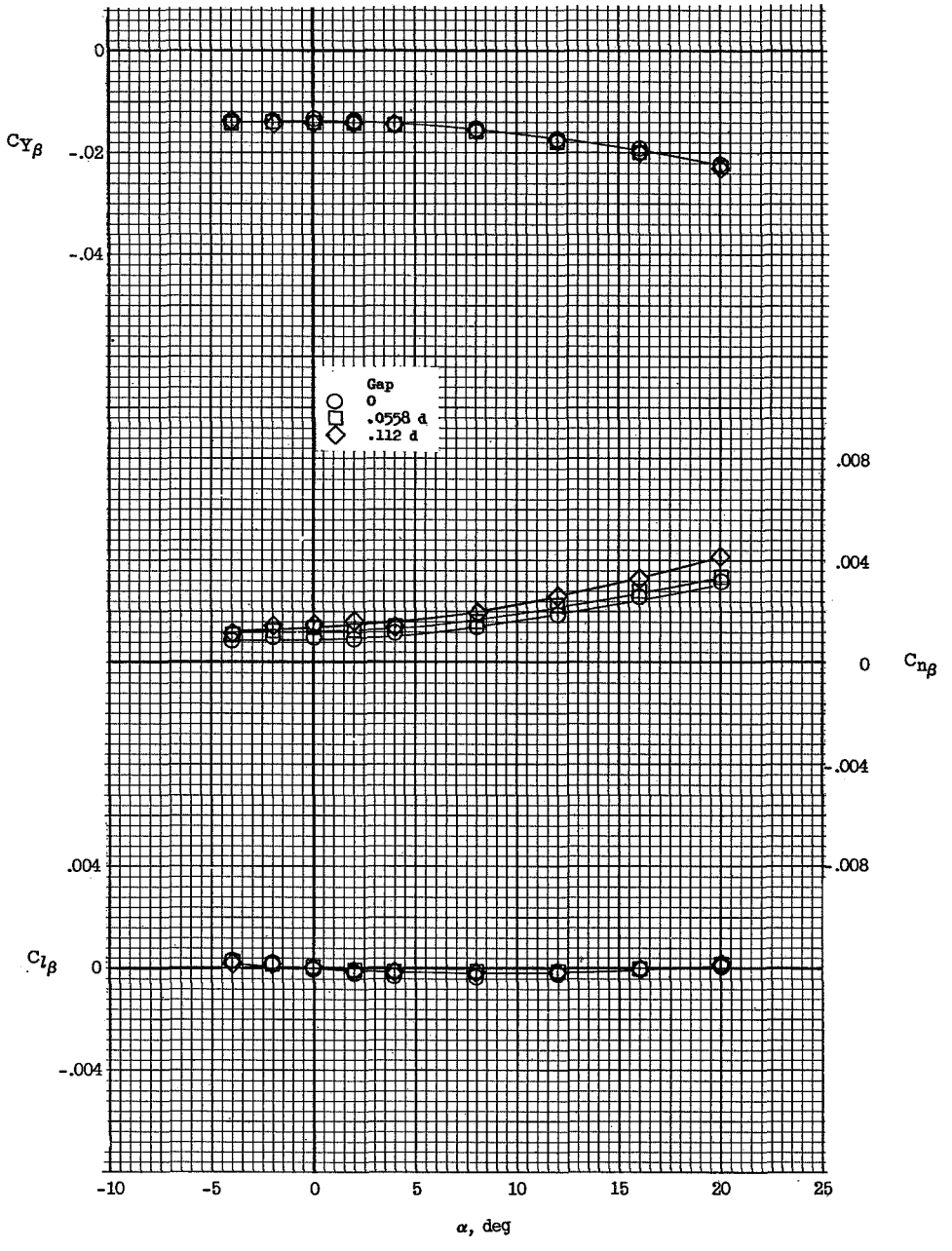

(a) $\delta_{J_F} = 40^\circ$.

Figure 39.- Effect of boundary-layer gap on the lateral and directional stability derivatives of configuration $B_2W_2X_3H_3V_{U4}V_{L5}J_F$ with various fairing speed-brake deflections. M = 6.83.

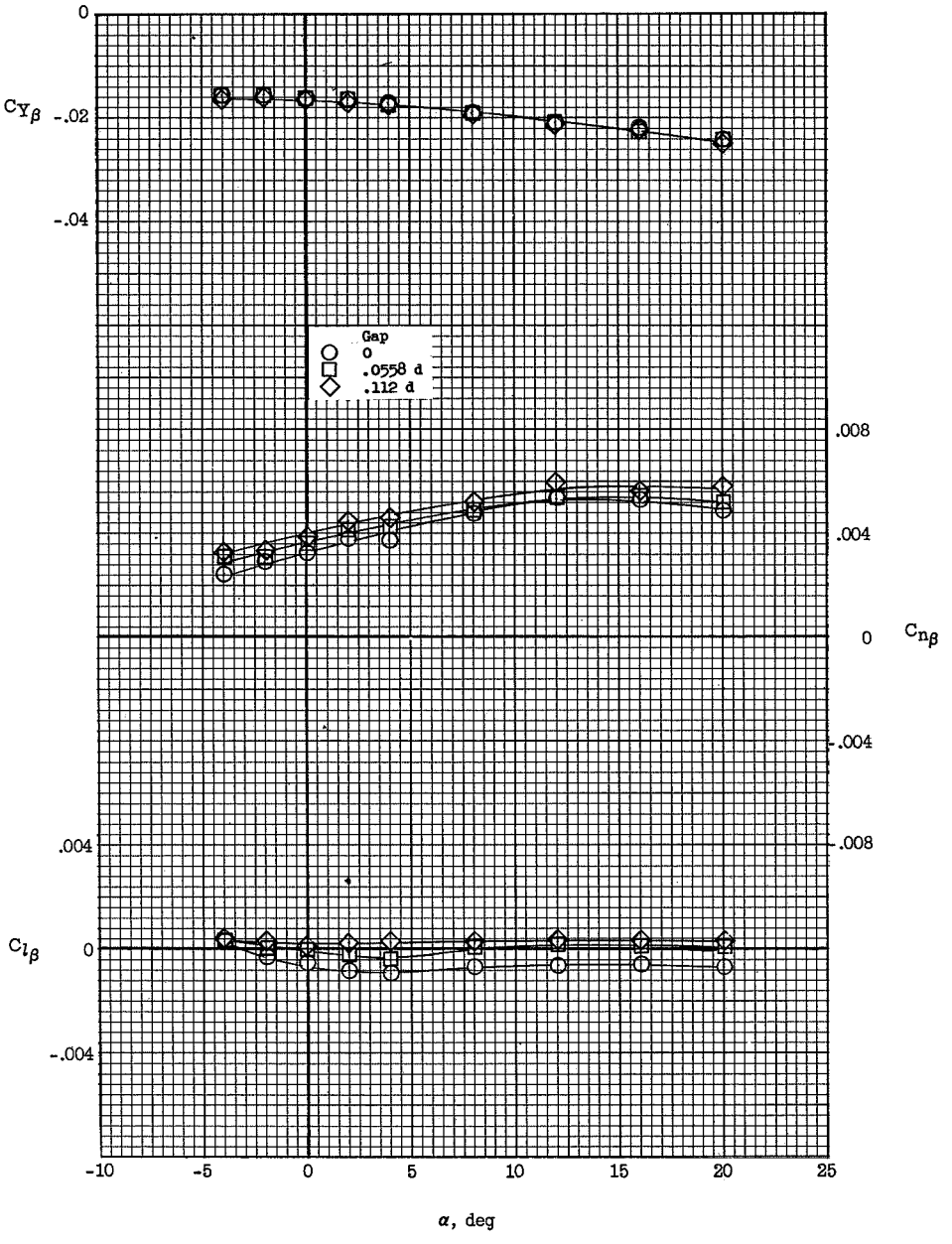

(b) $\delta_{J_F} = 75^\circ$.

Figure 39.- Concluded.

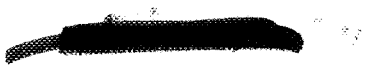

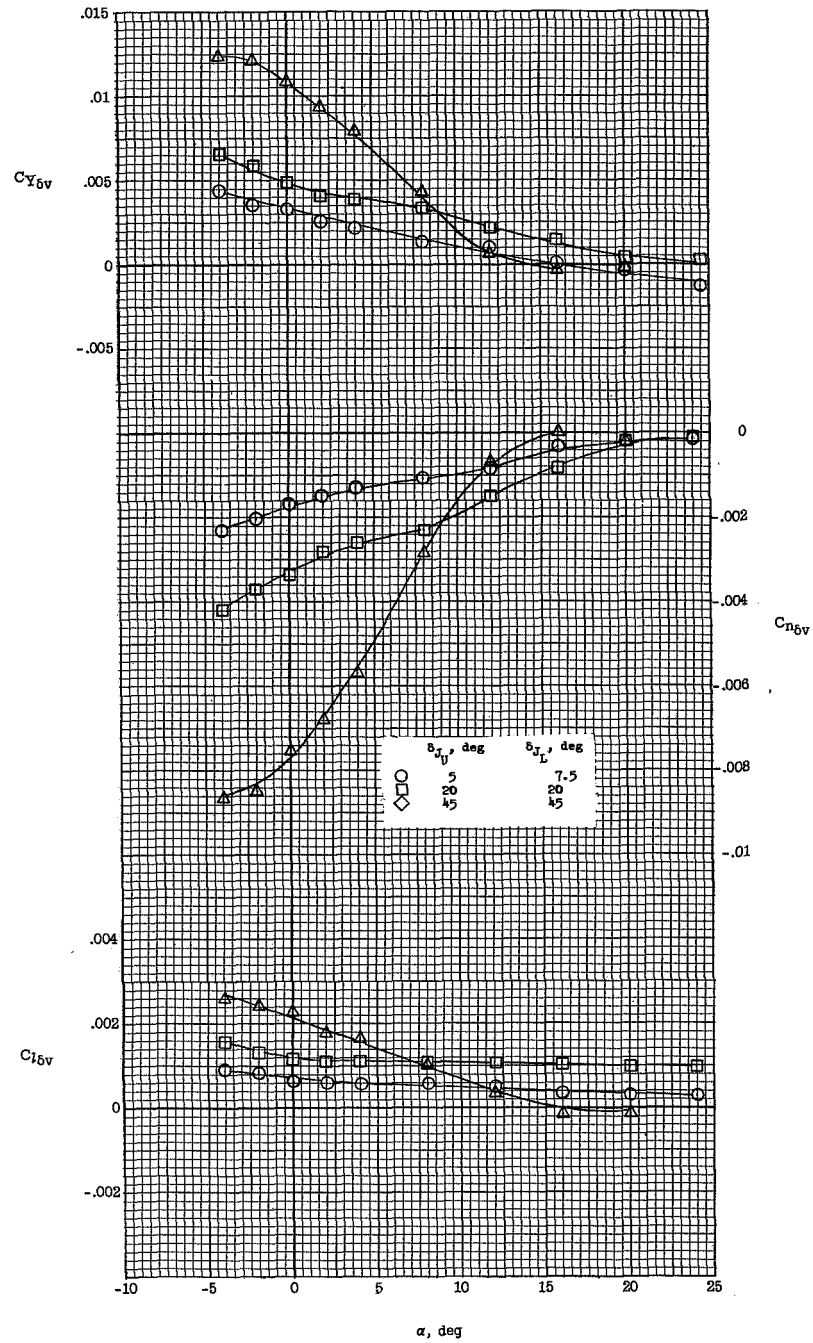

(a) Upper vertical-tail control parameters.

Figure 40.- Directional control derivatives for configuration $B_2W_2X_3H_3V_{U2}V_LJ_UJ_L$ with various speed-brake deflections. M = 6.83.

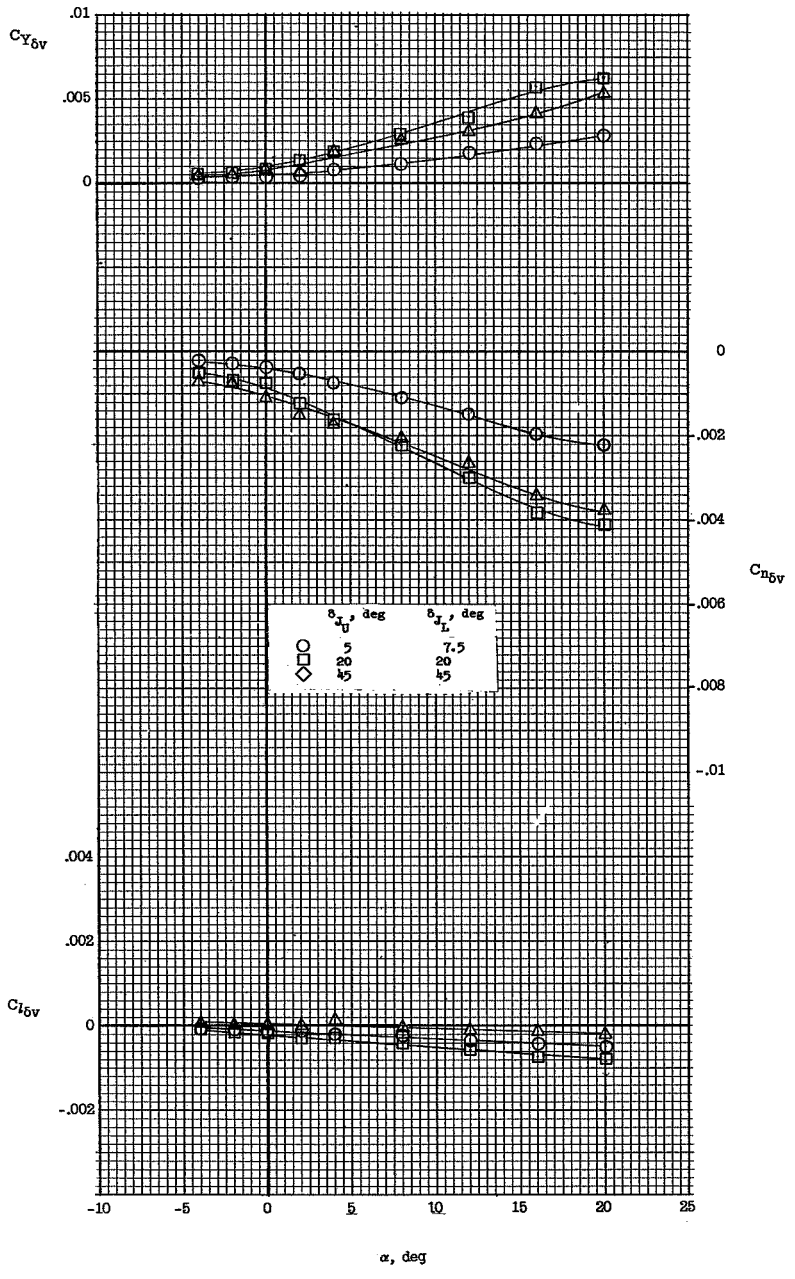

(b) Lower vertical-tail control parameters.

Figure 40.- Concluded.

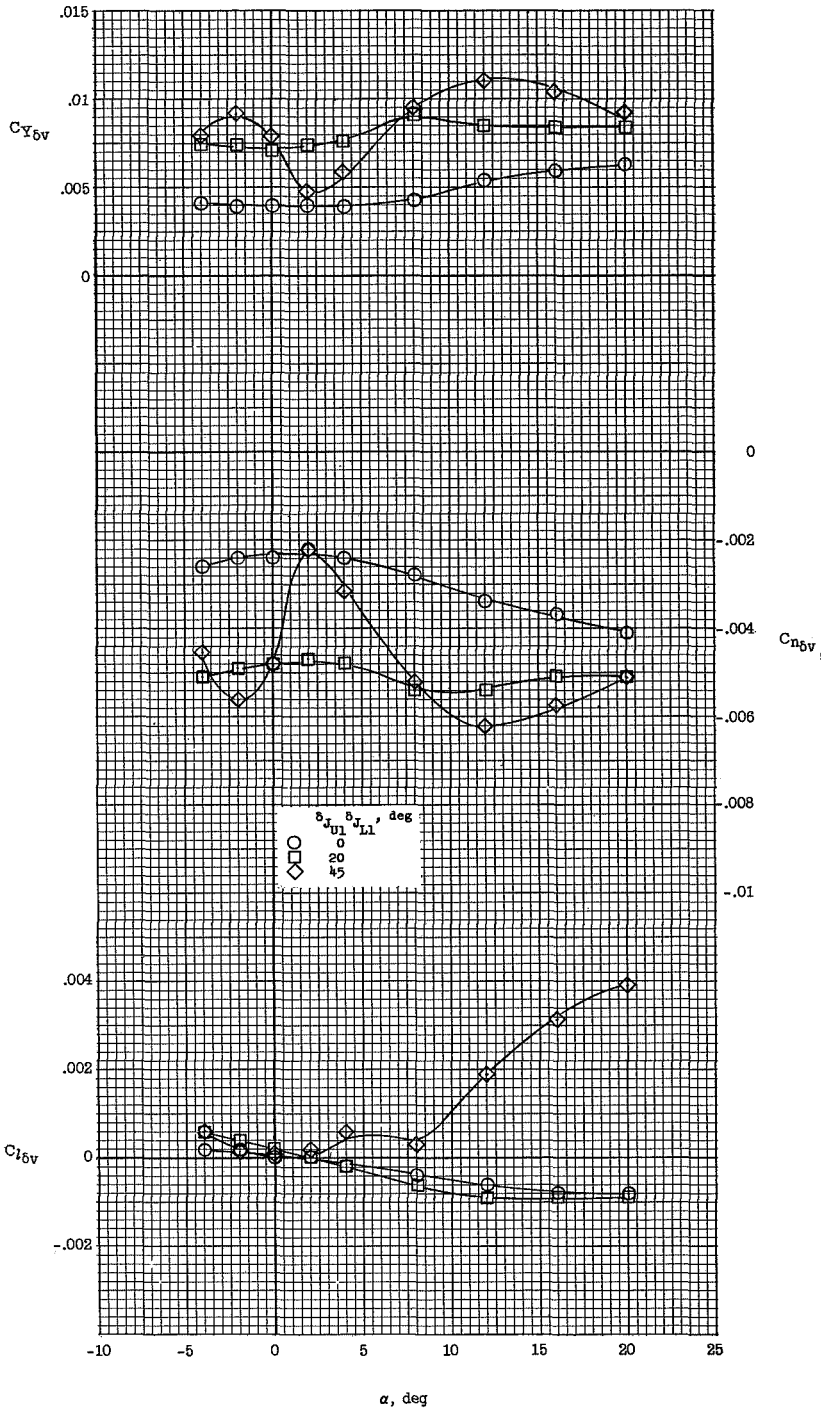

Figure 41.- Effect of speed-brake deflection on the directional control derivatives of configuration $B_2W_2X_3H_3V_{U4}V_{L5}J_{U1}J_{L1}$. M = 6.83.

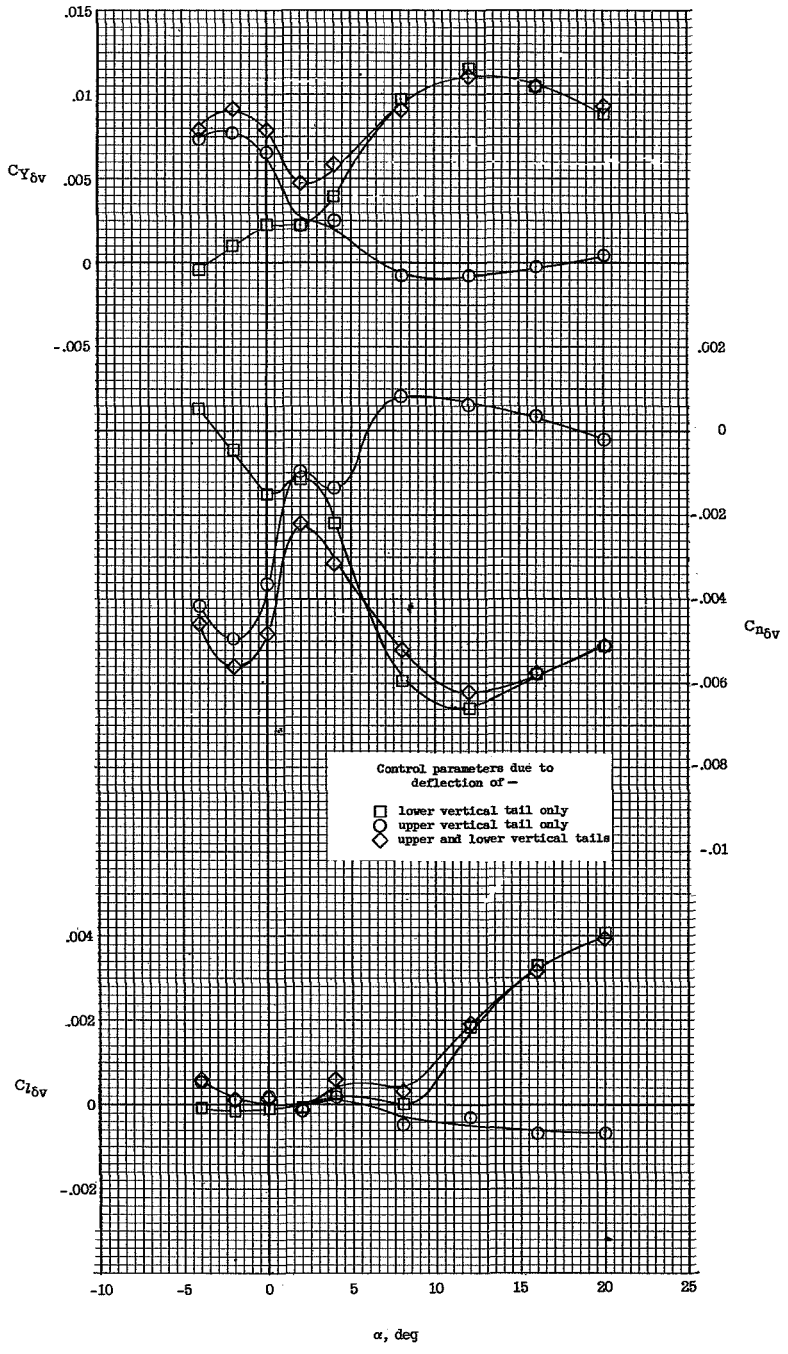

Figure 42.- Effect of vertical-tail components on the directional control derivatives of configuration $B_2W_2X_3H_3V_{U4}V_{L5}J_{U1}J_{L1}$. M = 6.83; $\delta_{J_{U1}} = \delta_{J_{L1}} = 45^\circ$.

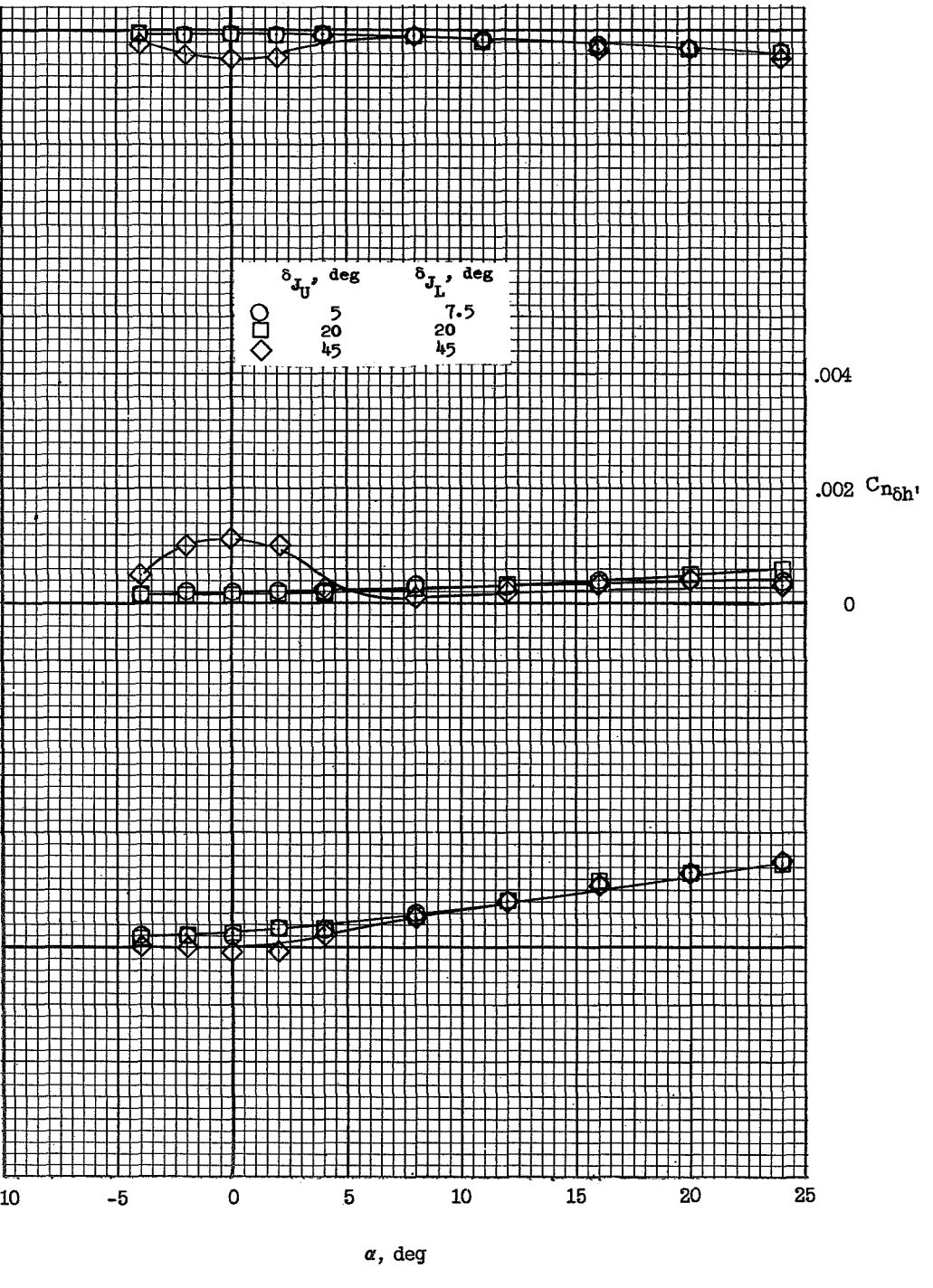

Figure 43.- Effect of speed-brake deflection on the lateral control derivatives of configuration $B_2W_2X_3H_3V_{U2}V_LJ_UJ_L$. M = 6.83.

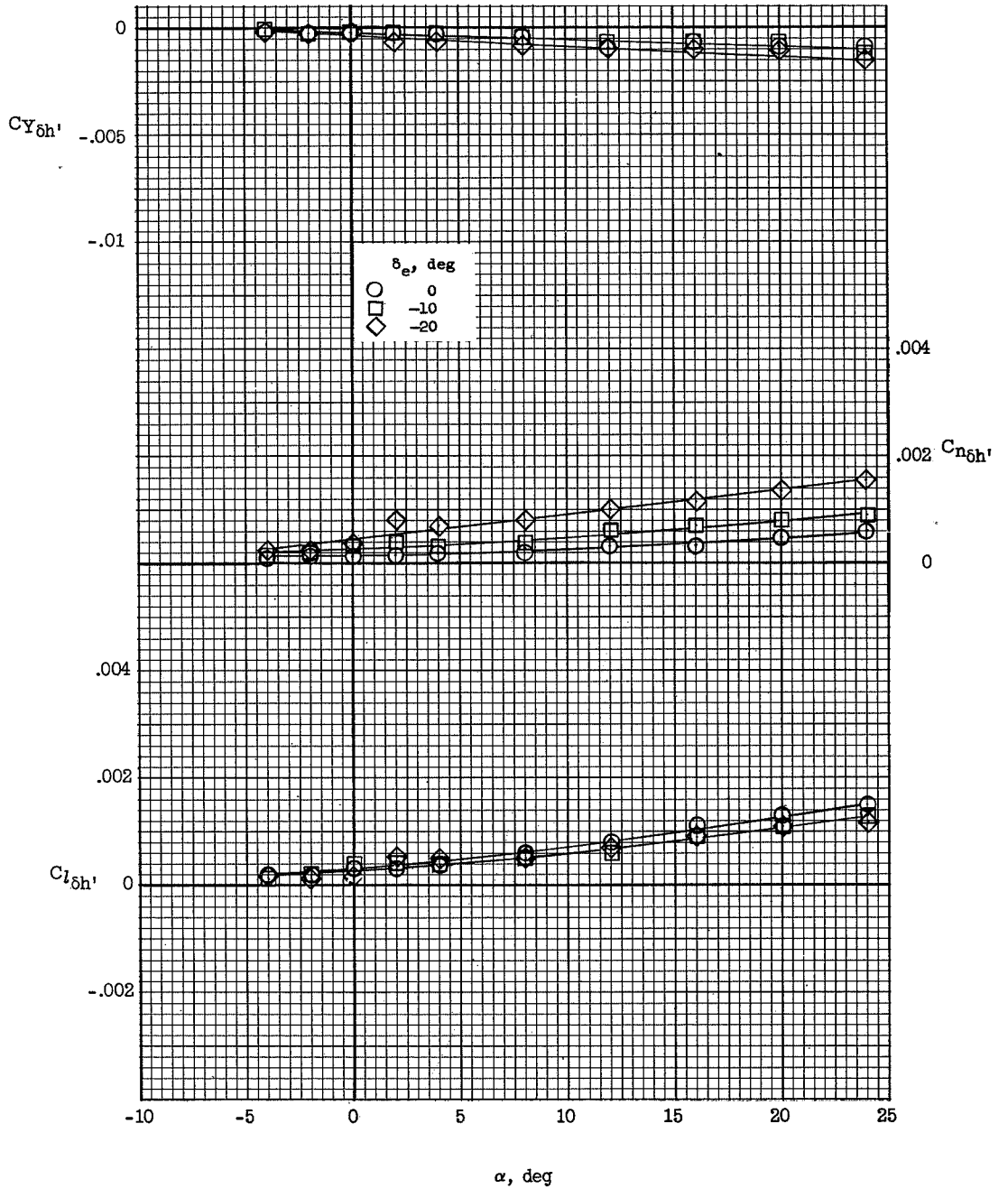

Figure 44.- Effect of equivalent horizontal-tail pitch deflection on the lateral control derivatives of configuration $B_2W_2X_3H_3V_{U2}V_LJ_UJ_L$. $M = 6.83$; $\delta_{J_U} = \delta_{J_L} = 20^\circ$.

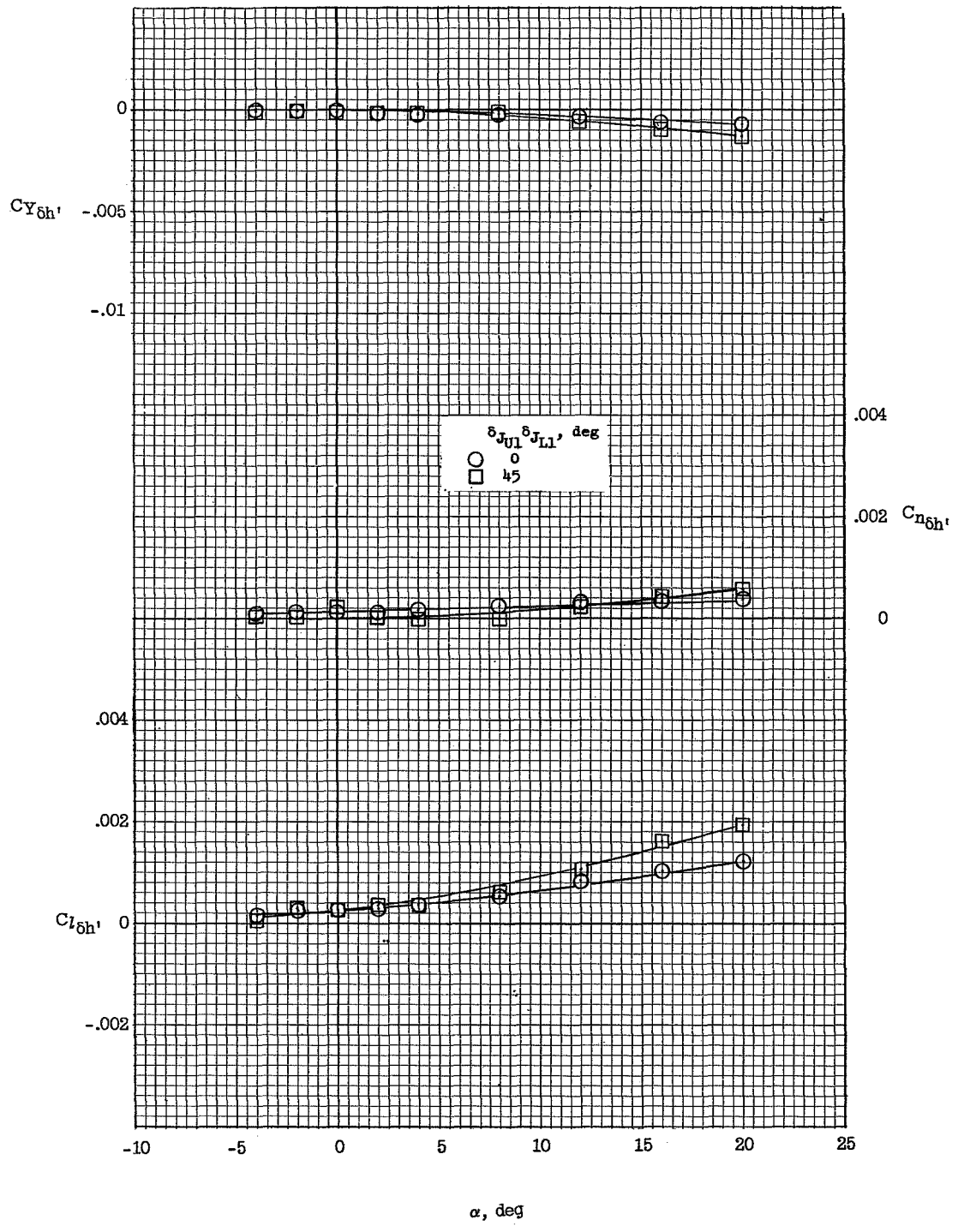

Figure 45.- Effect of speed-brake deflection on the lateral control derivatives of configuration $B_2W_2X_3H_3V_{U4}V_{L5}J_{U1}J_{L1}$. $\delta_e = 0^\circ$; M = 6.83.

[redacted]